

# STABILITY ANALYSIS OF MULTILEVEL INVERTER FED INDUCTION MOTOR DRIVE

## A DISSERTATION

*Submitted in partial fulfillment of the  
requirements for the award of the degree*

*of*

**MASTER OF TECHNOLOGY**

*in*

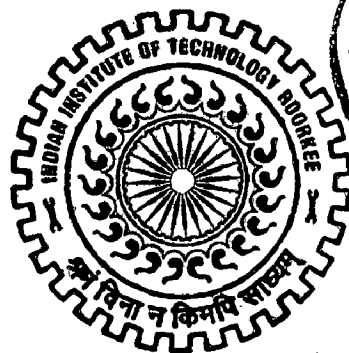
**ELECTRICAL ENGINEERING**

**(With Specialization in Power Apparatus and Electric Drives)**

*By*

**VIJAY KUMAR BHATT**

*IP*



**DEPARTMENT OF ELECTRICAL ENGINEERING  
INDIAN INSTITUTE OF TECHNOLOGY ROORKEE  
ROORKEE-247 667 (INDIA)**

**JUNE, 2006**

## Candidate's Declaration

I here by declare that the work which has been presented in the Dissertation Thesis entitled "Stability Analysis Of Multilevel Inverter Fed Induction Motor Drive" in partial fulfillment of the requirements for the award of the degree Master of Technology in electrical Engineering with specialization in Power Apparatus and Electric Drives, submitted in the department of electrical engineering Indian Institute of Technology Roorkee, INDIA-247667. This is an authentic record of my own work carried out in the period of the last two semesters from July 2005 to May 2006, under the supervision of Dr. Pramod Agarwal, professor and Dr.S.P.Srivastava associate professor, Department of Electrical Engineering ,Indian Institute of Technology, Roorkee INDIA-247667. The matter embodied in this Dissertation Thesis has not been submitted by me for the award of any other degree of diploma.

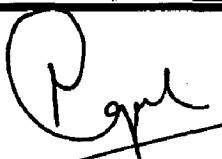
Date: 29/06/06  
Place: ROORKEE


  
(Vijay Kumar Bhatt)

## Certificate

This is to certify that the above statements made by the candidate are correct to the best of my knowledge.

---

  
(Dr. Pramod Agarwal)  
Professor  
Electrical Engineering Dept.  
Indian Institute of Technology  
Roorkee

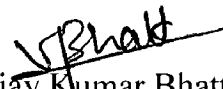
  
(Dr. S. P. Srivastava)  
Associate Professor  
Electrical Engineering Dept.  
Indian Institute of Technology  
Roorkee

## Acknowledgements

Many thanks extend to the people who have played a major role in the development and progress of this work. With their patience and guidance, this project has been a very enriching and enjoyable experience. I am especially grateful to **Dr. Pramod Agarwal, Professor and Dr. S. P. Srivastava, Associate Professor, Department of Electrical Engineering, Indian Institute of Technology Roorkee, Roorkee** for their whole heartedness and high dedication with which they involved in this work.

I am grateful to all my teachers of the PAED group for their suggestions and constant encouragement. I am also grateful to all Research Scholars of the PAED group for their suggestions and constant encouragement. Timely assistance and help from the laboratory staff of Drives Lab, Stores, and Workshop is sincerely acknowledged. Grateful acknowledgements also to my friends and other well wishers whose timely help has gone a long way in this work.

Date: 29/06/06  
Place: ROORKEE

  
(Vijay Kumar Bhatt)  
M.Tech (Elect.) PAED

## Abstract

---

The stability problem in an induction motor drive system has to be discussed essentially from two different angles. One is from the angle of the power source in relation to the achievement of quick response in electromagnetic torque. The other is closely related to the well known self-excitation phenomena in a self-excited type induction generator. The former is associated with the interaction between electric transients and rotor dynamics. For an induction motor driven by a voltage source of adjustable amplitude and frequency such as a PWM inverter the problem of occurrence of sustained oscillation has often been observed in the light loaded state. The two problems which should be considered are 1) under what condition is the oscillation excited, and how is the oscillating range determined in the stator voltage versus frequency (V/F) plane. If the matter is considered from the stand point of drive performance, the stability is quite easily interpreted. Whenever the electromagnetic torque is so controlled as to be kept, without delay, at a desired value required from the load side, the stability problem never occurs. Hence factors deteriorating the stability are the existence of the stator resistance and leakage inductances in both stator and rotor circuits or transient inductance.

## List of Figures

---

Figure No	Figure description	Page no.
Fig 2.1	Torque-frequency torque at variable voltage	9
Fig 2.2	Torque speed curves with variable stator voltage	10
Fig 2.3	Torque-speed curves at constant volts/Hz	11
Fig 2.4	Torque speed curves at variable voltage and variable Frequency up to field weakening region.	12
Fig 2.5	Stationary Frame a-b-c to ds-qs axis transformation	14
Fig 2.6	Dynamic $d^e - q^e$ equivalent circuit of machine (a) $q^e$ axis (b) $d^e$ axis.	15
Fig 2.7	Small signal control block diagram	19
Fig 2.8	Small signal transfer function block diagram	20
Fig 2.9	Unstable range	28
Fig 2.30	Three level inverter	29
Fig 3.1	Three level inverter circuit	34
Fig 3.2	Pulse amplification and isolation circuit	37
Fig 3.3	5 volt supply power circuit	37
Fig 3.4	$\pm 12V$ supply power circuit	38
Fig 3.5	MOSFET with snubber circuit	39
Fig 3.6	Delay circuit	39
Fig 3.7	Main program for open loop v/f control of npc inverter	42

Fig 3.8	Ts_ISR for Open Loop V/f Control of NPC Inverter	44
Fig 3.9	TaTbTc_ISR for Open Loop V/f Control of NPC Inverter	45
Fig 3.40	Regions in sector 1	46
Fig 3.41	Flow chart for the selection of region	47
Fig 4.1	Three level inverter	49
Fig 4.2	Three level space voltage vectors	50
Fig 4.3	Regions in sector 1	52
Fig 4.4 –Fig 4.27	Symmetrical pulse pattern for different regions.	56-70
Fig 4.28	Inverter phase voltage and its harmonic spectrum	71
Fig 4.29	Load current and its harmonic spectrum	72
Fig 4.30	Load current and its harmonic spectrum	73
Fig 4.31	Load current and its harmonic spectrum	74
Fig 4.32	Load current and its harmonic spectrum	75
Fig 4.33	Load current and its harmonic spectrum	76
Fig 4.34	Load current and its harmonic spectrum	77
Fig 4.35	Load current and its harmonic spectrum	78
Fig 4.36	Load current and its harmonic spectrum	79
Fig 4.37	Load current and its harmonic spectrum	80
Fig 4.38	Load current and its harmonic spectrum	81
Fig 4.39	Load current and its harmonic spectrum	82
Fig 4.40	Torque and Speed characteristic	83

## Nomenclature

---

$F_a, F_b, F_c$	Instantaneous quantity of voltage or current in phases a, b, and c, respectively
$\vec{F} = F_d + jF_q$	Instantaneous rotating spacial vector defined by $F_a, F_b, F_c$ .
$\vec{v}_1, \vec{i}_1, \vec{i}_2$	stator voltage and current and rotor current
$F =  \vec{F} $	magnitude of $\vec{F}$
$L_{11}, L_{22}, L_{12}$	stator winding self-inductance, rotor winding self-inductance, and mutual inductance between these two winding
$r_1, r_2$	stator winding resistance and rotor winding resistance
$\omega_r$	rotor electrical angular velocity
$T_e$	electromagnetic torque
$T_{sh}$	shaft torque
$J$	moment of inertia of rotor
$\vec{i}_0 = \vec{i}_1 + \left(\frac{L_{22}}{L_{12}}\right)\vec{i}_2$	equivalent magnetizing current proportional to rotor flux linkage

$$T_0 = \left( \frac{L_{22}}{r_2} \right)$$

rotor circuit time constant

$$L_0 = \left( \frac{L_{12}^2}{L_{22}} \right)$$

equivalent magnetizing inductance

$$L'_1 = L_{11} - L_0$$

transient inductance

$$\dot{\theta}(t) (= 2\pi f_1)$$

instantaneous angular frequency of  $\vec{v}_1$

$$\phi_0$$

rotating position of  $\vec{i}_0$  by phase angle measured from  $\vec{v}_1$

$$\dot{\phi}_0$$

instantaneous angular frequency deviation of  $\vec{i}_0$

$$L_k i_{k0}$$

specified magnetic flux linkage determining the value of  $V/f$  for  $\vec{v}_1$



**Introduction**

---

**1.1 Introduction**

Three-phase induction motor drive systems control by PWM voltage source inverter, which have been widely utilized in industrial fields have often shown undesirable hunting phenomena in the low speed range and in light load conditions. They are often called stability problem and many papers have already presented. There exists no problems if the desired electromagnetic torque is generated at any time without delay and the required driving performance is constantly achieved. The stability problem occurs when such a situation is interrupted and the rotor dynamic are forced into a kind of hunting state. The induction motor is apt to become very oscillatory and has some oscillating modes. These modes can easily be excited by three different causes (I) power source, (II) the rotor dynamics and (III) the potential of the occurrence self-excitation. An abrupt variation of the stator voltage or current not accompanied by right control of the air-gap flux can cause a disturbance and undesirable oscillating components can consequently be generated in the electromagnetic torque even under a constant rotor speed. The supply generated by the inverters is usually non-sinusoidal in nature; i.e. There is presence of harmonics which give rise to different undesired effects in the machine, like torque pulsation, additional power loss temperature rise etc. These problems are even of more concerns in large rating drives.

Motor winding failure have become a problem with some adjustable speed drives because the increased switching of contemporary power devices causes steep voltage waveforms to appear at the motor terminals. The voltage change rates some times can be high enough to induce corona between winding layers.

**1.2 Literature survey**

Ref [1]: In this reference Lawrenson and Bowes have shown that the direct-axis/quadrature-axis resistance ratio of the rotor circuits has a pronounced influence on machine stability. The optimum is given as 0.5 and, when the machine operates near this optimum ratio, the

beneficial effects on machine stability of a reduction in stator resistance or an increase in leakage reactance are considerably enhanced.

Ref [2, 3, 4]: Closed-loop feedback methods are developed in this reference. A synchronous reluctance motor is stabilized by altering the amplitude of the stator voltage in accordance with the fluctuations in rotor speed. An inverter-fed induction motor has been stabilized by controlling inverter frequency with the motor emf or a derivative of DC link current.

Ref [5]: Stability property of speed sensorless induction motor drives with stator resistance estimation is analyzed in this reference, using the averaging analysis technique. Explicit stability conditions are then derived to clarify analytically when the instability may occur and how the regressor vectors used in the estimation and the integral adaptation gains should be designed to assure stability. The derived stability conditions also reveal that the coupling between the speed and the stator resistance estimation loops is the main cause of instability.

Ref [6]: For an induction motor driven by a sinusoidal voltage source of adjustable amplitude and frequency such as a PWM inverter, the problem of the occurrence of sustained oscillation has often been observed in the light loaded state. This paper contributes to the solution of this problem from the point of view of a linearized model.

Ref [7]: This reference proposes two methods for analyzing a commonly used control scheme for AC inverters. The first method is based on an adaptive control theory and the second method is based on the well-known internal model principle. These methods give sufficient conditions for stability and allow the designers to analytically determine the stability margin and to specify range of stable operating condition.

Ref [8]: Stability analysis of systems with nonlinearities is considered in this reference. Multipliers that describe the nonlinearities are used for the analysis. The stability analysis can be approximated by a feasibility test for linear matrix inequalities. This requires that we choose a finite dimensional subspace for the set of multipliers. The choice of suitable

subspace is discussed and an example is given where a duality argument gives a bound for the possible performance of the multiplier for slope restricted nonlinearities.

Ref [9]: Stability improvement of  $V/f$  -controlled induction motor drive systems by a dynamic current compensator is proposed in this paper. The proposed method uses a dynamic current compensator to improve the stability of the  $V/f$ -controlled induction motor drive systems. This method is easy to implement and helps eliminate the oscillations causing the instability of  $V/f$ -controlled induction motor drive systems.

Ref [10]: The stability of pulse width modulated current-source rectifier/inverter fed induction motor drives is considered in this reference. To investigate the system stability successfully, an analysis without a complete simulation is performed by introducing synchronously rotating reference frames at the input and output terminals.

Ref [13]: This paper presents a new approach of  $V/f$  control, which is based on current feedback to improve the stability of the conventional  $V/f$  control. The proposed approach is based on the stator current derivatives. This new method has successfully damped the torque and speed oscillations in  $V/f$  control for low power IM drive system.

Ref [14]: This paper determines the controller parameter tuning range for a speed sensorless vector-controlled induction motor drive from the stability point of view. The tuning rules for conventional PI controllers are mostly based on experience. Trial and error procedures are used to tune the values of the controller parameters.

Ref [15]: This paper presents transformerless multilevel converters as an application for high-power and/or high-voltage electric motor drives. Multilevel converters 1) can generate nearsinusoidal voltages with only fundamental frequency switching; 2) have almost no electromagnetic interference or common-mode voltage; and 3) are suitable for large volt-ampere-rated motor drives and high voltages.

Ref [16]: This paper presents a new voltage source converter control approach. It is based on multivariable z-domain control techniques. Using time-averaging theory in the synchronous reference frame, a linear time-varying model of the converter is developed. The new model may be directly employed as an efficient simulation tool and used as a basis for developing discrete time inverter controls.

Ref [17]: A discrete time, linear time varying model of the three-phase voltage source converter (VSC) is developed. The model is employed to determine the steady-state operating characteristics of a VSC taking all ac-dc side harmonic interactions into account. The procedure is based on an exact closed form solution of the system equations and does not rely on iterative techniques. The steady-state operating curves from the proposed model are compared with those derived from a conventional continuous time  $dq$ -frame model.

Ref [18]: The aim of this paper is to develop a method to validate an equivalent internal circuit of the three-phase squirrel-cage induction machine for advanced signal processing including fault diagnosis. The proposed method is based on the computation of the stator and rotor current spectra. An experimental setup for an 11-kW induction machine was developed in order to get numerical data for voltages and currents from the stator side.

Ref [19]: This paper proposes a new software implementation for two level inverter using space vector modulation technique. This is performed by combining Matlab and Psim software packages. The switching pattern generation and sector identification for space vector modulation technique is generated using list of Matlab codes. Simcoupler modules provide interface between Matlab/simulink and Psim software packages for co-simulation.

Ref [20]: This paper comprehensively analyzes the relationship between space-vector modulation and three-phase carrier-based pulsewidth modulation (PWM). The relationships involved, such as the relationship between modulation signals (including zero-sequence component and fundamental components) and space vectors, the relationship between the modulation signals and the space-vector sectors, the relationship between the switching

pattern of space-vector modulation and the type of carrier, and the relationship between the distribution of zero vectors and different zero-sequence signal are systematically established.

Ref [21]: An adaptation of SVM modulation is presented in this paper. This system is called Bus Clamped Space Vector Modulation. This method has some practical advantages when compared to normal SVM. These include a reduced average switching frequency, easy digital implementation and asynchronous control and switching frequencies.

Ref [22]: The basic concept of direct torque control of induction machines is investigated in order to emphasize the effects produced by a given voltage vector on stator flux and torque variations. The low number of voltage vectors which can be applied to the machine using the basic DTC scheme may cause undesired torque and current ripple. An improvement of the drive performance can be obtained using a new DTC algorithm based on the application of the space vector modulation (SVM) for prefixed time intervals. In this way a sort of discrete space vector modulation (DSVM) is introduced.

Ref [23]: The PWM voltage generated by the space vector modulation method is compared with that generated by the subharmonic method for a permanent-magnet AC servo motor driven by a current-controlled PWM inverter. For the space vector modulation method, the on-times of its two zero voltage vectors are equalised.

Ref [24]: This paper describe the mechanism of generating undesirable narrow pulses in conventional three-level space vector PWM and suggest two new algorithms of space vector PWM using Non-Nearest three and four vector in a control period to avoid narrow pulse problem.

Ref [25]: The single-phase cascaded voltage-source inverter that uses series connection of insulated gate bipolar transistor (IGBT) H-bridge modules with isolated dc buses is presented. Next, a novel three-phase cascaded voltage-source inverter that uses three IGBT tri phase inverter modules along with an output transformer to obtain a 3-p.u. multilevel output voltage is introduced. The system yields in high-quality multistep voltage with up to four levels and

low, balanced operation of the inverter modules, each supplying a third of the motor rated kVA.

Ref [26]: This paper presents space vector PWM method for the three level GTO inverters. With the proposed PWM method harmonics components of the output voltage can be minimised by avoiding the minimum pulse width limitation problem of the GTO thyristors and keeping the voltage balancing of the dc-link capacitors.

Ref [27]: The paper proposes a new diode clamping inverter, which works without series association of the clamping diodes. An auxiliary resistive clamping network solving the indirect clamping problem of the inner devices is also discussed for both the new and conventional diode clamping inverter.

Ref [28]: This paper presents a simple pwm technique to control neutral point voltage of the multi-level inverter.

Ref [29]: A simple control method for balancing the dc-link voltage of three-level neutral point clamped inverters is presented in this reference, while providing enhanced ride-through and common mode voltage elimination.

Ref [30]: An MC68000, 16 bit microprocessor system is used to generate pulse width modulation (PWM) waveforms for a three level inverter. The MC68000 calculates the width of the pulses for only the first quarter cycle and sorts these into a table. The remaining pulses are calculated using the quarter or half wave symmetry.

## 1.3 Organization of Thesis

**Chapter 1:** This chapter gives brief introduction about the stability problems in induction motor drives fed by inverters. The main causes for the stability problem are highlighted.

**Chapter 2:** Basic introduction about the different application of the drive system is given. The complexity of the structure of the drive system is introduced. Different speed control methods of the drive is presented. Modeling of the induction motor is done using Park's transformation. Stability analysis is done by deriving the characteristic equation for the induction motor and then applying Hurwitz stability criterion for the stability the unstable and stable ranges are determined. Modeling of the three level voltage source inverter is also done using the switching function for the different switching.

**Chapter 3:** Development of multilevel inverter is presented. The implementation of the space vector modulation technique is done using microprocessor. An algorithm is given for implementing this technique. Advantages of using microprocessor is also given over the other conventional technique. Hardware requirements for the development of the three level inverter is given.

**Chapter 4:** This chapter gives the fundamental principles of the space vector modulation technique in detail. Different steps for the implementation of this technique is given. Simulation steps are given. Finally simulation results are presented for the different load conditions.

**Chapter 5:** This chapter concludes the whole work done in this thesis and discusses some important issues regarding the future scope of this and the related work. Some hardware and software trade-off are considered.

**Mathematical Modeling of Induction Motor Drive**

---

**2.1 Introduction**

Drive systems are widely used in applications such as pumps, fans, papers and textile mills, elevators, electric vehicle and subway transportation, home appliances, wind generation system, servos and robotics, computer peripherals, steel and cement mills, ship propulsion etc. A machine is a complex structure electrically, mechanically, and thermally. An engineer designing a high-performance drive system must have intimate knowledge about machine performance, the dynamic model, and parameter variations. Industrial drive applications are generally classified into constant-speed and variable-speed drives. In the last two or three decades, there is extensive research and development efforts for variable-frequency, variable-speed ac machine drive technology.

**2.2 Variable-Voltage, Constant Frequency Operation**

A very simple and economical method of controlling speed in a cage-type induction motor is to vary the stator voltage at constant supply frequency. Figure 2.1 shows the torque speed curve with variable stator voltage which have been plotted from the equation (2.1)

$$T_e = 3 \left( \frac{p}{2} \right) \frac{R_r}{S \omega_e} \cdot \frac{V_s^2}{(R_s + R_r / S)^2 + \omega_e^2 (L_{ls} + L_{lr})^2} \quad (2.1)$$

A load-torque curve for a pump or fan-type drive ( $T_L = k\omega_r^2$ ) is also shown in the Figure 2.1 where the points of intersection define stable points for variable-speed operation.



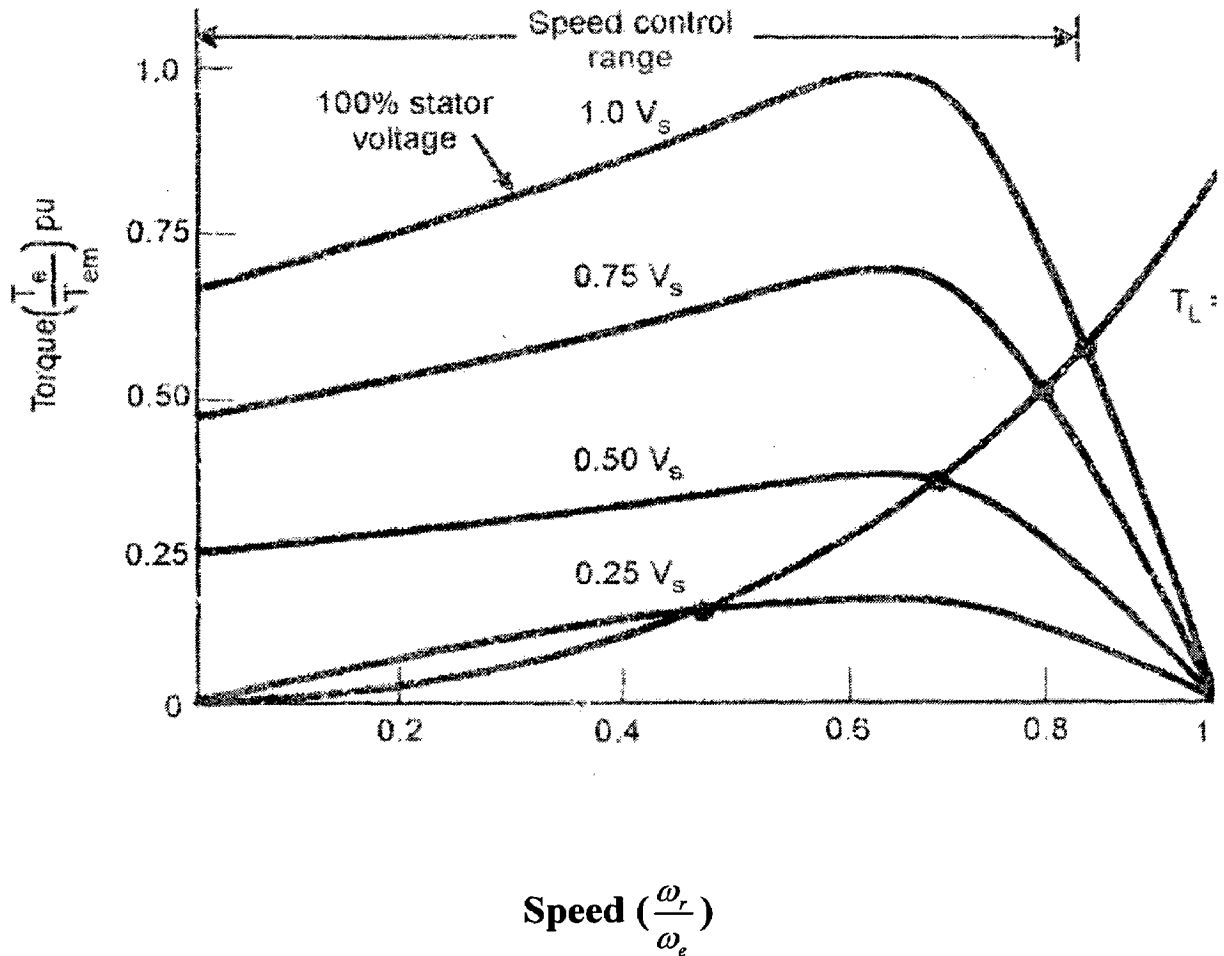


**Figure 2.1 torque-frequency curve at variable voltage**

### 2.3 Variable-Frequency Operation

If the stator frequency of a machine is increased beyond the rated value, but the voltage is kept constant, the torque speed curves can be plotted from equation (2.1), as shown below.

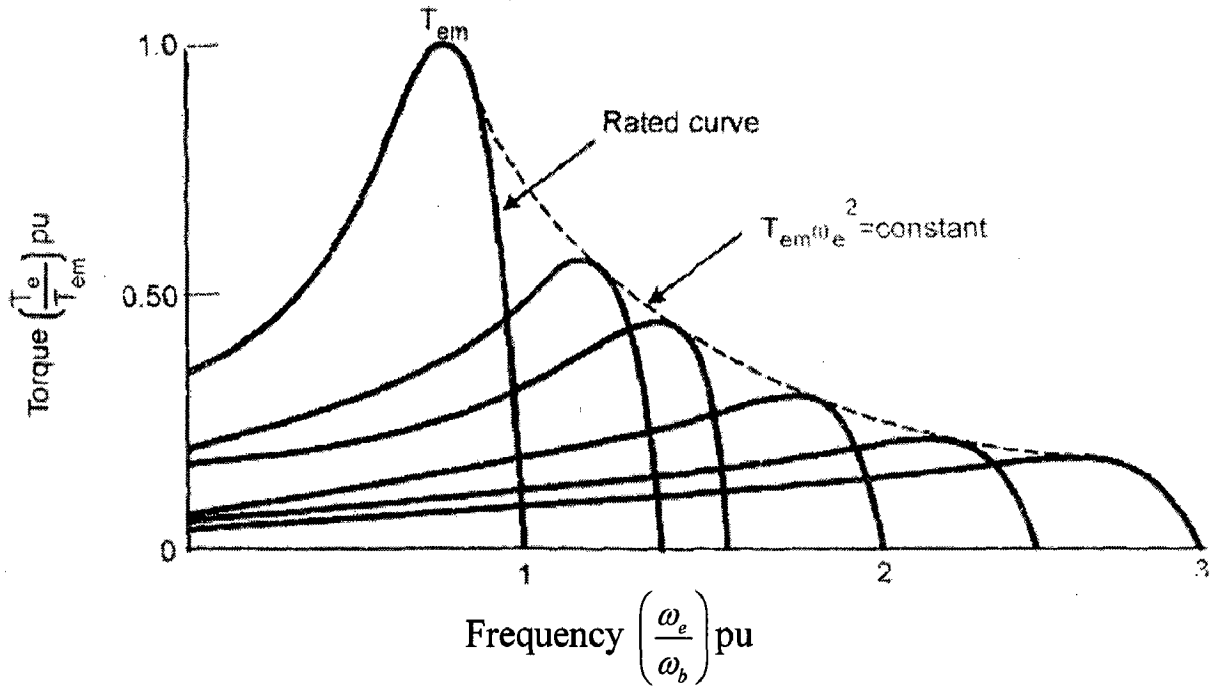


**Figure 2.2 Torque-speed curves with variable stator voltage**

The air gap flux and rotor current decrease as the frequency increases, and correspondingly, the developed torque also decreases. The breakdown torque is derived by differentiating equation (2.1) as

$$T_{em} = 3 \left( \frac{p}{2} \right) \left( \frac{V_s}{\omega_e} \right)^2 \frac{\omega_{slm} R_r}{Rr2 + \omega_{slm}^2 L_{lr}^2} \quad (2.2)$$

Where  $\omega_{slm} = \frac{R_r}{L_{lr}}$  is the slip frequency at maximum torque.

## 2.4 Constant volts/Hz Operation

If an attempt is made to reduce the supply frequency at the rated supply voltage, the air gap flux  $\psi_m$  will tend to saturate, causing excessive stator current and distortion of flux wave. Therefore the region below the base or rated frequency ( $\omega_b$ ) should be accompanied by the proportional reduction of stator voltage so as to maintain the air gap flux constant. Figure below shows the torque-speed curve at volts/Hz=constant.

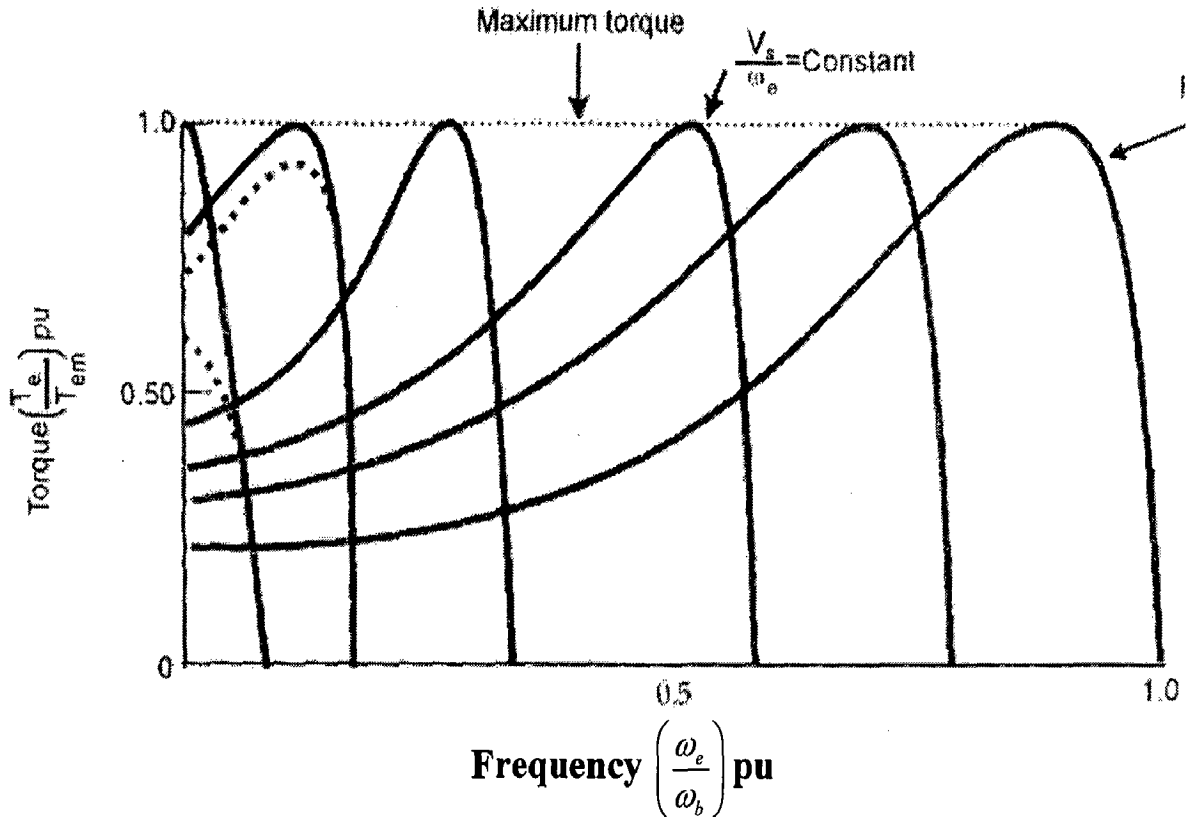


**Figure 2.3 Torque-speed curves at constant volts/Hz**

If the air gap flux of the machine is kept constant in the constant torque region, as shown in the Figure it can be shown that the torque sensitivity per ampere of stator current is high, permitting fast transient response of the drives with stator current control. The absence of a high in-rush starting current in a direct-start drive reduces stress and therefore improves the effective life of the machine [11]. By far, the majority of variable-speed ac drives operate with a variable-frequency, variable-voltage power supply.

## 2.5 Drive Operating Regions

The different operating regions of torque-speed curves for a variable-speed drive system with a variable-frequency, variable voltage supply is shown below.

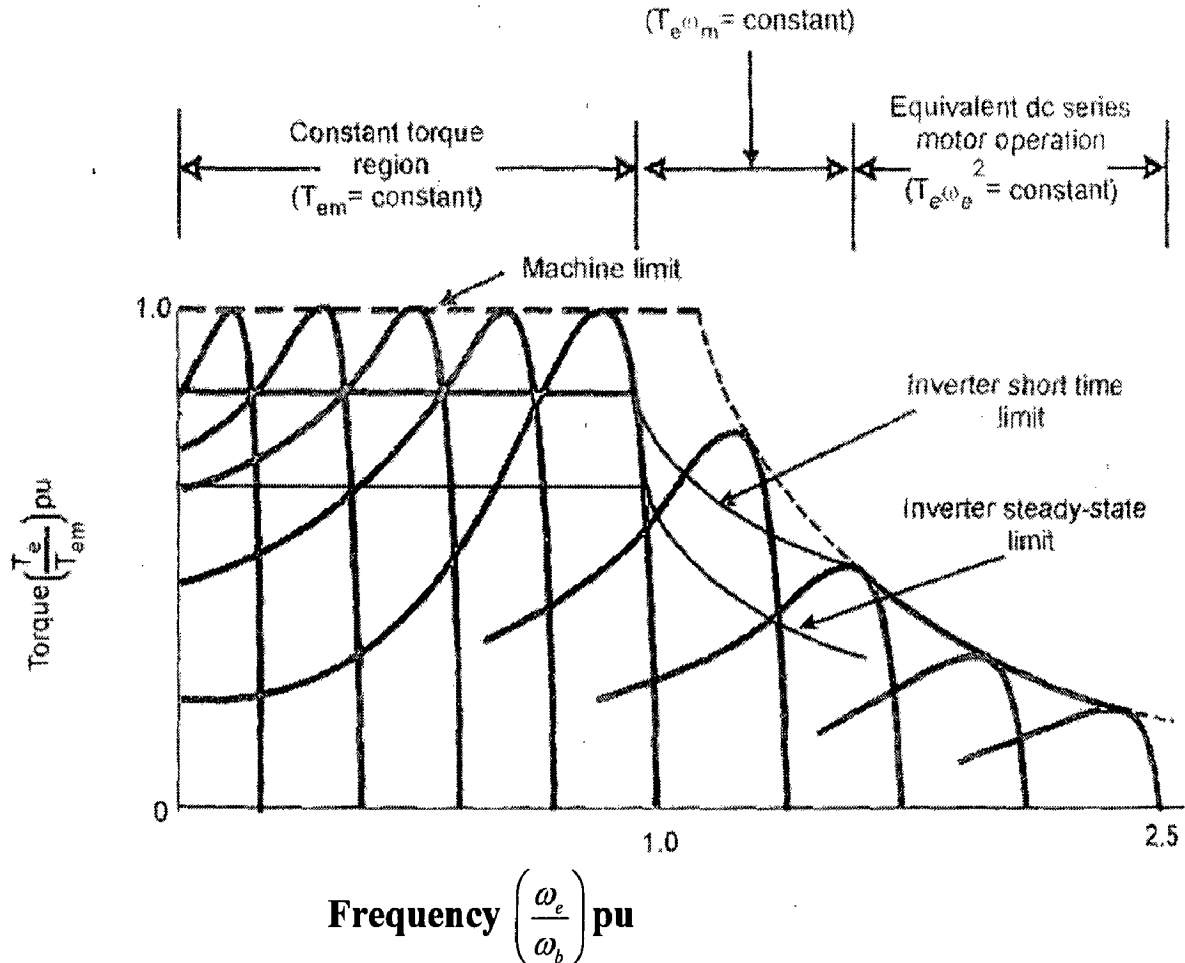


**Figure 2.4 Torque-speed curves at variable voltage and variable frequency up to field weakening region**

The inverter maximum, but short time or transient torque capability, is limited by the peak inverter current and is somewhat lower than the machine torque capability. The drive operating point can be anywhere within the inverter torque envelope. Since the inverter is more expensive than the machine, this margin is not too uneconomical. The steady state envelope, further limited by the power semiconductor junction temperature.

Typically, the inverter peak or short-time limit torque is 50 percent higher than steady state torque for 60-second duration (NEMA) standard. With improved cooling system design, the steady-state torque envelope can be increased [11].

## 2.6 Drive Model Development:

The per phase equivalent circuit of the machine is valid in steady-state condition only. In an adjustable-speed drive, the machine normally constitutes an element within a feedback loop, and therefore its transient behavior has to be taken into consideration. The dynamic performance of an ac machine is somewhat complex because the three-phase rotor windings move with respect to the three-phase stator winding. The machine model can be described by differential equations with time-varying mutual inductances but such a model tends to be very complex. R.H. Park in 1920s, proposed a new theory of electric machine analysis to solve this problem. He transformed or referred the stator variables to a synchronously rotating reference frame fixed in the rotor. With such a transformation (called Park's transformation), he showed that all the time varying inductances that occur due to an electric circuit in relative motion and electric circuits with varying magnetic reluctances can be eliminated. Later in the 1930s, H.C. Stanley showed that time-varying inductances in the voltage equation of an inductance machine due to electric circuits in relative motion can be eliminated by transforming the rotor variables to variables associated with fictitious stationary windings. Later, G. Kron proposed a transformation of both stator and rotor variable to synchronously rotating reference frame that moves with the rotating magnetic field. D.S. Brereton proposed a transformation of stator variables to a rotating reference frame that is fixed on the rotor. It was shown later by Krause and Thomas that time-varying inductances can be eliminated by referring the stator and rotor variables to a common reference frame which may rotate at any speed (arbitrary reference frame).

### 2.6.1 Axes Transformation

The transformation of three-phase stationary reference frame (as-bs-cs) variables into two phase stationary reference frame ( $d^s - q^s$ ) variables and then transformation of these to synchronously rotating reference frame ( $d^e - q^e$ ), and vice versa is given below.

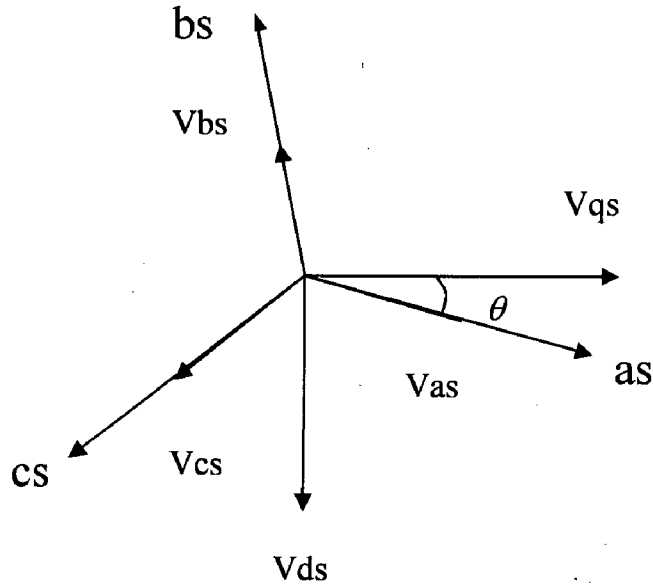


**Figure 2.5 Stationary frame a-b-c to  $ds$ - $qs$  axis transformation.**

The voltages  $V_{ds}^s$  and  $V_{qs}^s$  can be resolved into as-bs-cs components and can be represented in the matrix form as

$$\begin{pmatrix} V_{as} \\ V_{bs} \\ V_{cs} \end{pmatrix} = \begin{pmatrix} \cos \theta & \sin \theta & 1 \\ \cos(\theta - 120) & \sin(\theta - 120) & 1 \\ \cos(\theta + 120) & \sin(\theta + 120) & 1 \end{pmatrix} \begin{pmatrix} V_{qs} \\ V_{ds} \\ V_{0s} \end{pmatrix} \quad (2.3)$$

The corresponding inverse relation is

$$\begin{pmatrix} V_{qs} \\ V_{ds} \\ V_{0s} \end{pmatrix} = \frac{2}{3} \begin{pmatrix} \cos \theta & \cos(\theta - 120) & \cos(\theta + 120) \\ \sin \theta & \sin(\theta - 120) & \sin(\theta + 120) \\ 0.5 & 0.5 & 0.5 \end{pmatrix} \begin{pmatrix} V_{as} \\ V_{bs} \\ V_{cs} \end{pmatrix} \quad (2.4)$$

The current and flux linkages can be transformed by similar equations.

1 Stator circuit equations:

$$V_{qs}^s = R_s i_{qs}^s + p\psi_{qs}^s \quad (2.5)$$

$$V_{ds}^s = R_s i_{ds}^s + p\psi_{ds}^s \quad (2.6)$$

$\psi_{qs}^s$  is stator q axis flux linkage.

$\psi_{ds}^s$  is stator d axis flux linkage.

When these equations are converted to  $d^e - q^e$  frame, the following equations can be written as:

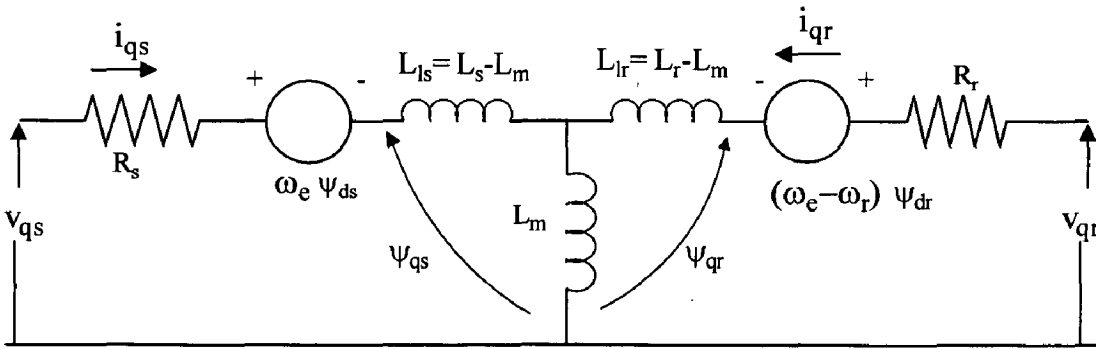
$$V_{qs}^s = R_s i_{qs}^s + p\psi_{qs}^s + \omega_e \psi_{ds}^s \quad (2.7)$$

$$V_{ds}^s = R_s i_{ds}^s + p\psi_{ds}^s - \omega_e \psi_{qs}^s \quad (2.8)$$

The rotor actually moves at speed  $\omega_r$ , the d-q axis fixed on the rotor moves at a speed  $\omega_e - \omega_r$  relative to the synchronously rotating reference frame. The rotor equations are as given below.

$$V_{qr} = R_r i_{qr} + p\psi_{qr} + (\omega_e - \omega_r) \psi_{dr} \quad (2.9)$$

$$V_{dr} = R_r i_{dr} + p\psi_{dr} - (\omega_e - \omega_r) \psi_{qr} \quad (2.10)$$



(a)

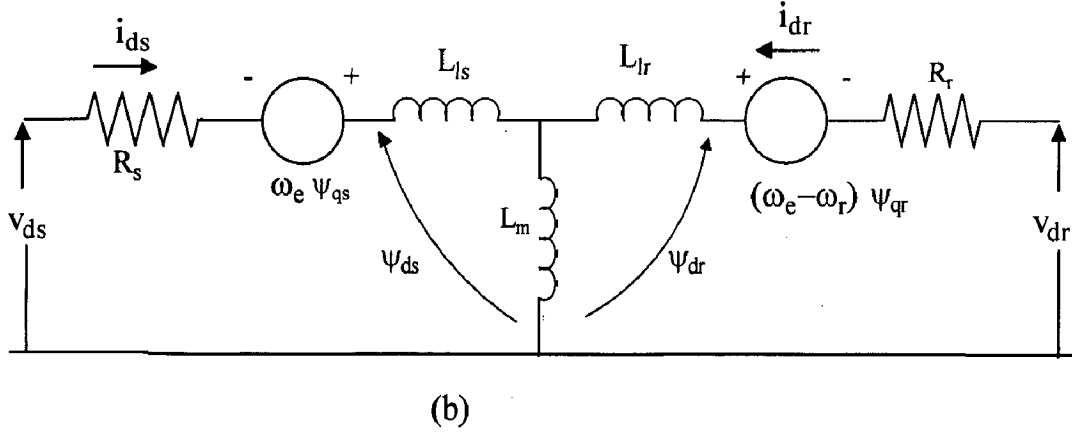


**Figure 2.6 Dynamic  $d^e - q^e$  equivalent circuit of machine (a)  $q^e$  axis circuit (b)  $d^e$  axis.**

The flux linkage expressions in terms of the currents can be written as follows:

$$\psi_{qs} = L_{ls} i_{qs} + L_m (i_{qs} + i_{qr}) \quad (2.11)$$

$$\psi_{qr} = L_{lr} i_{qr} + L_m (i_{qs} + i_{qr}) \quad (2.12)$$

$$\psi_{qm} = L_m (i_{qs} + i_{qr}) \quad (2.13)$$

$$\psi_{ds} = L_{ls} i_{ds} + L_m (i_{ds} + i_{dr}) \quad (2.14)$$

$$\psi_{dr} = L_{lr} i_{dr} + L_m (i_{ds} + i_{dr}) \quad (2.15)$$

$$\psi_{dm} = L_m (i_{ds} + i_{dr}) \quad (2.16)$$

Combining equations (2.7), (2.8), (2.9), (2.10), the electrical transient model in terms of voltages and currents can be given in matrix form as

$$\begin{pmatrix} V_{qs} \\ V_{ds} \\ V_{qr} \\ V_{dr} \end{pmatrix} = \begin{pmatrix} R_s + sL_s & \omega_e L_s & sL_m & \omega_e L_m \\ -\omega_e L_s & R_s + sL_s & -\omega_e L_m & sL_m \\ sL_m & (\omega_e - \omega_r) L_m & R_r + sL_r & (\omega_e - \omega_r) L_r \\ -(\omega_e - \omega_r) L_m & sL_m & -(\omega_e - \omega_r) L_r & R_r + sL_r \end{pmatrix} \begin{pmatrix} i_{qs} \\ i_{ds} \\ i_{qr} \\ i_{dr} \end{pmatrix} \quad (2.17)$$

for cage type induction motor,  $V_{qr} = V_{dr} = 0$ .



If the speed  $\omega_r$  is considered constant (infinite inertia load), the electrical dynamics of the machine are given by a fourth-order linear system. Then knowing the inputs  $V_{qs}$ ,  $V_{ds}$ , and  $\omega_e$ , the currents  $i_{qs}$ ,  $i_{ds}$ ,  $i_{qr}$ , and  $i_{dr}$  can be solved from equation 2.17.

The torque expression can be given as

$$T_e = \frac{3}{2} \left( \frac{p}{2} \right) (\psi_{dm} i_{qr} - \psi_{qm} i_{dr}) \quad (2.18)$$

The general control block diagram for variable-frequency speed control of an induction motor drive is shown in Figure 2.7.

It consists of a converter-machine system with hierarchy of control loops added to it. The converter-machine unit is shown with voltage and frequency as control inputs. The outputs are shown as speed, developed torque, stator currents and rotor flux. The machine's dynamic model given by equations 2.17 and 2.18 is nonlinear and multivariable. Besides there are coupling effects between the input and output variables. For example both the torque and flux of a machine are functions of voltage and frequency. Machine parameters may vary with saturation, temperature and skin effect, adding further nonlinearity to the machine model. The system becomes discrete time because of the converter and digital control sampling effects. Adding a high gain inner loop control provides the advantages of linearization, improved bandwidth and the ability to control the signals within the safe limits. Since an ac drive system is multivariable, nonlinear with internal coupling effect, and discrete-time in nature. Its stability analysis is very complex.

The converter machine system in Figure 2.6 can be linearized on a small signal perturbation basis at a steady state operating point and a transfer function model can be derived between a pair of input and output signals. The advantage of such a transfer function model is that the stability analysis of the drive system at the quiescent point is now possible using classical control theory such as Bode, Nyquist, or Root Locus techniques. Since the system is non-linear, the poles, zeros and gains of the transfer functions will vary as the steady state operating point shifts. The closed loop control

system can then be designed with controller parameters such that at the worst operating point, the system is adequately stable and the performances are acceptable.

Assembling equations 2.17 and 2.18 in matrix form and applying a small signal perturbation about a steady state operating point

$$\begin{pmatrix} V_{qs0} + \Delta V_{qs} \\ V_{ds0} + \Delta V_{ds} \\ V_{qr0} + \Delta V_{qr} \\ V_{dr0} + \Delta V_{dr} \\ T_{L0} + \Delta T_L \end{pmatrix} = \begin{pmatrix} R_s + sL_s & (\omega_{e0} + \Delta\omega_e)L_s & sL_m & (\omega_{e0} + \Delta\omega_e)L_m & 0 \\ -(\omega_{e0} + \Delta\omega_e)L_s & R_s + sL_s & -(\omega_{e0} + \Delta\omega_e)L_m & sL_m & 0 \\ sL_m & (\omega_{e0} + \Delta\omega_e)L_m & R_r + sL_r & (\omega_{e0} + \Delta\omega_e)L_r & -L_m(i_{ds0} + \Delta i_{ds}) - L_r(i_{dr0} + \Delta i_{dr}) \\ -(\omega_{e0} + \Delta\omega_e)L_m & sL_m & -(\omega_{e0} + \Delta\omega_e)L_r & R_r + sL_r & L_m(i_{qs0} + \Delta i_{qs}) + L_r(i_{qr0} + \Delta i_{qr}) \\ \frac{3p}{2}L_m(i_{dr0} + \Delta i_{dr}) & -\frac{3p}{2}L_m(i_{dr0} + \Delta i_{dr}) & 0 & 0 & -\frac{2}{p}J_s \end{pmatrix} \begin{pmatrix} i_{qs0} + \Delta i_{qs} \\ i_{ds0} + \Delta i_{ds} \\ i_{qr0} + \Delta i_{qr} \\ i_{dr0} + \Delta i_{dr} \\ \omega_{r0} + \Delta\omega_r \end{pmatrix} \quad (2.19)$$

Where load torque disturbance  $T_L$ , is considered an input signal. Parameters  $V_{qs0}$ ,  $V_{ds0}$ ,  $V_{qr0}$ ,  $V_{dr0}$ ,  $T_{L0}$ ,  $\omega_{e0}$ ,  $i_{qs0}$ ,  $i_{qr0}$ ,  $i_{ds0}$ ,  $i_{dr0}$  and  $\omega_{r0}$  describe the steady state operating point and cant be determined by solving the equations will all time derivatives set equal to zero. Linearizing equation 2.19 by neglecting the  $\Delta^2$  terms and eliminating steady state terms, we get the small signal linear state space equation in the form,

$$\frac{dX}{dt} = AX + BU \quad (2.20)$$

Where,

$$X = [\Delta i_{qs} \quad \Delta i_{ds} \quad \Delta i_{qr} \quad \Delta i_{dr} \quad \Delta \omega_r]^T \quad (2.21).$$

$$U = [\Delta V_s \quad 0 \quad 0 \quad 0 \quad \Delta \omega_e \quad \Delta T_L]^T \quad (2.22)$$

A

$$= \frac{-1}{L_s L_r - L_m^2} \begin{pmatrix} R_s L_r & (L_s L_r - L_m^2) \omega_{e0} + L_m^2 \omega_{r0} & -R_m L_m & L_m L_r \omega_{r0} & L_m^2 i_{ds0} + L_m L_r i_{dr0} \\ -(L_s L_r - L_m^2) \omega_{e0} - L_m^2 \omega_{r0} & R_s L_r & L_m L_r \omega_{r0} & -R_r L_m & -L_m^2 i_{qs0} - L_m L_r i_{qr0} \\ -R_s L_m & -L_m L_s \omega_{r0} & R_r L_s & (L_s L_r - L_m^2) \omega_{e0} - L_m^2 \omega_{r0} & -L_m L_s i_{ds0} - L_s L_r i_{dr0} \\ L_m L_s \omega_{r0} & -R_s L_m & (L_s L_r - L_m^2) \omega_{e0} - L_s L_r \omega_{r0} & R_r L_s & L_m L_s i_{qs0} + L_s L_r i_{qr0} \\ -\frac{3p^2}{8j} L_m (L_s L_r - L_m^2) i_{dr0} & \frac{3p^2}{8j} L_m (L_s L_r - L_m^2) i_{qr0} & \frac{3p^2}{8j} L_m (L_s L_r - L_m^2) i_{ds0} & \frac{3p^2}{8j} L_m (L_s L_r - L_m^2) i_{qs0} & 0 \end{pmatrix} \quad (2.23)$$

$$B = \frac{1}{L_s L_r - L_m^2} \begin{pmatrix} L_r & 0 & -L_m & 0 & -(L_s L_r - L_m^2) i_{d0} & 0 \\ 0 & L_r & 0 & -L_m & (L_s L_r - L_m^2) i_{q0} & 0 \\ -L_m & 0 & L_s & 0 & -(L_s L_r - L_m^2) i_{d0} & 0 \\ 0 & -L_m & 0 & L_s & (L_s L_r - L_m^2) i_{q0} & 0 \\ 0 & 0 & 0 & 0 & 0 & \frac{-p}{2j} (L_s L_r - L_m^2) \end{pmatrix} \quad (2.24)$$

The small signal block diagram is shown in Figure 2.7. The small signal transfer function block diagram derived from figure 2.7 is shown in figure 2.8.

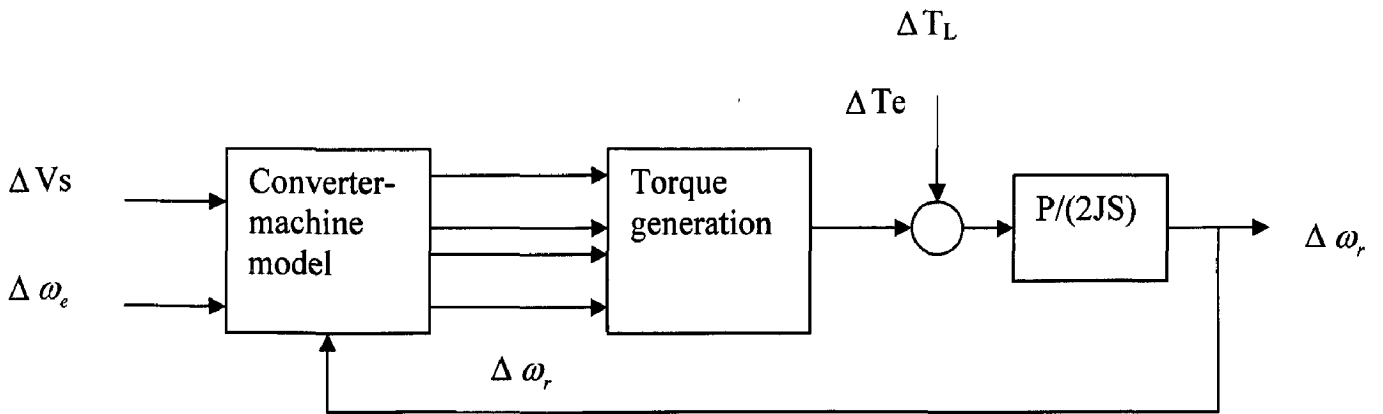
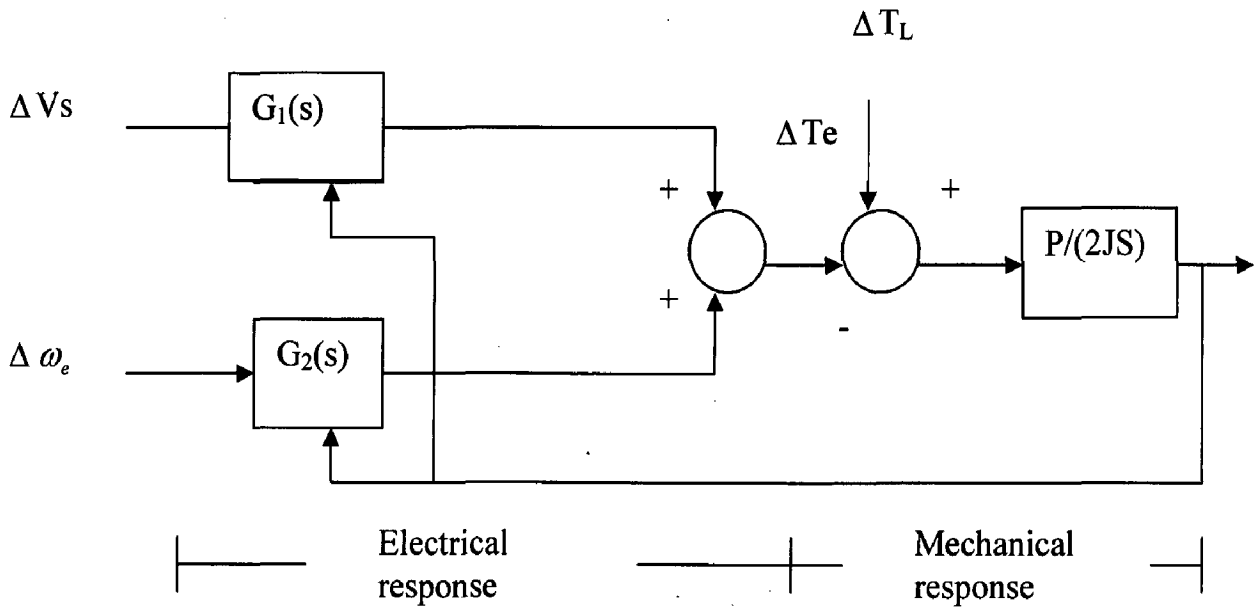


Figure 2.7 Small Signal Control Block Diagram



**Figure 2.8 Small Signal Transfer Function Block Diagram**

The transfer functions  $G_1(s)$  and  $G_2(s)$  are defined as

$$G_1(s) = \left. \frac{\Delta T_e}{\Delta V_s} \right|_{\Delta \omega_r = 0, \Delta \omega_e = 0} \quad (2.25)$$

$$G_2(s) = \left. \frac{\Delta T_e}{\Delta \omega_e} \right|_{\Delta \omega_r = 0, \Delta V_s = 0} \quad (2.26)$$

## 2.7 Drive Stability

When ac motors are operated on adjustable-frequency supplies, system instability may occur for certain critical frequency ranges and loading conditions. Machines that are perfectly stable on an ac utility network may become unstable with an inverter supply, machine that are stable when operated individually may become unstable when several of the motors are operated simultaneously as a group drive. Investigation of sources of this

instability shows that the two causes are (a) inherent low-frequency instability in the <sup>motor</sup>(b) instability due to interaction between the motor and inverter. An increase in stator and rotor leakage reactance also reduces the tendency of the machine to oscillate, and machine stability generally improves with an increase in pole number tendency. Lawrenson and Bowes [1] have shown that direct-axis/quadrature axis resistance ratio of the rotor circuits has a pronounced influence on machine stability. The transient response of the induction motor becomes more oscillatory as the supply frequency is reduced, but the normal machine does not usually become unstable on an infinite system. However, small motors with a low inertia constant may be unstable.

Instability due to interaction between motor and converter can occur with synchronous, synchronous reluctance or induction motors. It arises when the converter which supplies the adjustable speed motor has finite source impedance. The impedance may be introduced by transformer or by the filter which smooths the dc link supply in a static inverter drive. System instability usually occurs at frequencies below 25 HZ when an interchange of energy takes place between motor inertia and filter inductance and capacitance.

In an open-loop adjustable speed drive, the unstable region of operation is normally confined to a certain torque and frequency range. A torque frequency diagram can be prepared, as in fig 1.1 in which the unstable zone is enclosed by the contour. The critical contour can be predicted by application of the root locus technique or the Nyquist stability criterion to a linearized set of machine equations which are valid for small frequency excursions above and below a fixed base frequency it is found that the size of the unstable zone is affected by the system inertia, the load damping, and the electrical parameters of the motor and supply source. The harmonic content of the stator voltage waveform may slightly affect stability, particularly if the inertia is small. However, open-loop system stability can usually be assured over the desired range of torque and speed by proper coordination of motor and inverter. stability of the inverter-fed induction motor drive is generally enhanced (a) by increasing load torque and inertia, (b) by reducing stator voltage, and (c) by increasing filter capacitance and reducing filter inductance and resistance.

The PWM inverter has a step-down transformer action that reduces its effective output impedance at low frequencies and so improves drive stability. At low speeds, the fundamental output voltage is appreciably less than the dc link voltage, whereas output current is significantly greater than dc link current. If the dc link filter impedance is referred to the inverter output terminals, as in the case of a step-down transformer, the effective shunt capacitance is magnified and the series inductance is diminished. Both of these parameter changes are in the correct sense for an enhancement of drive stability, and consequently, the PWM inverter can give stable open loop operation at low speeds.

Appropriate modification of machine parameters can also help to eliminate instability in an open-loop adjustable-frequency drive, but the provision of special machine designs may be uneconomical and steady-state performance and efficiency may not be as good as in a normal motor. Various closed-loop feedback methods have therefore been developed to suppress rotor oscillations. An inverter-fed induction motor has been stabilized by controlling inverter frequency with the motor emf [2] or a derivative of dc link current [3]. Alternative feedback methods have also given satisfactory stabilization of adjustable-frequency drive [4]-[5].

Multilevel converter technologies are receiving increased attention recently especially for use in high power applications. This increased attention is probably due to the fact that the output waveforms are much improved over those of the two level converter technologies and that the voltage rating of the converter is increased due to the series connection of the devices. Multilevel converters are now receiving wide spread interest from the drives community for high power variable speed application. Indeed the three level inverter is being considered for both industrial and traction applications in Europe and various topologies for five and seven level systems are now being developed.

Multilevel inverters represents a high potential for realization of high power controllable conversion systems of different nature, rectifiers high power amplifiers etc. From the even more applied three level inverter to the multiple AC stages VSI different topologies are applied with an increasing quantity of possible levels.

Recent years have seen a sea change in factory automation. The manufacturing lines in an industrial plant typically involve one or more variable speed motor drives that serve to

various requirements of the plant like, power conveyor belts, robot arms, overhead cranes, steel process lines, paper mills and other processing lines. Prior to 1950s all such applications required the use of DC motor drive as the AC motor were not so flexible with respect to adjustable and smoothly varying speeds. But the inherent disadvantages of the DC drive promoted development on the side and eventually AC drives emerged as cost-effective and rugged compared to their DC counterparts. The reliability was also high. However the control flexibility with these drives is very limited and these proved to be suitable in applications where the speed need be regulated roughly like fan, pump, compressor etc. But high performance applications like machine tools, spindles; high-speed elevators etc need a much more sophisticated regulation of various variables such as speed, position, acceleration etc. Until recently this area was dominated by the DC drives. But with suitable control the induction motor drives are more than a match for DC drives in these high performance applications. The advances in microelectronics have simplified most of the control complexities of these drives and brought about an improved drive performance. The most common drive for the AC motor is the Voltage Source Inverter (VSI) Drive.

1.3 Stability analysis in induction motor driven by V/f controlled general-purpose inverter:

Fig 1.3 shows an equivalent circuit for an induction motor, and the motor is driven by the stator voltage given by

$$\vec{v}_1 = j\dot{\theta}(t)L_k i_{k0} \exp\{j\theta(t)\} \quad (1.1)$$

The corresponding magnetizing current  $\vec{i}_0$  is assumed to be represented by

$$\vec{i}_0 = i_0 \exp\{j(\theta + \psi_0)\} \quad (1.2)$$

Substituting this into appendix B and deleting stator current  $\vec{i}_1$  and rotor current  $\vec{i}_2$  using the relation

$$\vec{i}_0 = i_1 + \left(\frac{L_{22}}{L_{12}}\right)\vec{i}_2 \quad (1.3)$$

the following are derived:

$$L_1' T_0 (\ddot{i}_0 - \dot{\phi}_0^2 i_0) + (r_1 T_0 + L_{11}) \dot{i}_0 - L_1' T_0 (2\dot{\theta} - \omega_r) \dot{\phi}_0 i_0 + \{r_1 - L_1' T_0 \dot{\theta} (\dot{\theta} - \omega_r)\} i_0 = \dot{\theta} L_k i_{k0} \sin \phi_0 \quad (1.4)$$

$$L_1' T_0 (\ddot{\phi}_0 i_0 + 2\dot{\phi}_0 \dot{i}_0) + (r_1 T_0 + L_{11}) \dot{\phi}_0 i_0 + L_1' T_0 (2\dot{\theta} - \omega_r) i_0 + \{r_1 T_0 (\dot{\theta} - \omega_r) + \dot{\theta} L_{11} + L_1' T_0 (\ddot{\theta} - \dot{\omega}_r)\} i_0 = \dot{\theta} L_k i_{k0} \cos \phi_0 \quad (1.5)$$

$$T_e = k L_0 T_0 i_0^2 (\dot{\phi}_0 + \dot{\theta} - \omega_r) \quad (1.6)$$

$$(J/n) \dot{\omega}_r = T_e - T_{sh} \quad (1.7)$$

Taking into account the small deviation in the state variables  $(i_0, \phi_0, \omega_r)$  from an equilibrium point  $(i_{00}, \phi_{00}, \omega_{r0})$  as

$$i_0 = i_{00} + \Delta i_0 \rightarrow \dot{i}_0 = \Delta \dot{i}_0$$

$$\phi_0 = \phi_{00} + \Delta \phi_0 \rightarrow \dot{\phi}_0 = \Delta \dot{\phi}_0 \quad (1.8)$$

$$\omega_r = \omega_{r0} + \Delta \omega_r \rightarrow \dot{\omega}_r = \Delta \dot{\omega}_r$$

Substituting these into equations (1.4)-(1.7), and neglecting higher order terms, the linearized equations are derived as follows:

$$L_1' T_0 \Delta \ddot{i}_0 + (r_1 T_0 + L_{11}) \Delta \dot{i}_0 + \{r_1 - L_1' T_0 \dot{\theta} (\dot{\theta} - \omega_{r0})\} \Delta i_0 - L_1' T_0 (2\dot{\theta} - \omega_r) i_{00} \Delta \dot{\phi}_0 - \{r_1 T_0 (\dot{\theta} - \omega_{r0}) + \dot{\theta} L_{11}\} i_{00} \Delta \phi_0 + L_1' T_0 i_{00} \dot{\theta} \Delta \omega_r = 0 \quad (1.9)$$

$$L_1' T_0 i_{00} \Delta \ddot{\phi}_0 + (r_1 T_0 + L_{11}) i_{00} \Delta \dot{\phi}_0 + \{r_1 - L_1' T_0 \dot{\theta} (\dot{\theta} - \omega_{r0})\} i_{00} \Delta \phi_0 + L_1' T_0 (2\dot{\theta} - \omega_r) \Delta \dot{i}_0 + \{r_1 T_0 (\dot{\theta} - \omega_{r0}) + \dot{\theta} L_{11}\} \Delta i_0 - L_1' T_0 i_{00} \Delta \dot{\omega}_r - r_1 T_0 i_{00} \Delta \omega_r = 0 \quad (1.10)$$



$$i_{00}\Delta\dot{\omega}_r = k_1(\dot{\theta} - \omega_{r0})\Delta i_0 + k_2 i_{00}(\Delta\dot{\phi}_0 - \Delta\omega_r) \quad (1.11)$$

Where the following relations are used in the process of the derivation given above regarding the equilibrium point:

$$\begin{aligned} \{r_1 - L_1' T_0 \dot{\theta}(\dot{\theta} - \omega_{r0})\} i_{00} &= \dot{\theta} L_k i_{k0} \sin \phi_{00} \\ \{r_1 T_0 (\dot{\theta} - \omega_{r0}) + \dot{\theta} L_{11}\} i_{00} &= \dot{\theta} L_k i_{k0} \cos \phi_{00} \end{aligned} \quad (1.12)$$

$$\begin{aligned} K_1 &= 2k i_{00}^2 (\dot{\theta} - \omega_{r0}) \frac{L_0 T_0}{J} \\ K_2 &= k L_0 T_0 \frac{i_{00}^2}{J} \end{aligned} \quad (1.13)$$

$i_{00}\Delta\phi_0$  and  $i_{00}\Delta\omega_r$  are replaced as state variables by  $\Delta\phi_0'$  and  $\Delta\omega_r'$ , respectively, Equations (1.9)-(1.11) are summarized as

$$[A][\Delta i_0, \Delta\phi_0', \Delta\omega_r']^T = 0 \quad (1.14)$$

$$A = \begin{pmatrix} \alpha_{11}p_2 + \beta_{11}p + \gamma_{11} & -\alpha_{12}p - \beta_{12} & \beta_{13} \\ \alpha_{12}p + \beta_{12} & \alpha_{11}p_2 + \beta_{11}p + \gamma_{11} & -\alpha_{23}p - \beta_{23} \\ -K_1 = 0 & -K_2p & p + K_2 \end{pmatrix}$$

Where

$$\alpha_{11} = L_1' T_0$$

$$\beta_{11} = r_1 T_0 + L_{11}$$

$$\gamma_{11} = \{r_1 - L_1' T_0 \dot{\theta}(\dot{\theta} - \omega_{r0})\}$$

$$\beta_{12} = r_1 T_0 \dot{\theta}(\dot{\theta} - \omega_{r0})$$

$$\beta_{13} = L_1' T_0 \dot{\theta}$$

$$\alpha_{23} = L'_1 T_0$$

$\beta_{23} = r_1 T_0$ ; P is the differential operator.

Stability analysis is carried out by assuming  $r_1 \neq 0$  and  $L' = 0$ .

Then  $\alpha_{11} = 0$ ,  $\beta_{11} = r_1 T_0 + L_{11}$ ,  $\gamma_{11} = r_1$ ,  $\alpha_{12} = 0$ ,  $\beta_{13} = 0$ ,  $\alpha_{23} = 0$ ,  $\beta_{23} = r_1 T_0$  and  $K_1 = 0$ .

Substituting these equations into equation (1.14) and the characteristic equation is given as:

$$f(p) = \alpha_0 p^3 + \alpha_1 p^2 + \alpha_2 p + \alpha_3 = 0 \quad (1.15)$$

Where  $\alpha_0 = (T_0 + T_s^2)$ ,  $\alpha_1 = (T_0 + T_s)(2 + K_2 T_s)$ ,  $\alpha_2 = 1 + \dot{\theta}^2 T_s^2 + K_2(2T_s + T_0)$

$\alpha_3 = K_2(1 + \dot{\theta}^2 T_s^2)$  and  $T_s = \frac{L_{11}}{r_1}$ . The condition for instability is (applying Hurwitz criterion).

$$H2 = \alpha_1 \alpha_2 - \alpha_0 \alpha_1 < 0 \quad (1.16)$$

This implies that  $(1 + \dot{\theta}^2 T_s^2)(T_0 K_2 - 2) > (T_0 + 2T_s)K_2(K_2 T_s + 2)$  (1.17)

This equation never holds if  $r_1 = 0$ . This means existence of  $r_1$  is the cause of instability.

Equation (1.17) yields

$$T_0 K_2 > 2 \quad (1.18)$$

$$1 + \dot{\theta}^2 T_s^2 > \frac{(T_0 + 2T_s)K_2(K_2 T_s + 2)}{(T_0 K_2 - 2)} \quad (1.19)$$

From equation (1.18)

$$i_{00} > \{2j/(kL_0 T_0^2)\}^{1/2} = i_{00}, c_1 \quad (1.20)$$

Where  $i_{00,c_1}$  gives the lower limit of  $i_0$  for instability and has a constant value. If  $L_0$  and  $T_0$  is larger, the motor may become more oscillatory. If  $J$  becomes smaller the motor will be more unstable. From equation (1.18).

$$T_0 > 2T_m$$

When the rotor circuit time constant is larger than two times the mechanical time constant

the motor falls into an unstable state. If  $r_1$  is sufficiently small then from equation (1.19)

$$\dot{\theta}^2 = \frac{2K_2}{T_0} \tag{1.21}$$

$$\text{Or } \dot{\theta}^2 > \frac{2KL_0 i_{00}^2}{j} \tag{1.22}$$

$$\text{Or } i_{00} < \{j/(2kL_0)\}^{1/2} \dot{\theta} = i_{00,c_2} \tag{1.23}$$

Where  $i_{00,c_2}$  is the upper limit of  $i_{00}$  for instability. When  $i_{00,c_2} > i_{00,c_1}$  the probability of occurring oscillation in the practical induction machine is high.

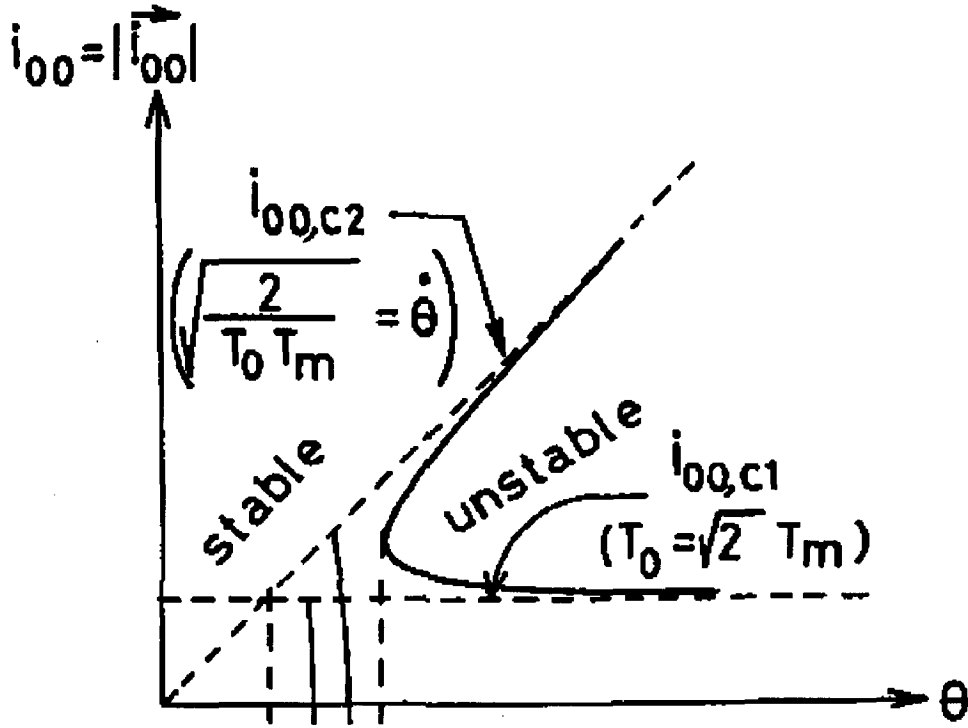


Fig 2.9 Unstable range (dotted lines are asymptotes)

Now assuming

$r_1 = 0$  and  $L' \neq 0$  the characteristic equation is given by

$$\alpha_0 p^5 + \alpha_1 p^4 + \alpha_2 p^3 + \alpha_3 p^2 + \alpha_4 p + \alpha_5 = 0 \quad (1.24)$$

Where

$$\alpha_0 = 1; \alpha_1 = 2\mu; \alpha_2 = \mu K_2 + \dot{\theta}^2 + \mu^2; \alpha_3 = \mu^2 K_2 + 2\dot{\theta}\mu; \alpha_4 = \dot{\theta}^2 \mu(\mu + K_2)$$

$$\alpha_5 = (\dot{\theta}\mu)^2 K_2, \text{ and } \mu = \frac{L_{11}}{L_1' T_0}. \text{ Applying Hurwitz stability criterion.}$$

$$H2 = \alpha_1 \alpha_2 - \alpha_0 \alpha_3 > 0$$

$$\text{Or } \mu^2 (2\mu + K_2) > 0$$

$$\text{and } H3 = \alpha_1 (\alpha_2 \alpha_3 - \alpha_1 \alpha_4) - \alpha_0 (\alpha_3^2 - \alpha_1 \alpha_5) = \mu^4 K_2 (2\mu + K_2) > 0$$

motor is absolutely stable in the sense of dynamic stability since both  $H2$  and  $H3$  are independent of  $\dot{\theta}$  and  $\omega_{r0}$ .

When a small deviation in rotor speed from a steady state-equilibrium point is taken for  $T_0 > T_m$ , the electrical transient in the rotor circuit is longer than the mechanical one. The response of  $T_e$  is delayed and the restoring force that reduces the deviation of rotor speed to zero does not work. For large value of  $i_{00}$  the slope of torque verses speed becomes steep this steepness stabilizes the motor. If the variation in  $T_e$  becomes large, the variation in rotor speed will be quite small.

## 2.8 Modeling Of Voltage Source Inverter

The three level converter consists of six number of pairs of switches and thus, it needs six switching functions.

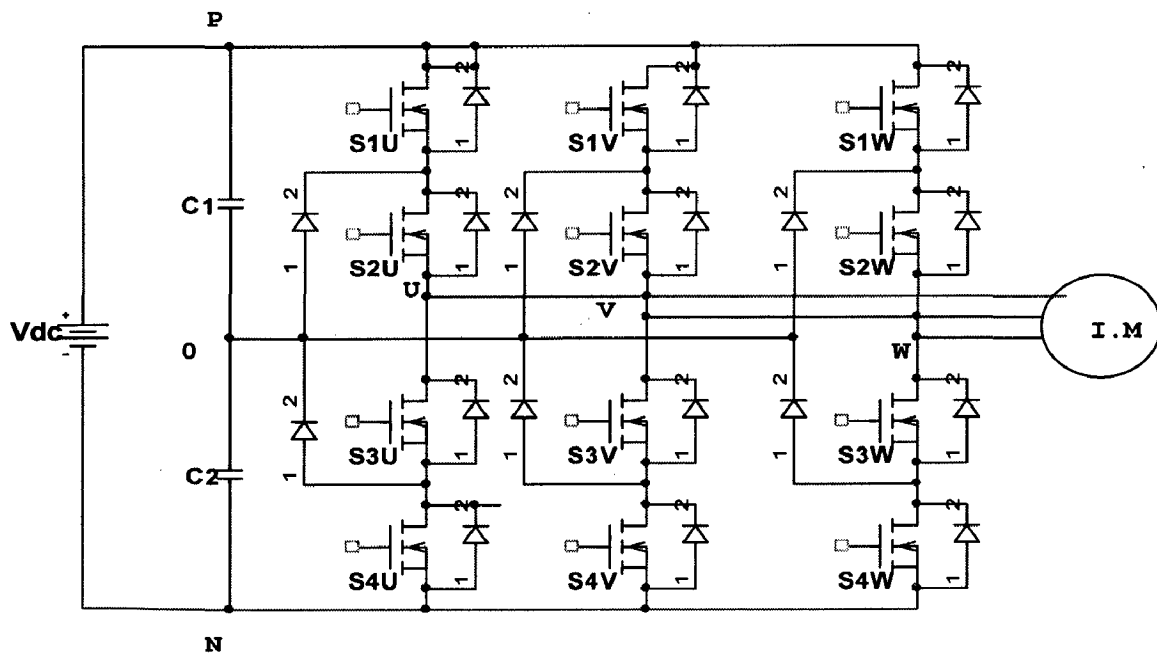


**Fig 2.30 Three Level Inverter**

Let the S1U, S1V, and S1W are represented by  $h_1, h_3$ , and  $h_5$  respectively and S4U, S4V, and S4W are represented by  $h_4, h_6$ , and  $h_2$  respectively. The switching function  $h_1, h_3$  and  $h_5$  are selected at appropriate time corresponding to  $120^\circ$  phase lag. The switching function of  $h_2, h_4$  and  $h_6$  are applied in similar manner. The only difference here is that the second set of switching function ( $h_2, h_4$  and  $h_6$ ) are  $180^\circ$  out of phase with respective first set of parameters (i.e.  $h_1, h_3$  and  $h_5$ ). The output can be varied by varying the duty ratio of the above switches. Considering the phase U the output is measured at point U.

when both S1 and S4 are OFF then the output voltage at U is zero. When S1 is made ON then the voltage at U is  $\frac{V_{dc}}{2}$ . By then S4 is OFF. When the switch S4 is made ON then of point U is  $-\frac{V_{dc}}{2}$ . Here again S1 is made OFF.

So voltage at U is represented by

$$V_U = (h_1 - h_4) \frac{V_{dc}}{2} \quad (2.27)$$

Similarly for the rest of the phases, the voltages can be represented as follows:

$$V_V = (h_3 - h_2) \frac{V_{dc}}{2} \quad (2.28)$$

$$V_W = (h_5 - h_6) \frac{V_{dc}}{2} \quad (2.29)$$

The line to phase equivalent voltage at the output of the converter can be given by

$$\begin{bmatrix} V_{Ug} \\ V_{Vg} \\ V_{Wg} \end{bmatrix} = \frac{V_{dc}}{2} \begin{bmatrix} \frac{2}{3} & -\frac{1}{3} & -\frac{1}{3} \\ -\frac{1}{3} & \frac{2}{3} & -\frac{1}{3} \\ -\frac{1}{3} & -\frac{1}{3} & \frac{2}{3} \end{bmatrix} \begin{bmatrix} h_1 - h_4 \\ h_3 - h_6 \\ h_5 - h_2 \end{bmatrix} \quad (2.30)$$

The above set of equations can be transformed to two phase system as

$$h_2 = \sum_{n=1,3,5,\dots}^{\infty} \frac{2}{\pi} \cos n\left(-\frac{7\pi}{3}\right)$$

$$h_2 = \sum_{n=1,3,5,\dots}^{\infty} \frac{2}{\pi} \left[ \frac{\sin(n\pi d)}{n} \right] \cos n\left(\omega t - \frac{7\pi}{3}\right) \quad (2.31)$$

$$V_d = \left[ -\frac{2V_{dc}}{\pi} \sin(\pi d) \right] \sin(\omega t)$$

$$\begin{bmatrix} V_q \\ V_d \end{bmatrix} = \frac{V_{dc}}{2} \begin{bmatrix} \frac{2}{3} & -\frac{1}{3} & -\frac{1}{3} \\ 0 & -\frac{1}{\sqrt{3}} & -\frac{2}{\sqrt{3}} \end{bmatrix} \begin{bmatrix} h_1 - h_4 \\ h_3 - h_6 \\ h_5 - h_2 \end{bmatrix} \quad (2.32)$$

Let the switching function S1 be taken as reference. Thus the switching function can be expressed as

$$h_1 = \sum_{n=1,3,5,\dots}^{\infty} \frac{2}{\pi} \left[ \frac{\sin(n\pi d)}{n} \right] \cos(n\omega t) \quad (2.33)$$

$$h_4 = \sum_{n=1,3,5,\dots}^{\infty} \frac{2}{\pi} \left[ \frac{\sin(n\pi d)}{n} \right] \cos n(\omega t - \pi) \quad (2.34)$$

$$h_3 = \sum_{n=1,3,5,\dots}^{\infty} \frac{2}{\pi} \left[ \frac{\sin(n\pi d)}{n} \right] \cos n\left(\omega t - \frac{2\pi}{3}\right) \quad (2.35)$$

$$h_6 = \sum_{n=1,3,5,\dots}^{\infty} \frac{2}{\pi} \left[ \frac{\sin(n\pi d)}{n} \right] \cos n\left(\omega t - \frac{5\pi}{3}\right) \quad (2.36)$$

$$h_5 = \sum_{n=1,3,5,\dots}^{\infty} \frac{2}{\pi} \left[ \frac{\sin(n\pi d)}{n} \right] \cos n\left(\omega t - \frac{4\pi}{3}\right) \quad (2.37)$$

$$h_2 = \sum_{n=1,3,5,\dots}^{\infty} \frac{2}{\pi} \left[ \frac{\sin(n\pi d)}{n} \right] \cos n\left(\omega t - \frac{7\pi}{3}\right) \quad (2.38)$$

Thus the equation (2.32) can be solved for the fundamental frequency. The results are as follows

$$V_q = \left[ \frac{2V_{dc}}{\pi} \sin(\pi d) \right] \cos(\omega t) \quad (2.39)$$

$$V_d = \left[ -\frac{2V_{dc}}{\pi} \sin(\pi d) \right] \sin(\omega t) \quad (2.40)$$

This is the vary simple relation between the rms value of the output voltage of the inverter and the control parameter d.

## **2.9 Conclusion**

This chapter gives drive performance for different operating conditions. Different speed control methods of the drive is presented. Modeling of the induction motor is done using park's transformation. Stability analysis is done by deriving the characteristic equation for the induction motor and then applying Hurwitz stability criterion for the stability the unstable and stable ranges are determined. Modeling of the three level voltage source inverter is also done using the switching function for the different switching.



### Development of Multilevel Inverter

---

#### 3.1 Introduction

The space-vector PWM (SVM) method is an advanced, computation-intensive PWM method and is possibly the best among all the PWM techniques for variable-frequency drive applications. Because of its superior performance, it has been finding widespread application in recent years.

The current generation of adjustable speed drives (ASD) and static power converters (SPC) are generally based on the real-time digital generation of pulse-width modulated (PWM) waveform using either microprocessors or application –specific integrated circuits (ASICs). Digital PWM generation techniques have eliminated the component drift and tolerance problems associated with earlier analogue implementations. In addition, accurate real-time PWM waveform generation, giving virtually instantaneous control of the amplitude and frequency can be provided, as required by the more advanced ASD and SPC applications.

Although microprocessor-based PWM generation techniques offer significant advantages, particularly for optimizing the PWM waveform, the maximum switching frequency of the can be severely limited by the computation time needed to generate the PWM switching times in the microprocessor. This is particularly when advanced PWM strategies are used, for example, the harmonic minimization or harmonic elimination PWM strategies, involving considerable “on-line”, “real-time” computing.

### 3.2 Hardware Requirements

The hardware requirements for the realization of neutral point clamped three level inverter along with the various design aspects like modular construction testing and assembling etc. are discussed. The protection of the MOSFET has been discussed. Delay circuit has been used to provide delay and to protect the devices in the same leg from short circuit thus avoiding shoot through problem. Hardware requirements have been discussed briefly. PC interfacing with the hardware and data acquisition cards has been described briefly.

#### 3.2.1 Power Circuit

Fig 3.1 shows the power circuit of the neutral point clamped three level voltage sources inverter.

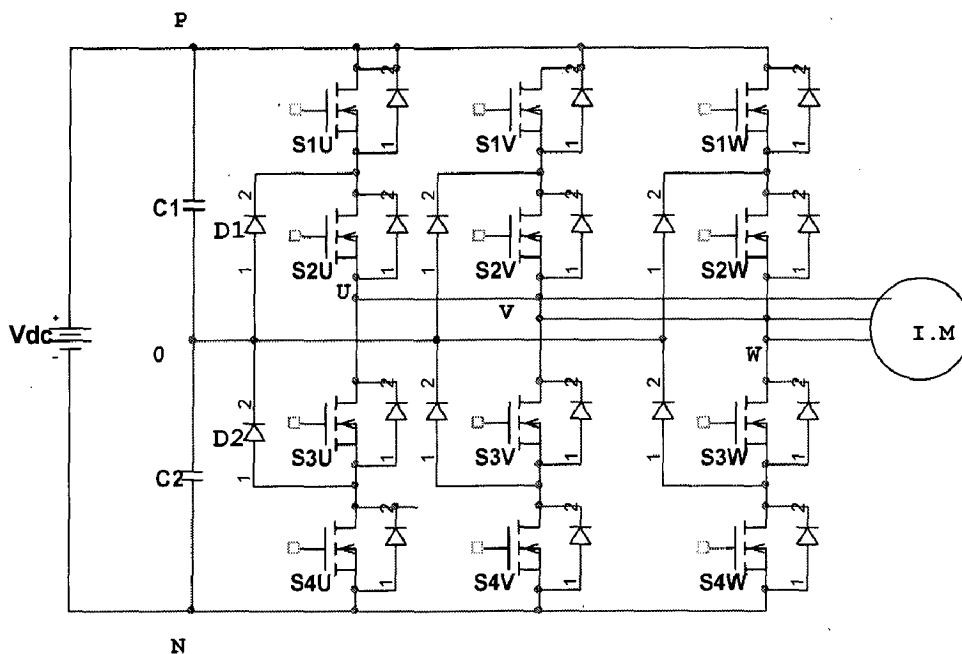


**Fig 3.1 Three level inverter circuit.**

The number of switching devices required, in general for x level inverter, per phase leg is  $2(x-1)$ .

Capacitors required are  $(x-1)$ .

Clamping diodes required per phase are  $(x-1)*(x-2)$ .

Here for three level inverter  $x=3$ . So two capacitors, six clamping diodes and total of twelve switches are required.

Switches used are MOSFET IRF 740 and MOSFET IRF P460. Short description of these devices given below.

**(A) IRFP460:**

N-CHANNEL 500V-0.22 $\Omega$ -20 TO-247 Power Mesh MOSFET

**FEATURES:**

- Typical  $R_{ds}=0.22\Omega$
- Extremely high  $dv/dt$  capability
- 100% avalanche tested
- Very low intrinsic capacitances
- Gate charge minimized

This power MOSFET is designed using the company's consolidated strip layout-based MESH OVERLAY process. This technology matches and improves the performance compared with standard parts from various sources.

**(B) IRF 740:**

10A, 400, 0.550 $\Omega$ , N-Channel power MOSFET.

This N-channel enhancement mode silicon gate power field effect transistor is an advanced power MOSFET designed, tested and guaranteed to withstand a specified level of energy in the breakdown avalanche mode of operation.

**FEATURES:**

- 10A, 400V.
- $R_{ds(0n)}=0.550\Omega$
- Single pulse avalanche energy rated.
- SOA is power dissipation limited
- Nanosecond switching speeds.
- Linear transfer characteristics.
- High input impedance.

Each MOSFET switch is used in the circuit consists of an inbuilt anti parallel free wheeling diode. Switching of these devices is done through gate pulses. The load inductance restricts large  $di/dt$  through MOSFETs hence only turn off snubber is required for protection. An RCD (resistor, capacitor and diode) turn off circuit is connected to protect the circuit against high  $dv/dt$  and is protected against power voltage by connecting MOV (metal oxide varistor).

### **3.2.2 Pulse Amplification And Isolation Circuit**

Pulse amplification and isolation circuit is shown in fig 3.2. The Opto-coupler (MCT-2E) provides the necessary isolation between the low voltage isolation circuit and high voltage power circuit. The pulse amplification is provided by the output amplifier transistor 2N222. When the input gating pulse is at +5V level, the transistor saturates, the LED conducts and the light emitted by it falls on the base of phototransistor, thus forming its base drive. The output transistor thus receive no base drive and, therefore remains in cut-off state and a +12 v pulse (amplified) appears across its collector terminal (w.r.t. ground). When the input gating pulse reaches the ground level (0V), the input switching transistor goes into the cut-off state and LED remains off, thus emitting no light and therefore a photo transistor of the opto-coupler receives no base drive and, therefore remains in cut-off state. A sufficient

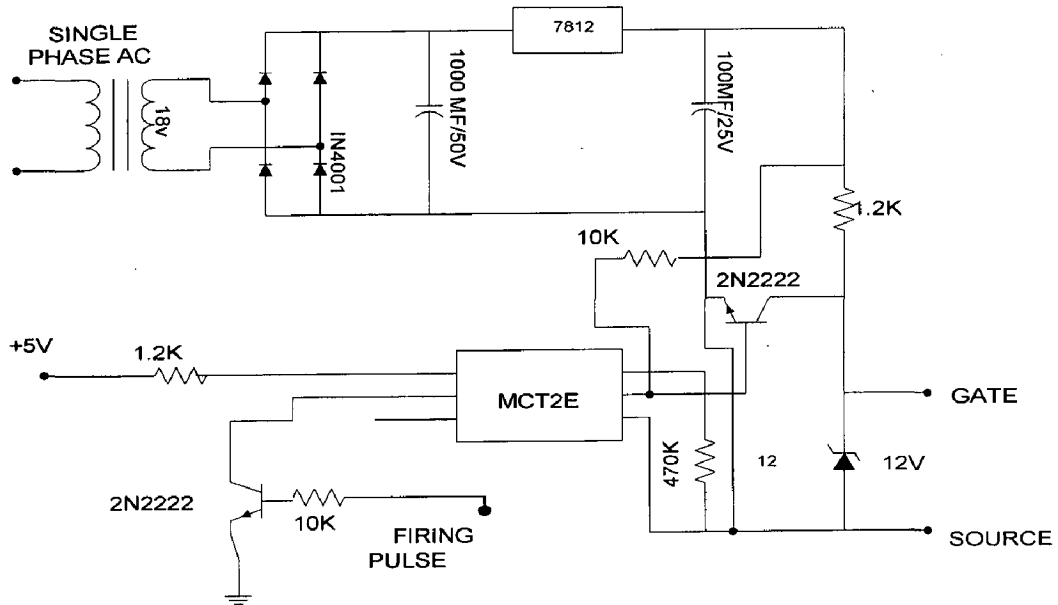


**Fig 3.2 Pulse amplification and isolation circuit**

Base drive now applies across the base of the output amplifier transistor it goes into the saturation state and hence the output falls to ground level. Therefore circuit provides proper amplification and isolation. Further, since slightest spike above 20v can damage the MOSFET, a 12 V zenor diode is connected across the output of isolation circuit. It clamps the triggering voltage at 12 V.

### 3.2.3 Power Supplies

D.C regulated power supplies ( $\pm 12$  V and +5 V) are required for providing the biasing to various ICs, etc. the system development has in-built power supplies for this purpose. The circuit diagram for various dc regulated power supplies are shown in Fig below.

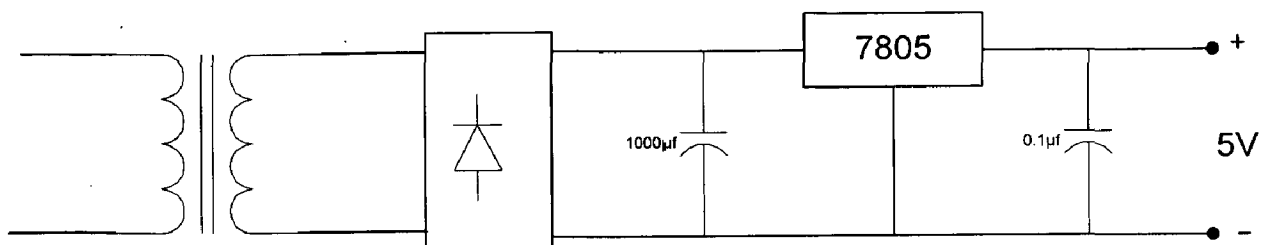


**Fig 3.3. 5 volt supply power circuit**

As, shown the single phase AC voltage is stepped down and the rectified using diode bridge rectifier. A capacitor of  $1000\mu\text{F}$ ,  $50\text{V}$  is connected at the output of the bridge rectifier for smoothing out the ripples in the rectified dc voltage of each supply. IC voltage regulated chips, 7812, 7912, 7805 are used for obtaining the dc-regulated voltages. A capacitor of  $0.1\mu\text{F}$ ,  $50\text{V}$  is connected at the output of the IC voltage regulator of each supply for obtaining the constant, ripple-free dc voltage.

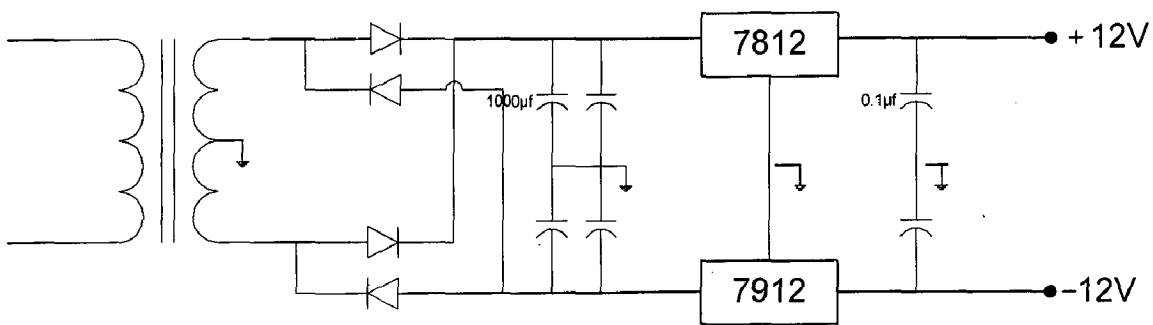


**Fig 3.4  $\pm 12\text{V}$  supply power circuit**

DC VOLTAGE	IC REGULATOR
+5V	7805
+12V	7812
-12V	7912

**Table 3.1**

### 3.2.4 Protection of Mosfet

An RC snubber circuit has been used for the protection of the main switching devices. Circuit diagram is shown in fig 3.5 given below.

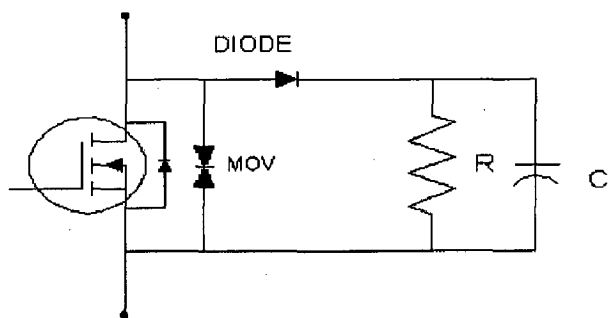


**Fig 3.5 MOSFET with snubber circuit.**

### 3.2.5 Delay Circuit

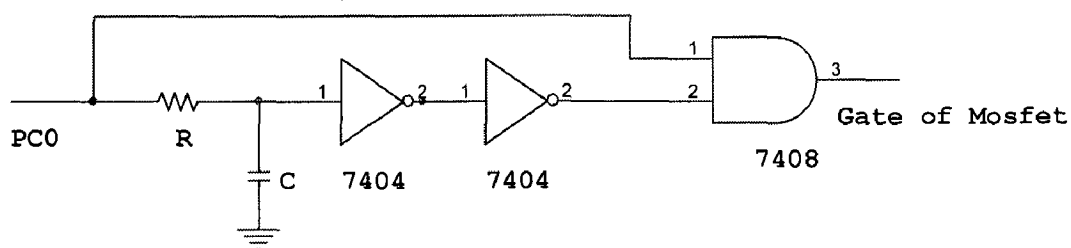
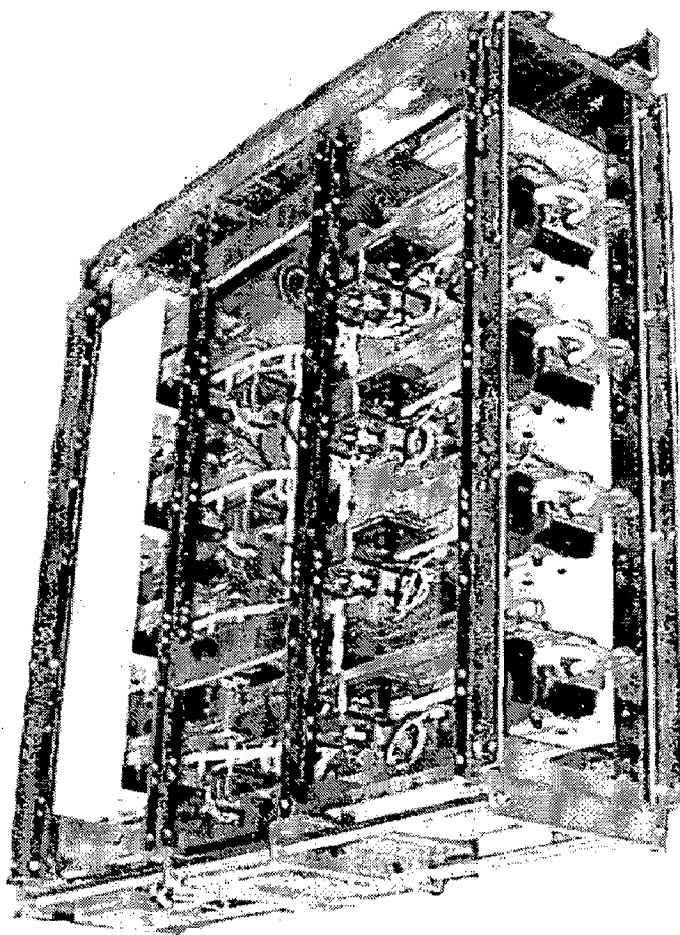


**Fig 3.6 Delay circuit.**



**Inverter phase leg rated at 6.5 KV DC, 1000 A RMS**



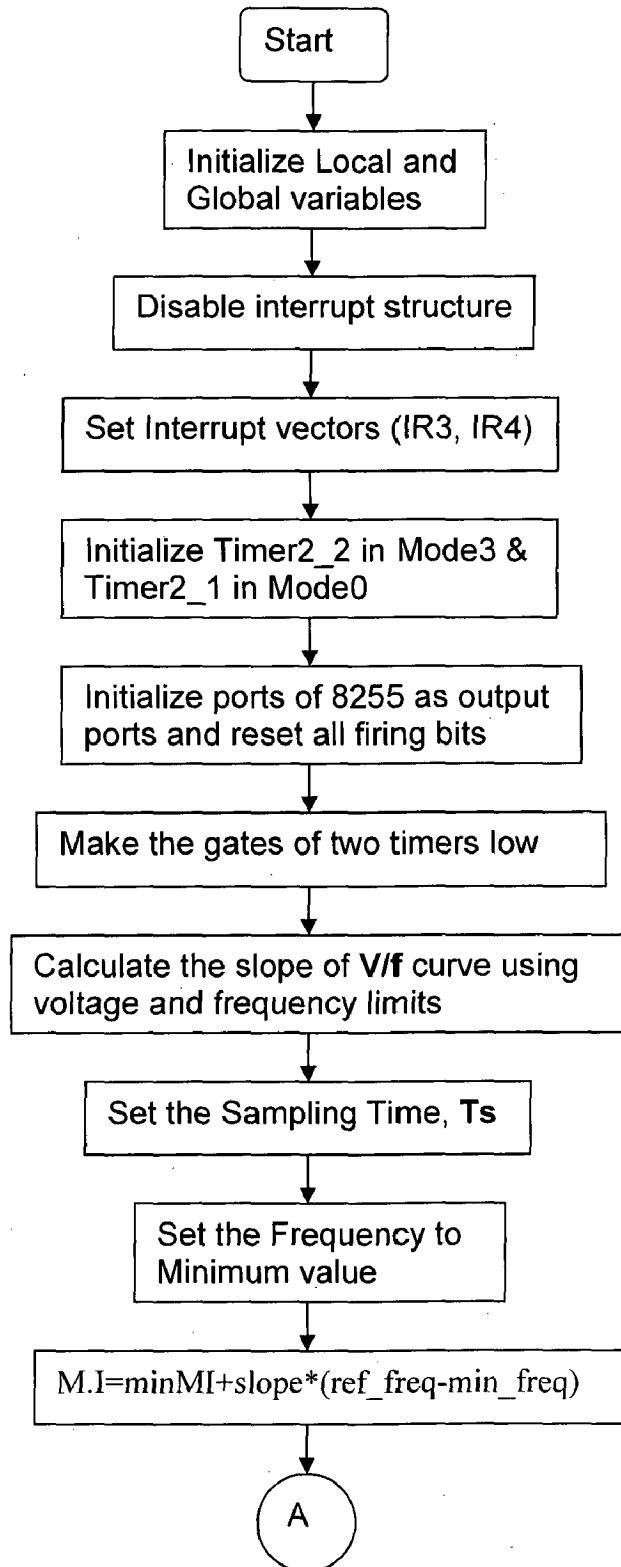
### **3.3 Pc Interfacing**

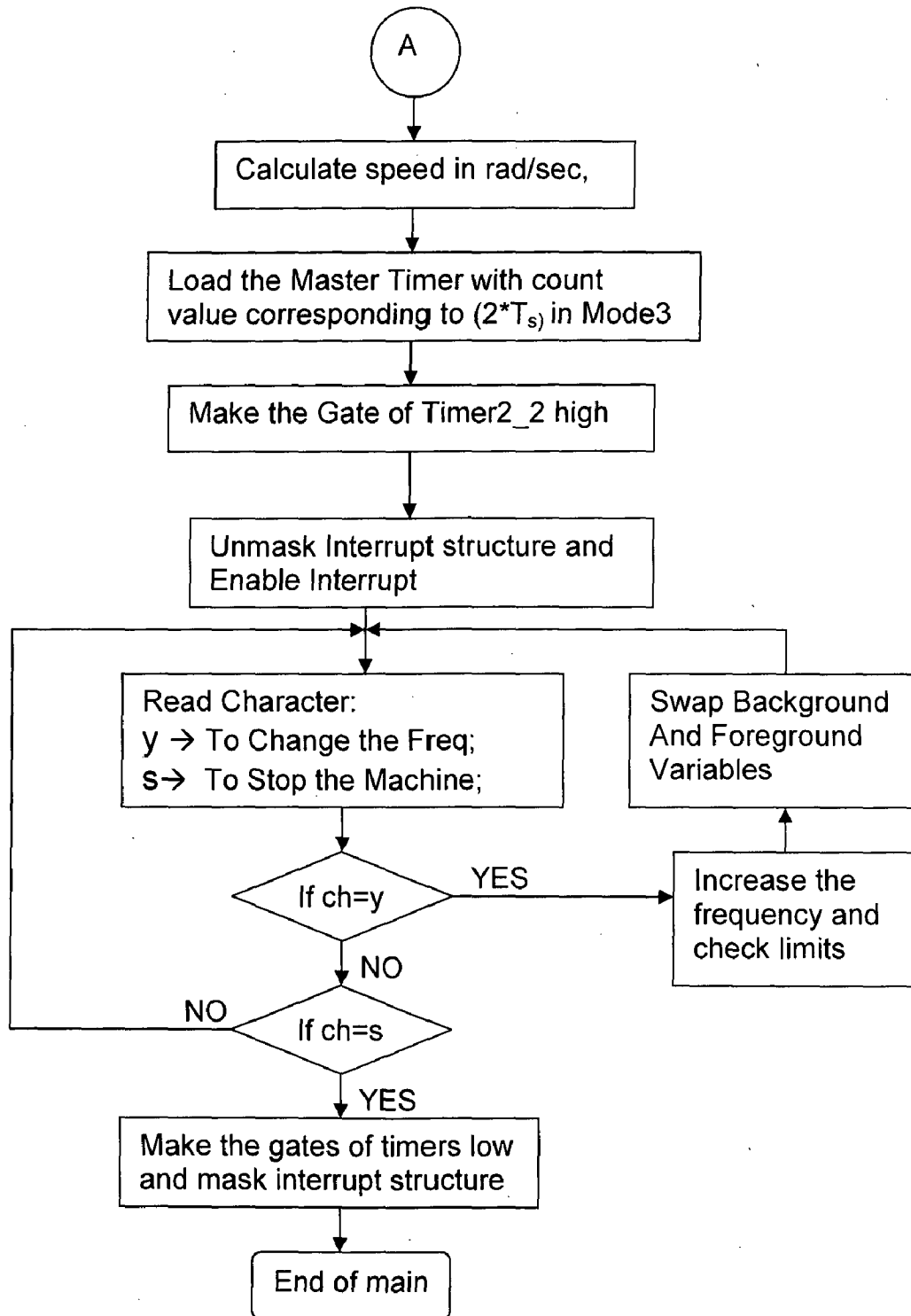
Pentium 80486 Processor based PC with clock frequency 2 MHz along with the Timer I/O card and ADC has been used for this application. This card provides two 8255 each having three I/O ports A, B, C. Since there are 12 switches in Neutral Point Clamped Inverter, six bits from PORT A are being used as firing bits of Upper half of 3-level inverter and inverted signals are used as a firing bits of upper half of 3-level inverter and six bits from port C are being used as firing bits for the lower half of the inverter after providing appropriate delay. The card has two timer chips 8253-1 and 8253-2. Each chip has three counters TIMER1\_0, TIMER1\_1, and TIMETR1\_2 and TIMER2\_0, TIMER2\_1, and TIMER2\_2 respectively. The interrupt used are IR3, IR4, and IR7. To avoid any damage to the ports, a buffer circuit has been fabricated (using 74245 buffers) and all firing bits are first buffered and then applied to the switching devices. The source code has been written in 'C' language. The same configuration can be used to operate conventional three-phase inverter.

### **3.4 Control Technique And Software Development**

The performance of any drive depends on the control technique and its implementation. In the present drive, the control is implemented through 80486 processor based PC and Data acquisition cards. Microprocessor based control reduces the complexity of the system hardware, increases the reliability and makes the control system fast. Space vector modulation technique is used to control the inverter. The complete drive is controlled using TIMER I/O. For superior performance of the drive system suitable software is to be developed, flow char for the software is given below.

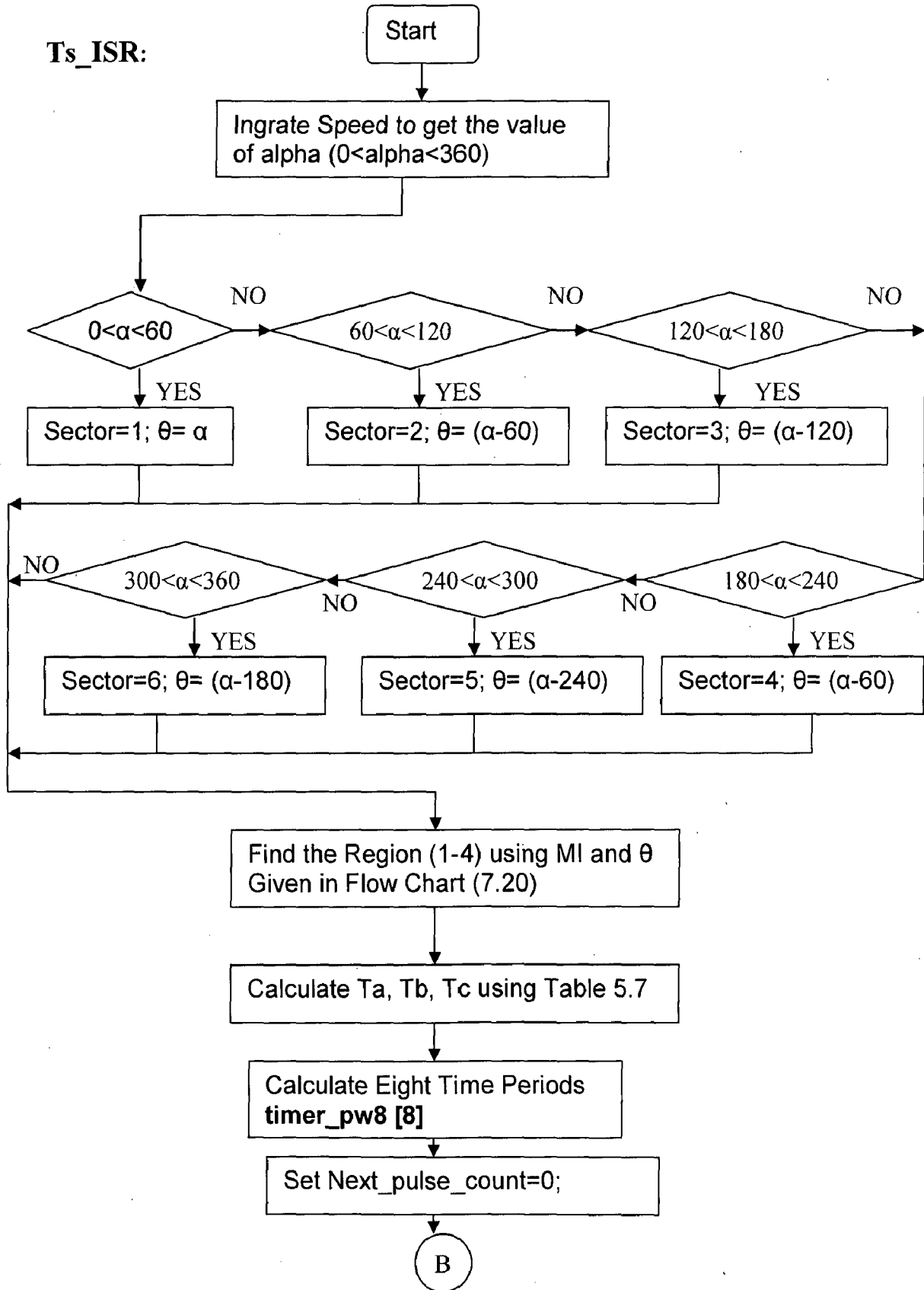
**MAIN PROGRAM:**





**Fig 3.7 Main Program for Open Loop V/f Control of NPC Inverter**

Ts\_ISR:



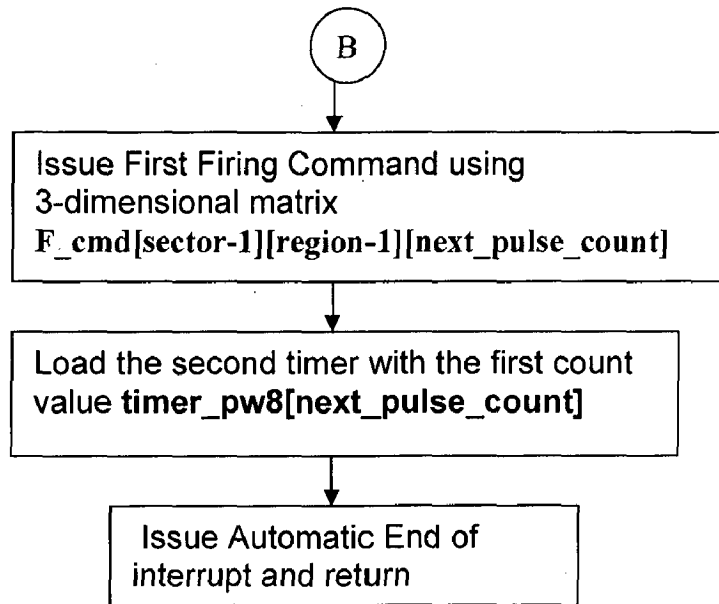


**Fig 3.8 Ts\_ISR for Open Loop V/f Control of NPC**

**TaTbTc\_ISR:**

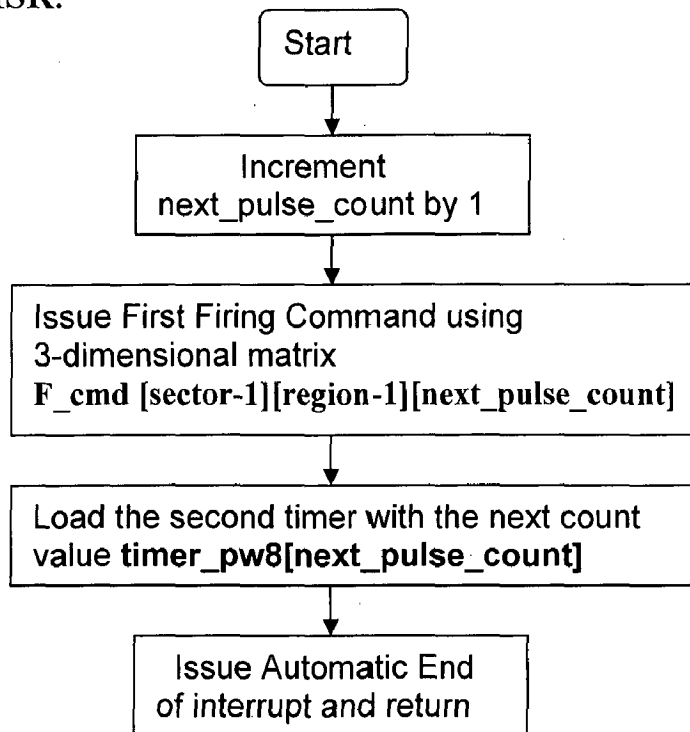


**Fig 3.9 TaTbTc\_ISR for Open Loop V/f Control of NPC**

### 3.4.1 How To Find The Region Using MOD\_INDEX And $\theta$ Values

Fig. 3.40 shows Regions in sector 1. By using simple geometry the logic for the region selection can be found as given below.

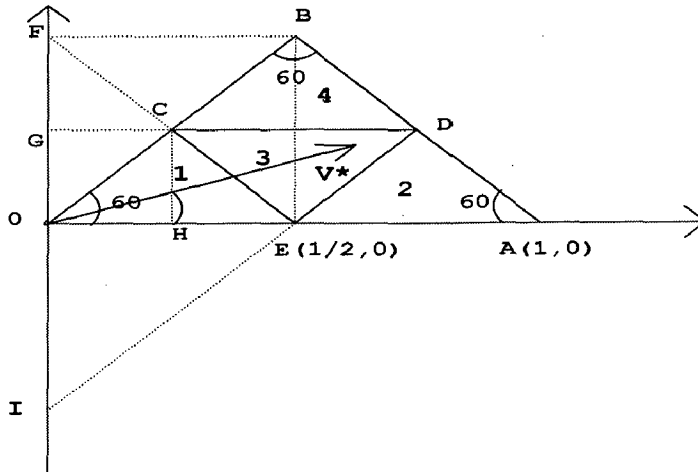


**Fig 3.40 Regions In Sector 1**

Let the side of the equilateral triangle is 1. The coordinate of different point in the equilateral triangle (sector one) are as follows:

$$C\left(\frac{1}{4}, \frac{\sqrt{3}}{4}\right), D\left(\frac{3}{4}, \frac{\sqrt{3}}{4}\right), E\left(\frac{1}{2}, 0\right)$$

$$\text{CE line Equation} \quad y_1 = -\sqrt{3}x_1 + \frac{\sqrt{3}}{2}$$

$$\text{DE line Equation,} \quad y_2 = \sqrt{3}x_2 - \frac{\sqrt{3}}{2}$$

$$\text{DC line Equation,} \quad y_3 = \frac{\sqrt{3}}{4}$$

Using the line equations given above we can find the region in which the reference vector is lying. The algorithm is follows.

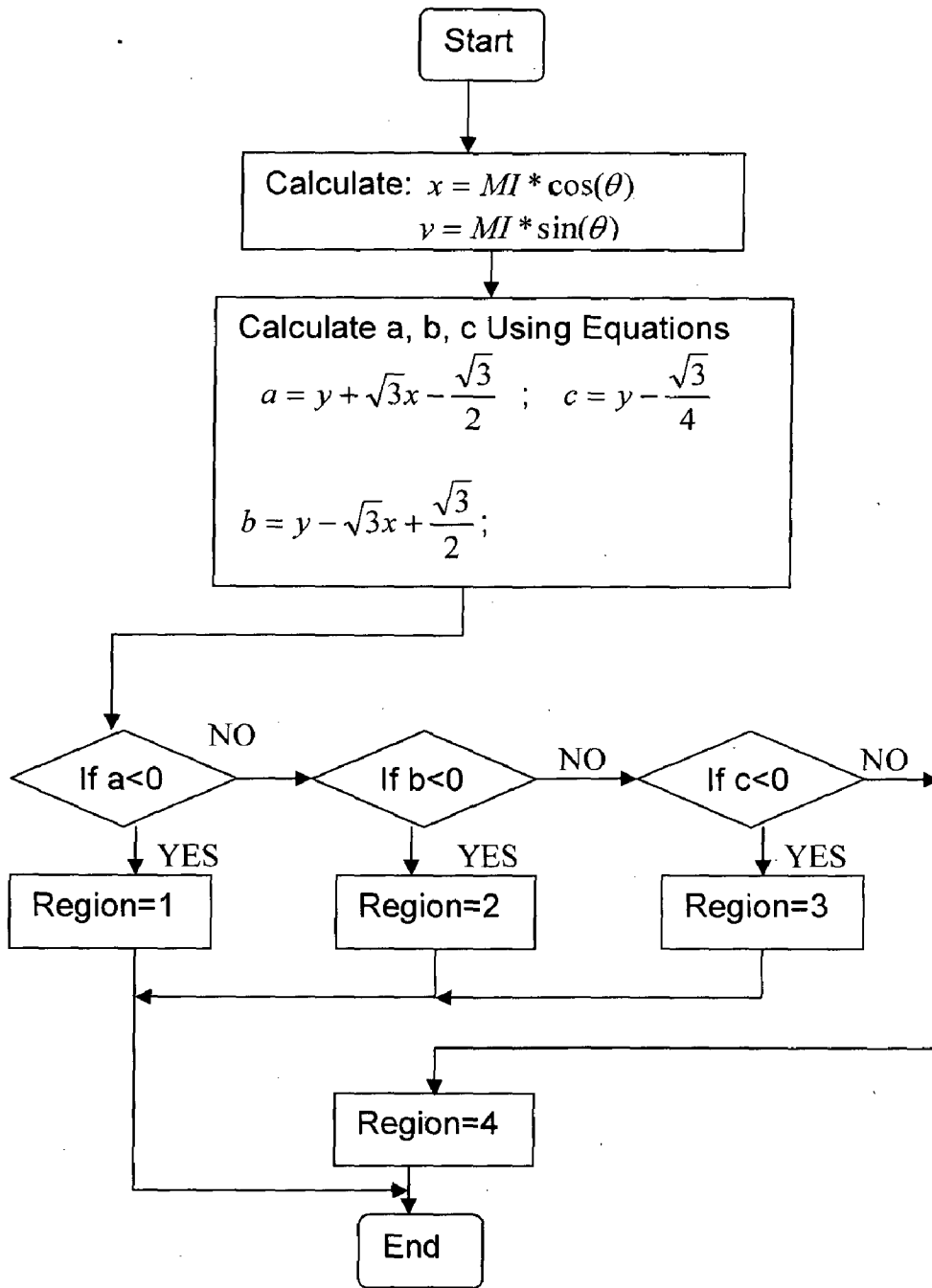


**Fig 3.41 Flow chart for the selection of region**

### **3.5 Conclusion**

Development of multilevel inverter is presented in this chapter. Implementation of the space vector modulation technique is done using microprocessor and using C language. An algorithm is given for implementing this technique. Advantages of using microprocessor is also given over the other conventional technique. Hardware requirements for the development of the three level inverter is given.



Simulation Study

4.1 Introduction

This chapter presents a PWM method for the three level inverter based on space voltage vectors. The principle of the proposed PWM method and the voltage vector output sequences are described in detail. Computer simulation's results verify that the proposed PWM method is suitable for high voltage and large capacity three level inverters.

Three-level inverters are able to generate five level output line-to-line voltage without output transformer or reactor. The main aim of any modulation technique is to obtain variable output having a maximum fundamental component with minimum harmonics. Therefore, the harmonic components of the output voltage are fewer than those of the conventional two-level inverters at the same switching frequency [4]-[9].

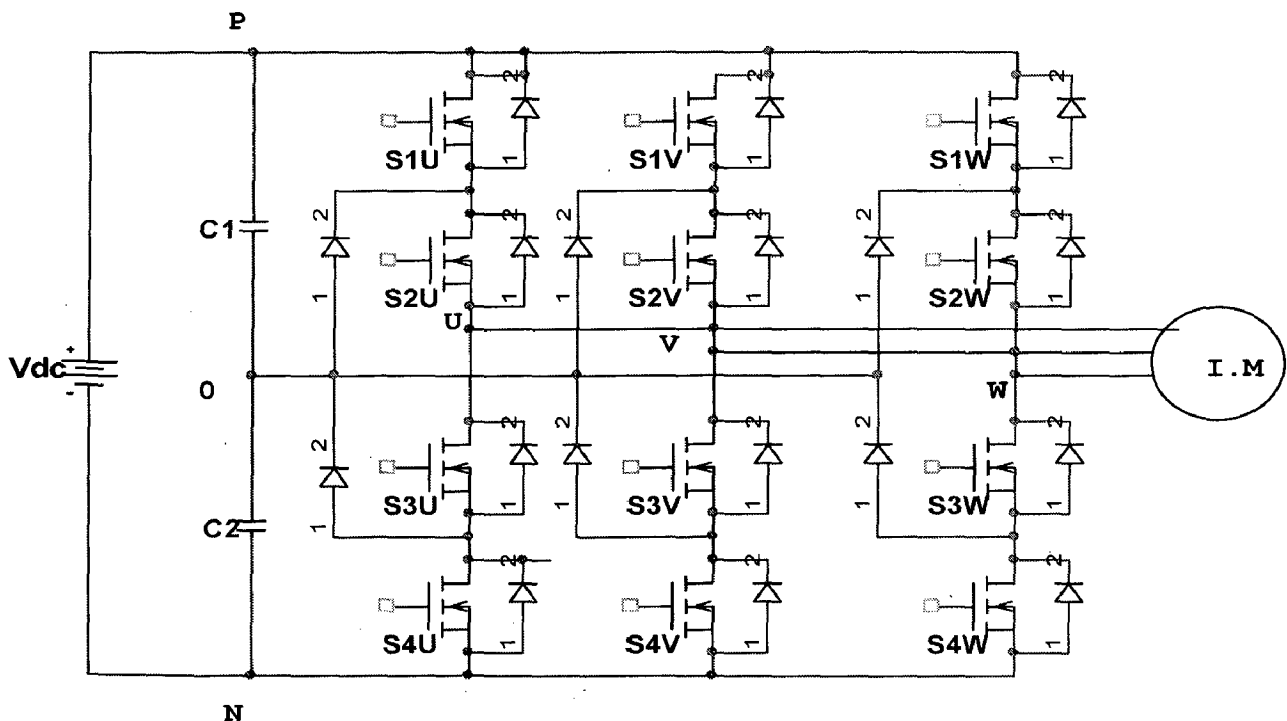
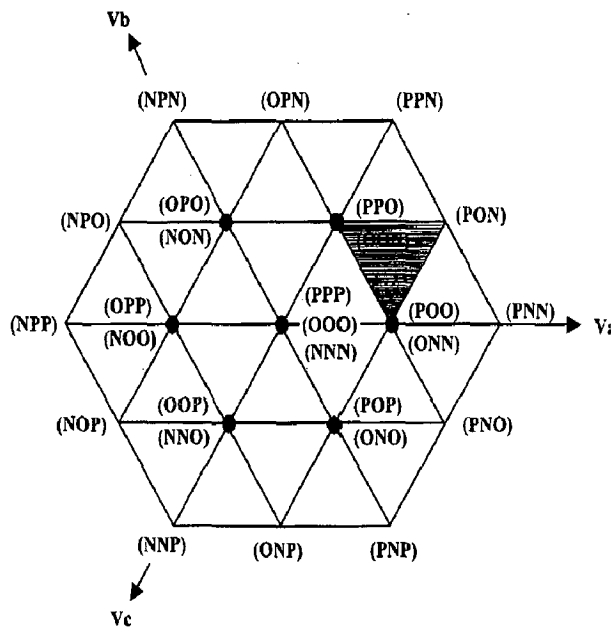


Fig 4.1 Three level inverter

Space vector PWM technique is a more sophisticated technique for generating sine wave that provides a higher voltage to the motor with lower total harmonic distortion. This technique is based on the space vector representation of voltage in the  $\alpha - \beta$  plane.

The  $\alpha - \beta$  components are found by transformations [2]-[4]. The determination of switching instants may be achieved using space vector modulation technique based on the representation of switching vectors in  $\alpha - \beta$  plane. Space vector representation of the three phase quantity is given in appendix B.



**Fig 4.2 Three level space voltage vectors**

Switching States	S <sub>1X</sub>	S <sub>2X</sub>	S <sub>3X</sub>	S <sub>4X</sub>	V <sub>X0</sub>
P	ON	ON	OFF	OFF	+V <sub>dc</sub> /2
0	OFF	ON	ON	OFF	0
N	OFF	OFF	ON	ON	-V <sub>dc</sub> /2

**Table 4.1 Switching states of three level inverter**

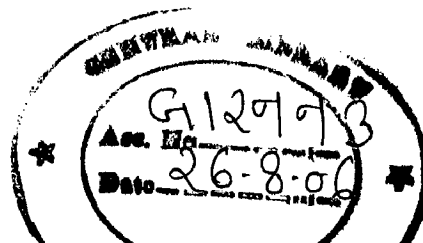


Table 4.1 shows the switching states of a three-level inverter. Three switching states exist in three level inverter therefore total space vectors are 27. Fig 4.2 shows the space voltage vectors for three level-inverter.

## 4.2 Implementation of Space Vector Modulation

Space vector can be implemented by the following steps.

**Step 1.** Determine  $V_d$ ,  $V_q$ ,  $V_{ref}$ , and angle ( $\alpha$ ).

**Step 2.** Determine time duration  $T_a$ ,  $T_b$ ,  $T_c$  for different regions.

**Step 3.** Determine the switching time of each switch.

**Step 1.** Determine  $V_d$ ,  $V_q$ ,  $V_{ref}$ , and angle ( $\alpha$ )

$$V_d = V_{an} - V_{bn} \cdot \cos 60 - V_{cn} \cdot \cos 60 \quad (4.1)$$

$$= V_{an} - \frac{1}{2} V_{bn} - \frac{1}{2} V_{cn}$$

$$V_q = 0 + V_{bn} \cdot \cos 30 - V_{cn} \cdot \cos 30 \quad (4.2)$$

$$= V_{an} + \frac{\sqrt{3}}{2} V_{bn} - \frac{\sqrt{3}}{2} V_{cn}$$

$$\begin{bmatrix} V_d \\ V_q \end{bmatrix} = \frac{2}{3} \begin{bmatrix} 1 & -\frac{1}{2} & -\frac{1}{2} \\ 0 & \frac{\sqrt{3}}{2} & \frac{\sqrt{3}}{2} \end{bmatrix} \begin{bmatrix} V_{an} \\ V_{bn} \\ V_{cn} \end{bmatrix} \quad (4.3)$$

$$|\bar{V}_{ref}| = \sqrt{V_d^2 + V_q^2} \quad (4.4)$$

$$\alpha = \tan^{-1} \left( \frac{V_d}{V_q} \right) \quad (4.5)$$

The voltage  $V_d$ ,  $V_q$ ,  $V_{ref}$ , and angle ( $\alpha$ ) are calculated using the above equation.

Step 2: Determine time durations  $T_a$ ,  $T_b$ ,  $T_c$  of vectors for different regions

Fig 4.3 shows the sector one consisting of four regions 1, 2, 3, and 4 and voltage vectors  $V_0$ ,  $V_1$ ,  $V_2$ ,  $V_3$ ,  $V_4$ ,  $V_5$ . Reference voltage vector is formed by its nearest three voltage vector in order to minimize the harmonic components of the line-to-line voltage. For the location of the  $\overline{V^*}$  vector shown in fig 4.3 a convenient way to generate the PWM output is to use the adjacent vectors  $V_1$ ,  $V_3$  and  $V_4$  of region 3 on a part time basis to satisfy the average output demand.

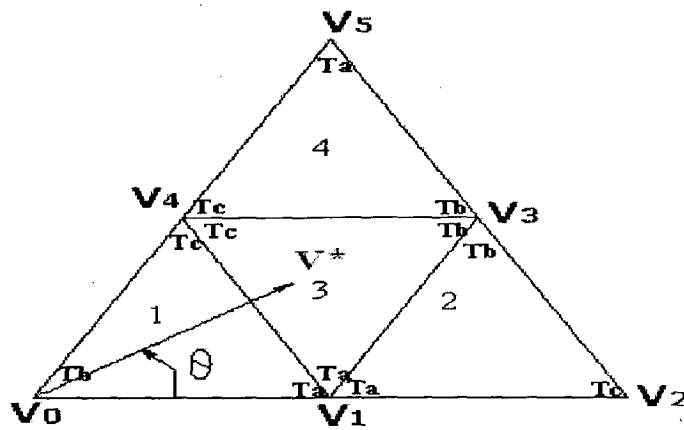


Fig 4.3 regions in sector 1.

The voltage vectors of the sector 1 in exponential form are given below

$$V_0 = 0, V_1 = \frac{1}{2}e^{j \cdot 0}, V_2 = e^{j \cdot 0}, V_3 = \frac{\sqrt{3}}{2}e^{j \frac{\pi}{6}}, V_4 = \frac{1}{2}e^{j \frac{\pi}{3}}, V_5 = e^{j \frac{\pi}{3}} \dots (4.1)$$

In the fig 4.3 space vector lies in the third region. The duration for which the voltage vectors should be applied is calculated as shown below.

$$V_1 \cdot T_a + V_3 \cdot T_b + V_4 \cdot T_c = V^* \cdot T_s \quad (4.2)$$

$$T_a + T_b + T_c = T_s \quad (4.3)$$

Substituting the values of voltage vector  $V_1$ ,  $V_3$ ,  $V_4$  from equation 4.1 to equation 4.2 and using equation 4.3 we get.

$$\frac{1}{2}T_a + \frac{\sqrt{3}}{2}\left(\cos\frac{\pi}{6} + j\sin\frac{\pi}{6}\right)T_b + \frac{1}{2}\left(\cos\frac{\pi}{3} + j\sin\frac{\pi}{3}\right)T_c = V(\cos\theta + j\sin\theta)T_s \quad (4.4)$$

Equating real and imaginary parts.

$$\frac{1}{2}T_a + \frac{\sqrt{3}}{2}\left(\cos\frac{\pi}{6}\right)T_b + \frac{1}{2}\left(\cos\frac{\pi}{3}\right)T_c = V(\cos\theta)T_s \quad (4.5)$$

$$\frac{\sqrt{3}}{2}\left(\sin\frac{\pi}{6}\right)T_b + \frac{1}{2}\left(\sin\frac{\pi}{3}\right)T_c = V(\sin\theta)T_s \quad (4.6)$$

From equation 4.3, 4.5, and 4.6  $T_a$ ,  $T_b$ , and  $T_c$  are given as.

$$T_a = (1 - 2k \sin\theta) \quad (4.7)$$

$$T_b = T_s \left[ 2k \sin\left(\theta + \frac{\pi}{3}\right) - 1 \right] \quad (4.8)$$

$$T_c = T_s \left[ 2k \sin\left(\theta - \frac{\pi}{3}\right) + 1 \right] \quad (4.9)$$

Where  $k = \frac{2V}{\sqrt{3}} \quad (0 < k < 1)$

For all the regions of sector one the values for the timings of the voltage vectors is given in the table below. Since the timings of the voltage vectors of the different regions of the others sectors are symmetrical so these equations of timings are used for the vectors lying in sector other than one by transforming the angle into sector one.

Step 3: Determine the switching time of each switch

SECTOR	REGION	SEQUENCE OF VECTORS
1	1	ONN, OON, OOO, POO, POO, OOO, OON, ONN
	2	ONN, PNN, PON, POO, POO, PON, PNN, ONN
	3	POO, PON, OON, ONN, ONN, OON, PON, POO
	4	OON, PON, POO, PPO, PPO, POO, PON, OON
2	1	PPO, OPO, OOO, OON, OON, OOO, OPO, PPO
	2	PPO, PPN, OPN, OON, OON, OPN, PPN, PPO
	3	OON, OPN, OPO, PPO, PPO, OPO, OPN, OON
	4	OPO, OPN, NPN, NON, NON, NPN, OPN, OPO
3	1	NON, NOO, OOO, OPO, OPO, OOO, NOO, NON
	2	NON, NPN, NPO, OPO, OPO, NPO, NPN, NON
	3	OPO, NPO, NOO, NON, NON, NOO, NPO, OPO
	4	NOO, NPO, NPP, OPP, OPN, NPN, NPO, NOO
4	1	OPP, OOP, OOO, NOO, NOO, OOO, OOP, OPP
	2	OPP, NPP, NOP, NOO, NOO, NOP, NPP, OPP
	3	NOO, NOP, OOP, OPP, OPP, OOP, NOP, NOO
	4	OOP, NOP, NNP, NNO, NNO, NNP, NOP, OOP
5	1	NNO, ONO, OOO, OOP, OOP, OOO, ONO, NNO
	2	NNO, NNP, ONP, OOP, OOP, ONP, NNP, NNO
	3	OOP, ONP, ONO, NNO, NNO, ONO, ONP, OOP
	4	ONO, ONP, PNP, POP, POP, PNP, ONP, ONO
6	1	POP, POO, OOO, ONO, ONO, OOO, POO, POP
	2	POP, PNP, PNO, ONO, ONO, PNO, PNP, POP
	3	ONO, PNO, POO, POP, POP, POO, PNO, ONO
	4	POO, PNO, PNN, ONN, ONN, PNN, PNO, POO

**Table 4.3 Switching sequence in all regions and sectors**

<b>R</b>	<b>T<sub>a</sub></b>	<b>T<sub>b</sub></b>	<b>T<sub>c</sub></b>
1	$2kT_s \sin\left(\frac{\pi}{3} - \theta\right)$	$T_s \left[1 - 2k \sin\left(\frac{\pi}{3} + \theta\right)\right]$	$2kT_s \sin\theta$
2	$2T_s \left[1 - k \sin\left(\frac{\pi}{3} + \theta\right)\right]$	$2kT_s \sin\theta$	$T_s \left[2k \sin\left(\frac{\pi}{3} - \theta\right) - 1\right]$
3	$T_s [1 - 2k \sin\theta]$	$T_s \left[2k \sin\left(\frac{\pi}{3} + \theta\right) - 1\right]$	$T_s \left[2k \sin\left(\theta - \frac{\pi}{3}\right) + 1\right]$
4	$T_s [2k \sin\theta - 1]$	$2kT_s \sin\left(\frac{\pi}{3} - \theta\right)$	$2T_s \left[1 - k \sin\left(\frac{\pi}{3} + \theta\right)\right]$

**Table 4.2 Durations of voltage vectors in 4 regions of sector 1**

Symmetrical pulse pattern for three phases (U, V, W) for different regions of six sectors is shown below. Symmetrical pattern gives minimal output harmonics [7].

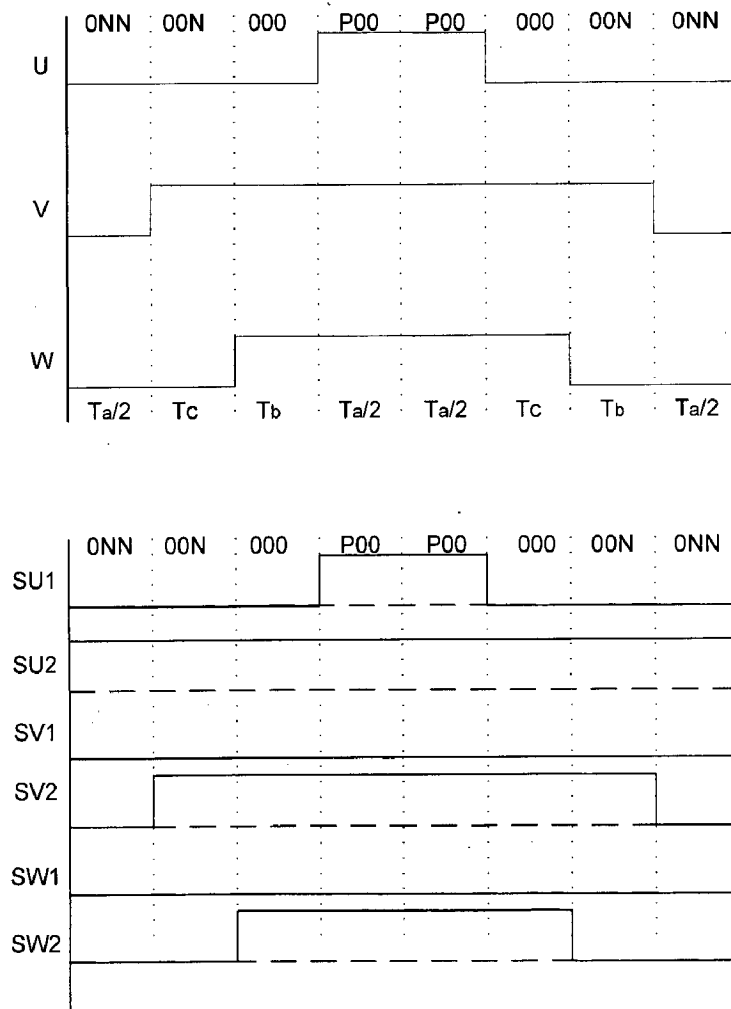


**Figure 4.4 Sector 1- Region 1**



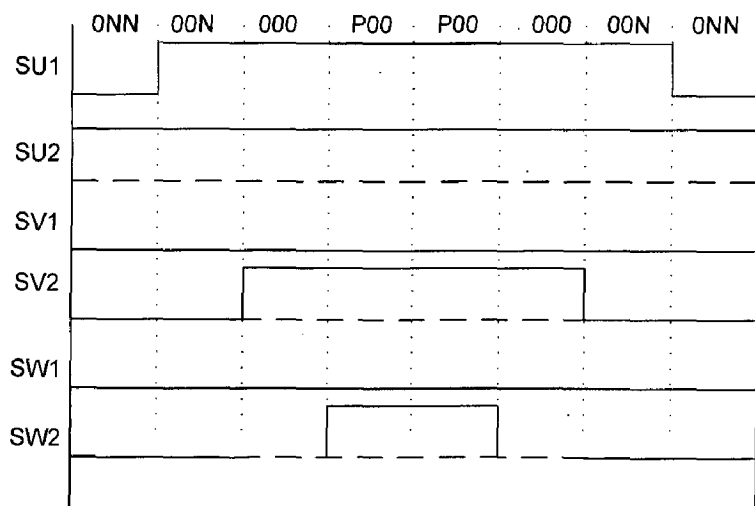
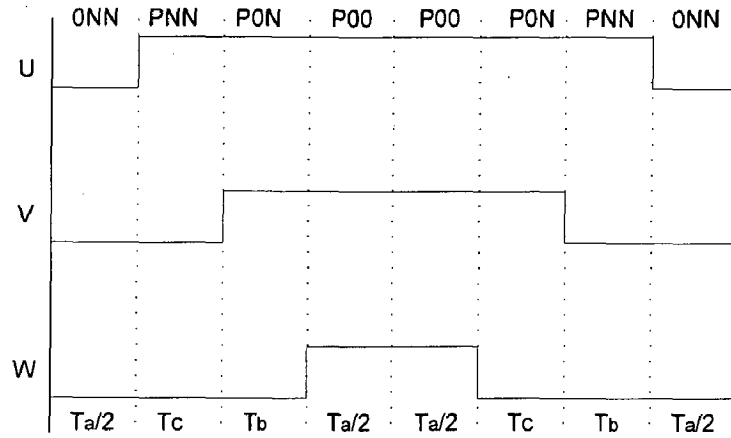


**Figure 4.5 Sector 1- Region 2**

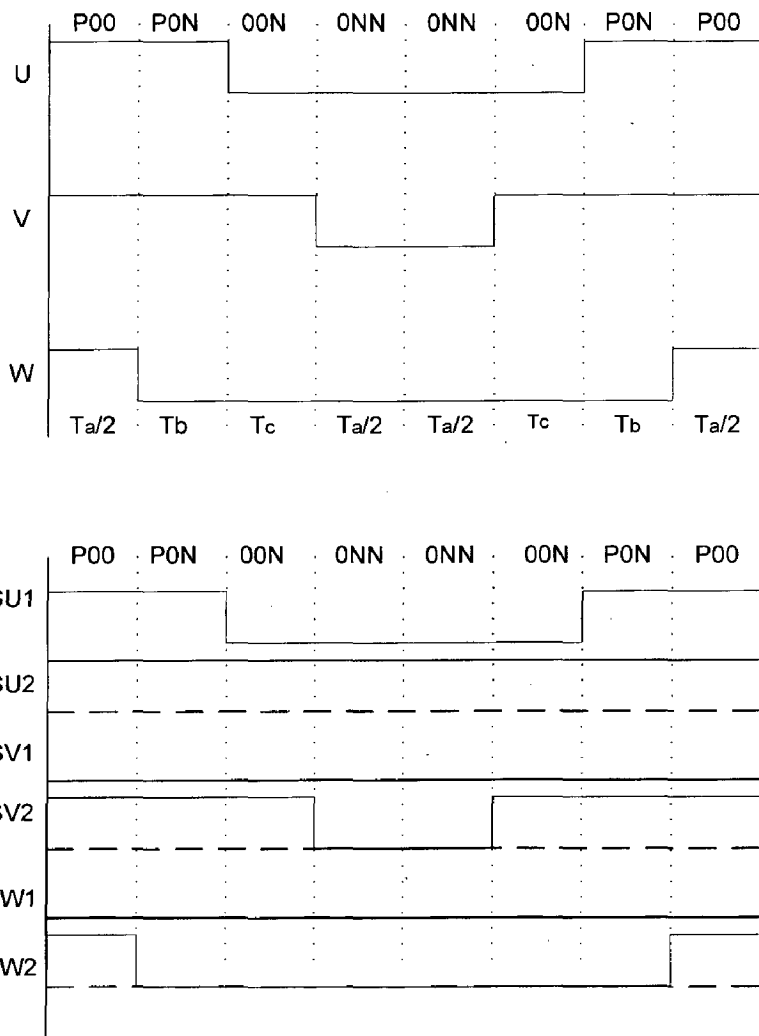


**Figure 4.6 Sector 1- Region 3**

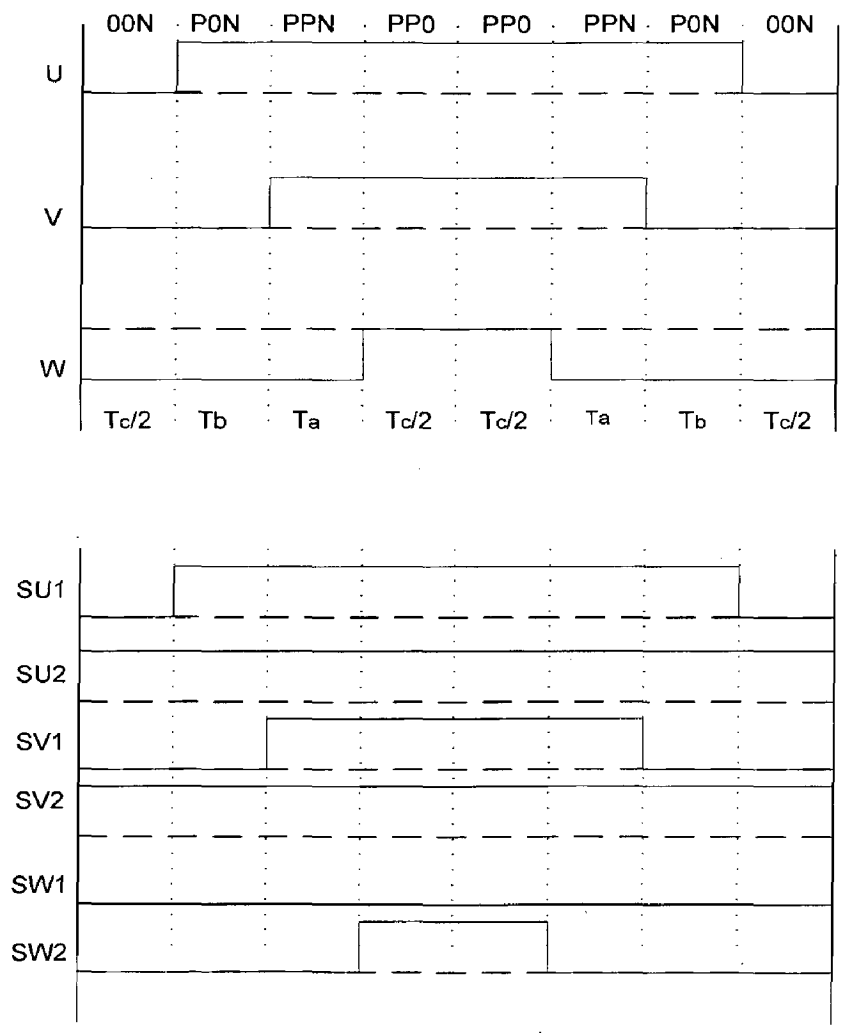


**Figure 4.7 Sector 1- Region 4**

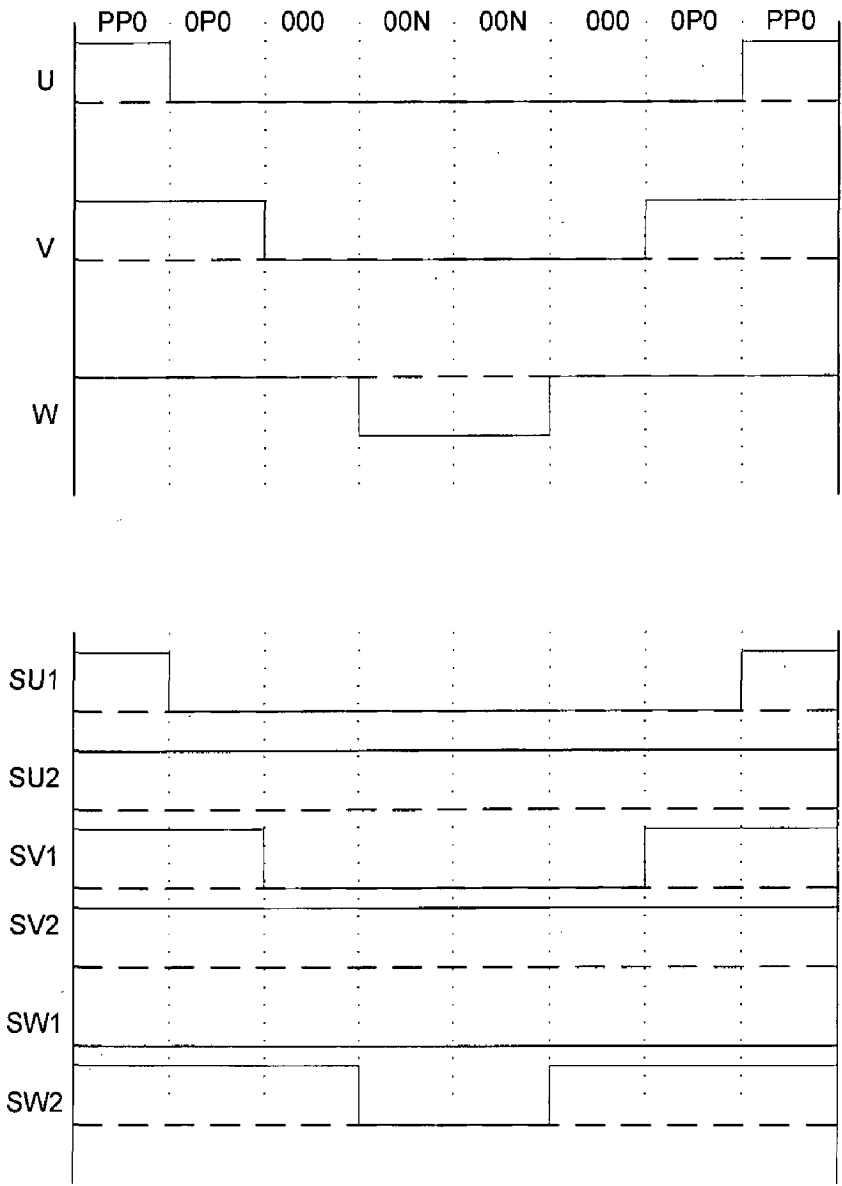


**Figure 4.8 Sector 2- Region 1**

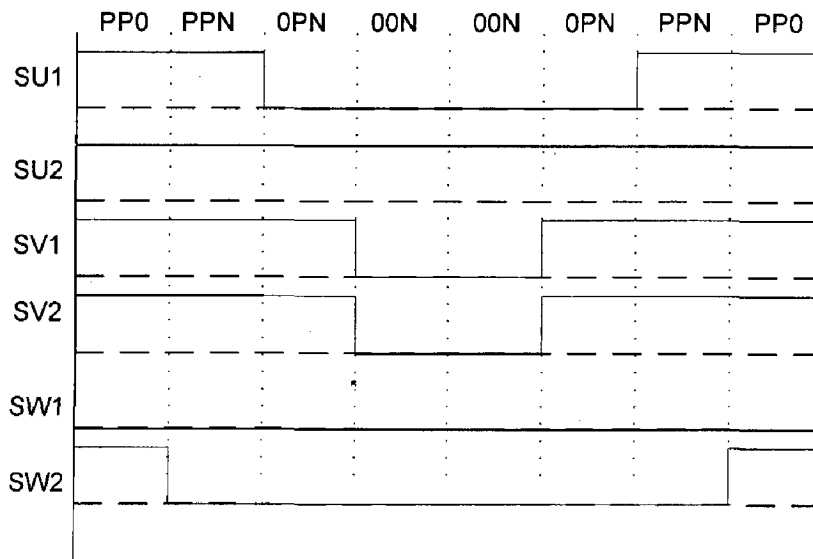


**Figure 4.9 Sector 2- Region 2**

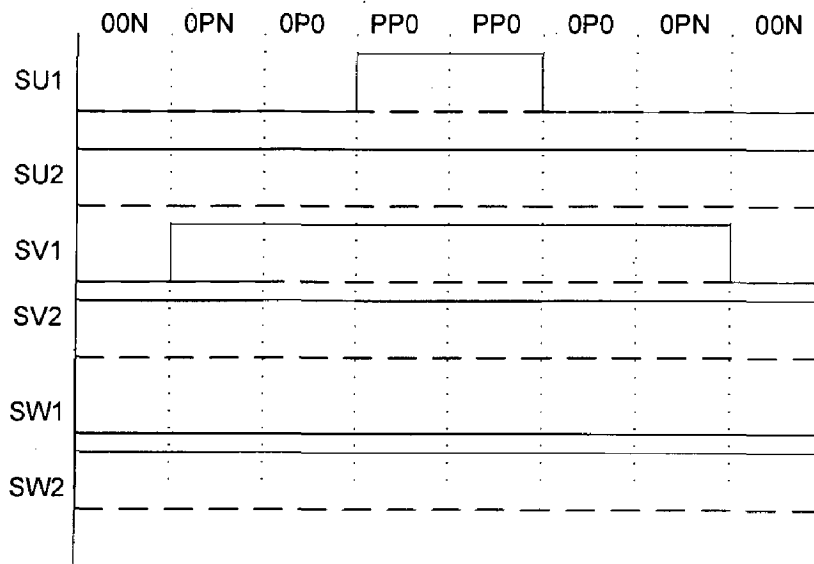


**Figure 4.10 Sector 2- Region 3**

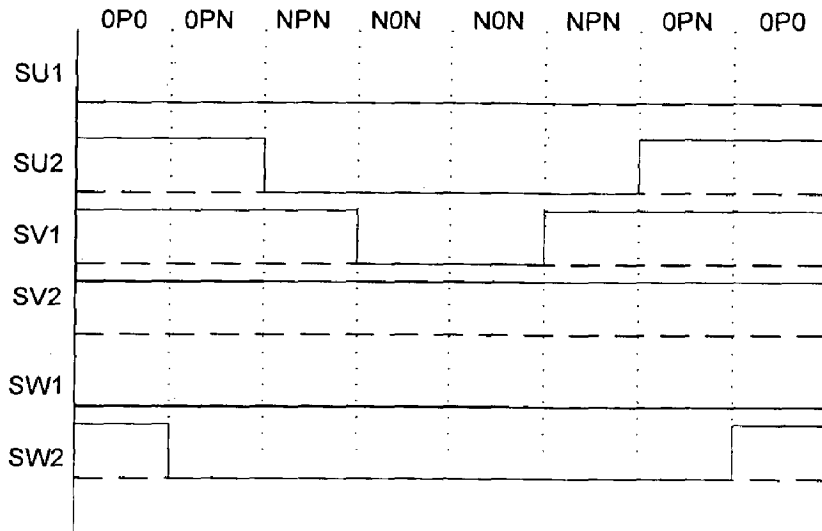


**Figure 4.11 Sector 2- Region 4**

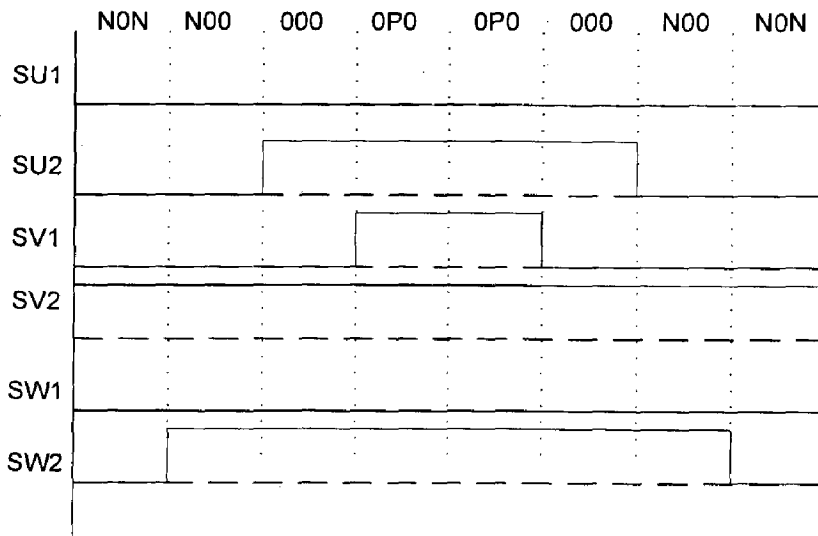


**Figure 4.12 Sector 3- Region 1**

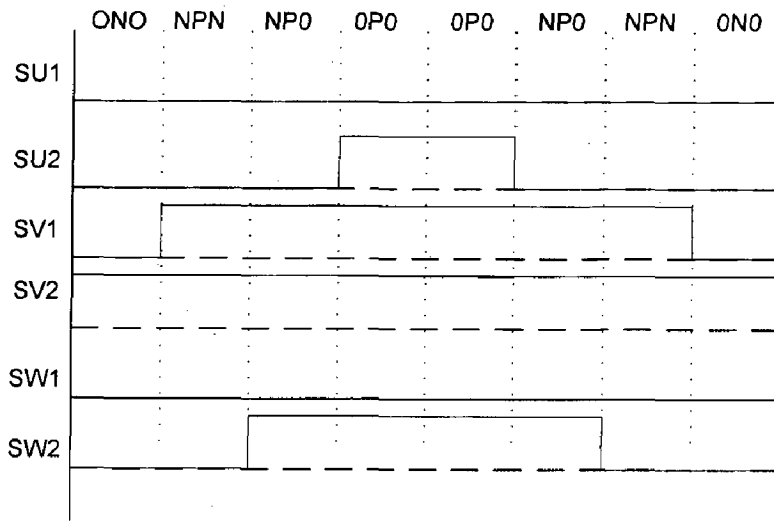


**Figure 4.13 Sector 3- Region 2**

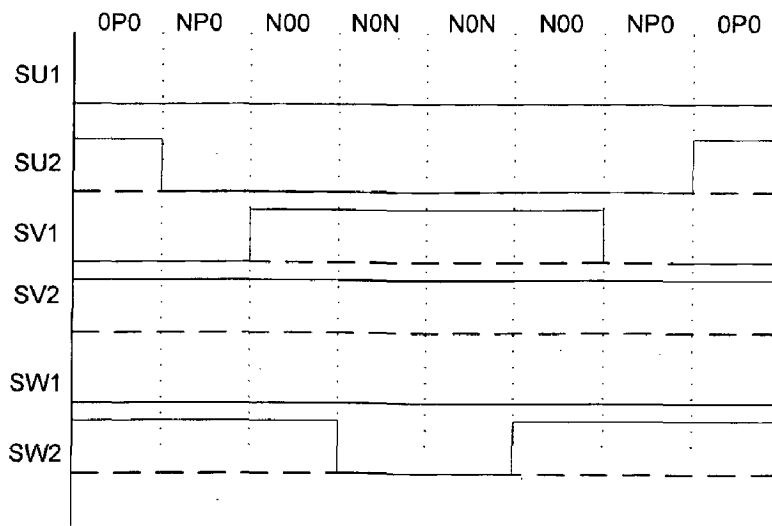


**Figure 4.14 Sector 3- Region 3**

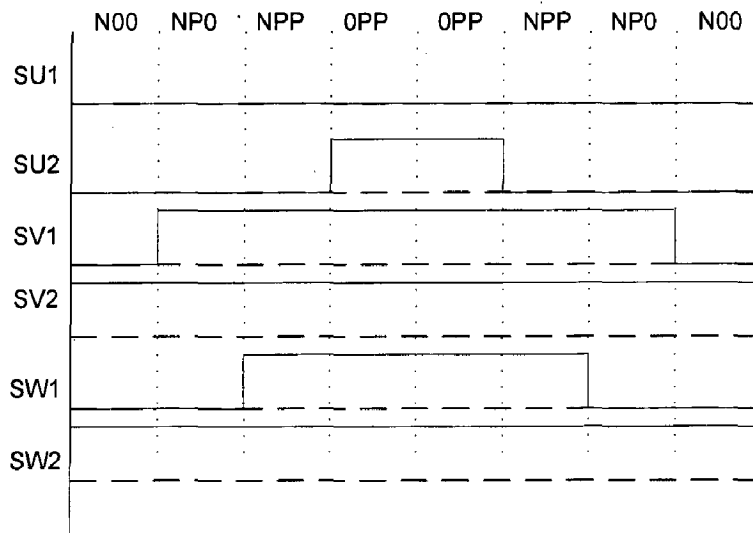


**Figure 4.15 Sector 3- Region 4**

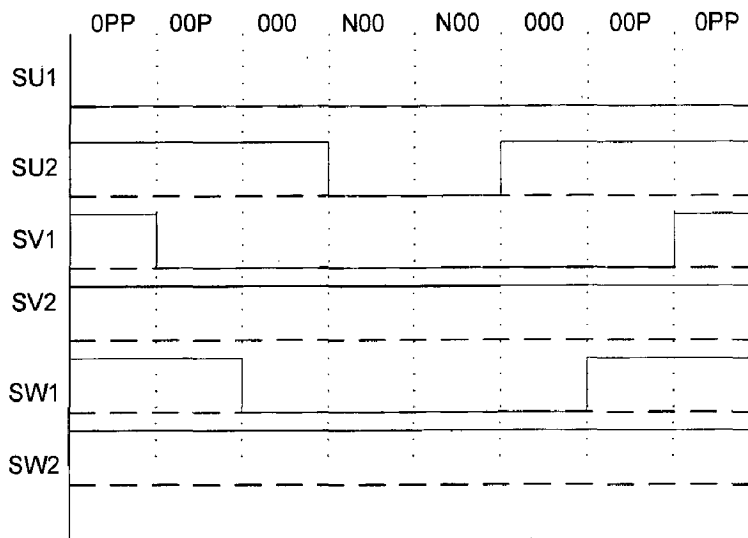


**Figure 4.16 Sector 4- Region 1**



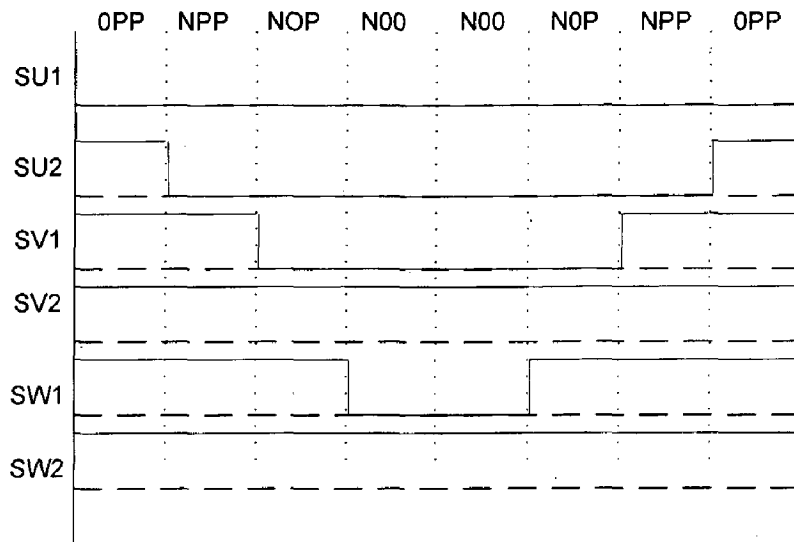


**Figure 4.17 Sector 4- Region 2**

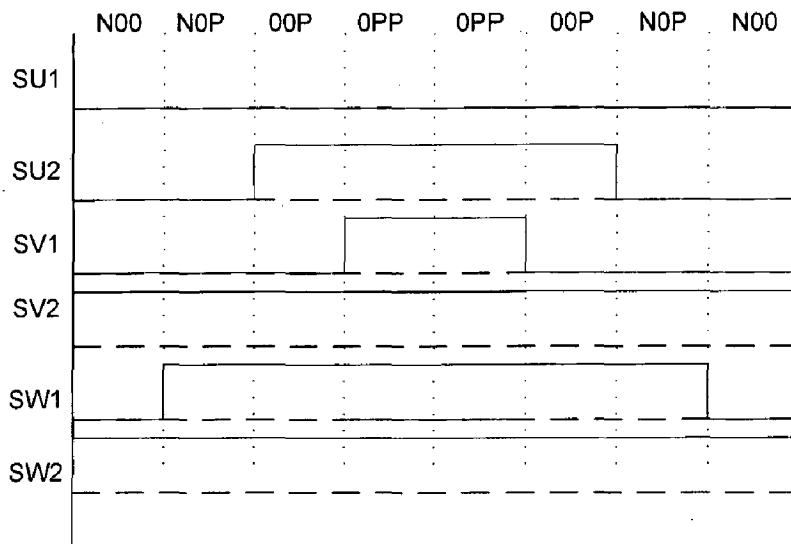


**Figure 4.18 Sector 4- Region 3**

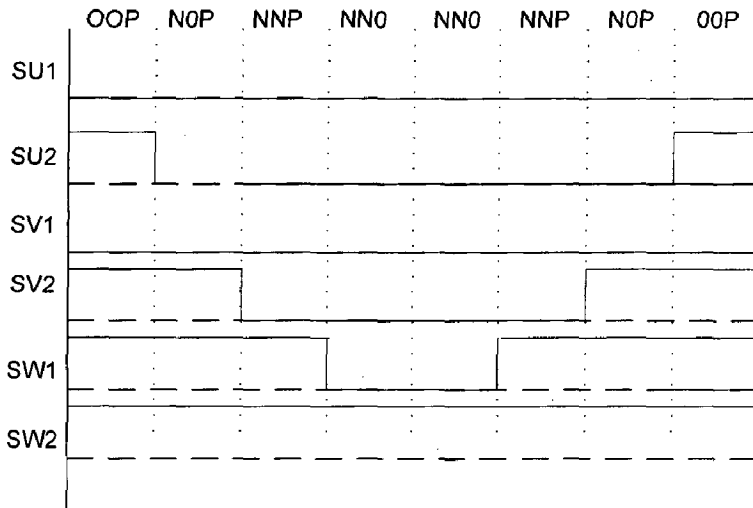


**Figure 4.19 Sector 4- Region 4**

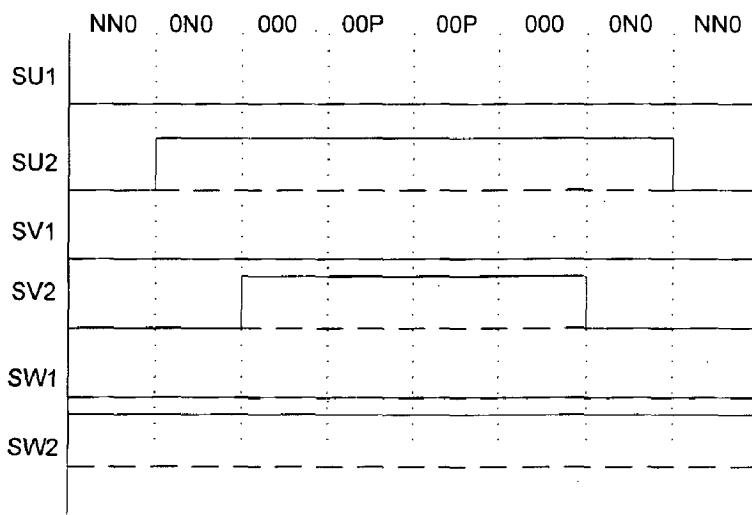


**Figure 4.20 Sector 5- Region 1**

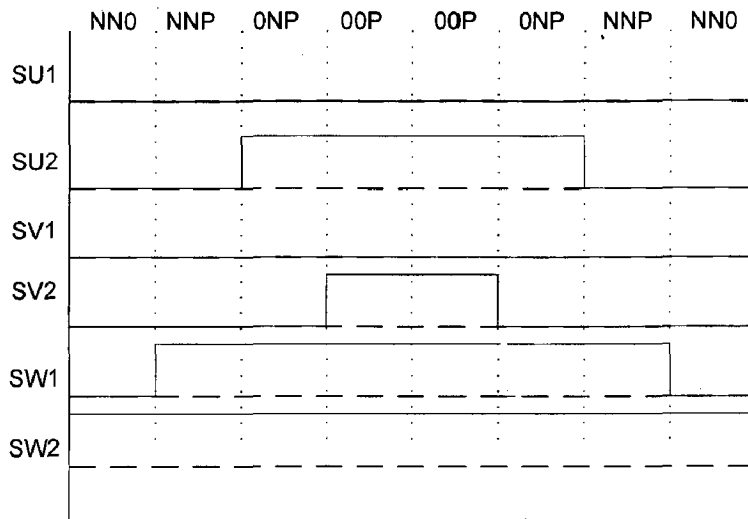


**Figure 4.21 Sector 5- Region 2**

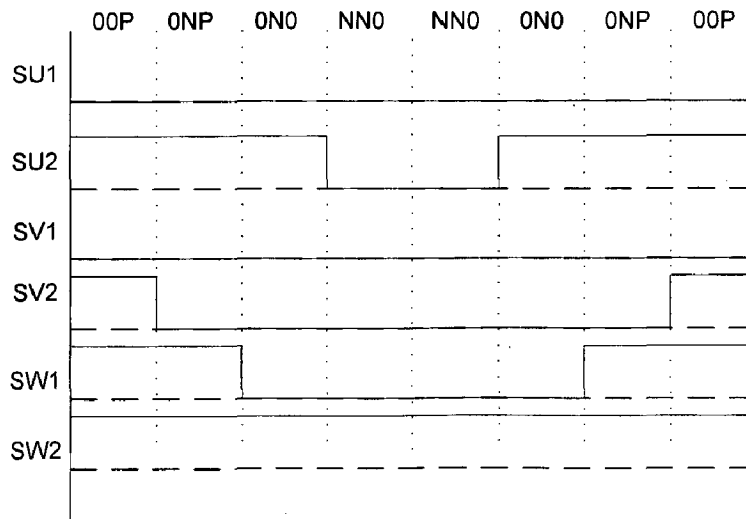


**Figure 4.22 Sector 5- Region 3**

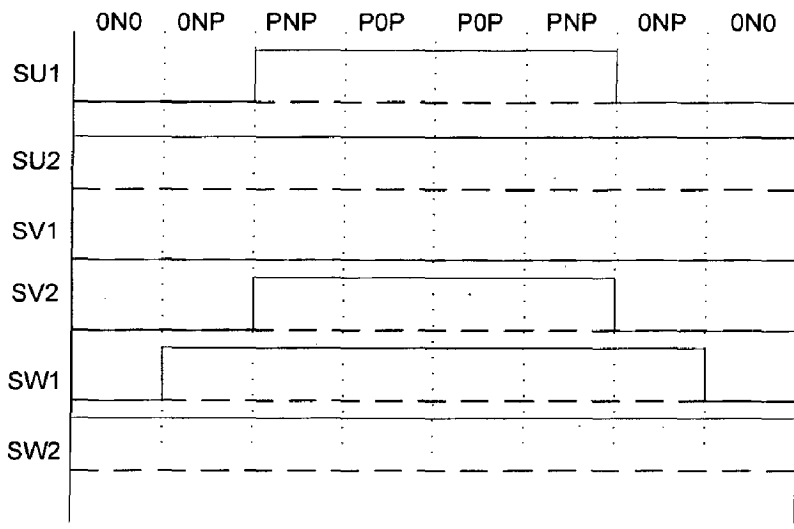


**Figure 4.23 Sector 5- Region 4**

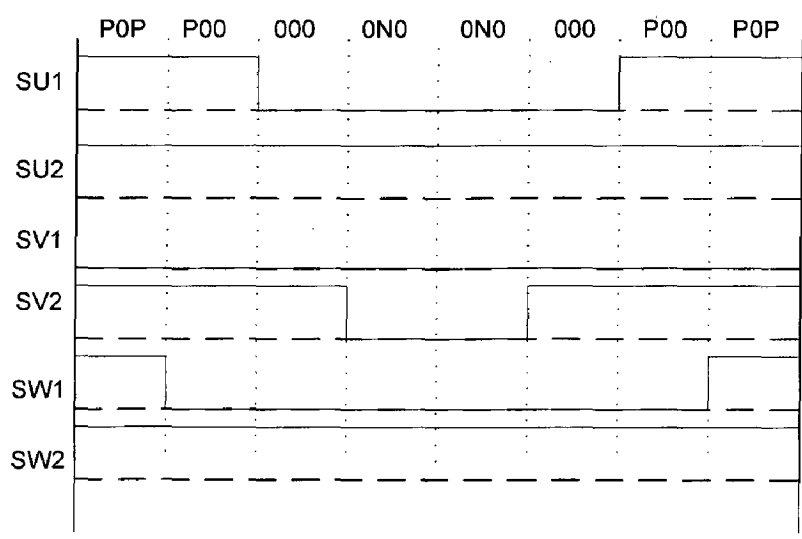


**Figure 4.24 Sector 6- Region 1**

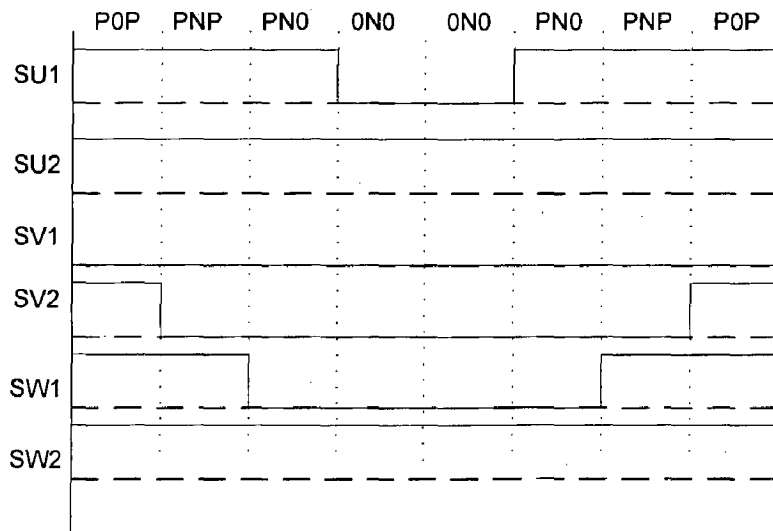


**Figure 4.25 Sector 6- Region 2**

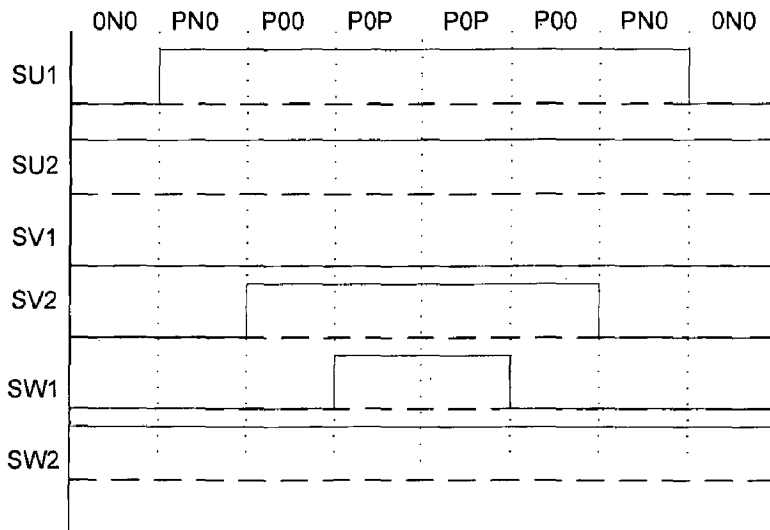


**Figure 4.26 Sector 6- Region 3**

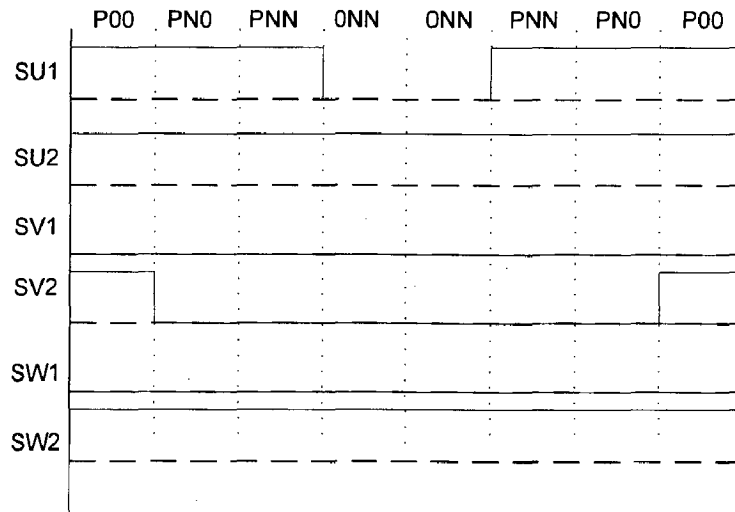


**Figure 4.27 Sector 6- Region 4**

The construction of symmetrical pulse pattern for two consecutive  $T_Z$  intervals are shown and  $T_S=2 T_Z=1/f_s$  ( $f_s$  switching frequency) is the sampling time. The null time has been conveniently distributed between the vectors to describe the symmetrical pulse pattern. The over modulation region where the reference voltage vector  $V$  exceeds the hexagon boundary is not discussed in this thesis.

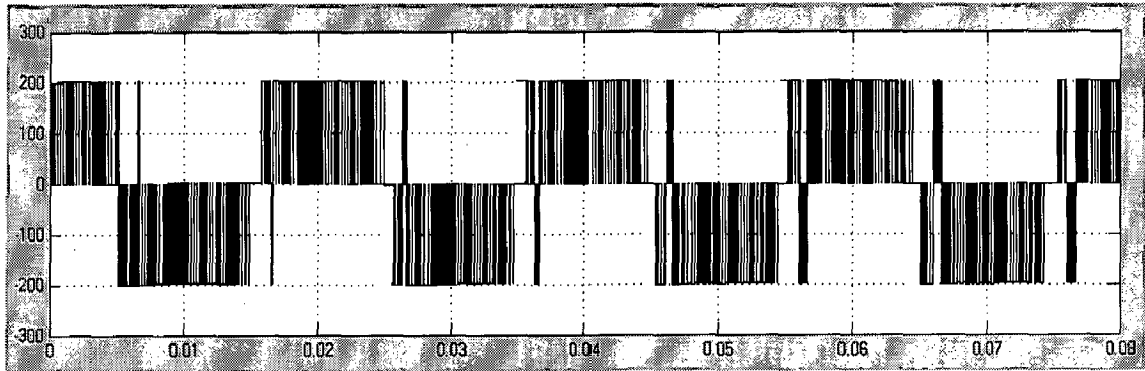
### 4.3 simulation steps

- 1). Initialize system parameters using Matlab
- 2). Build Simulink Model
  - Determine sector
  - Transform reference vector into sector one
  - Determine regions in sector one
  - Determine time duration  $T_a, T_b, T_c$

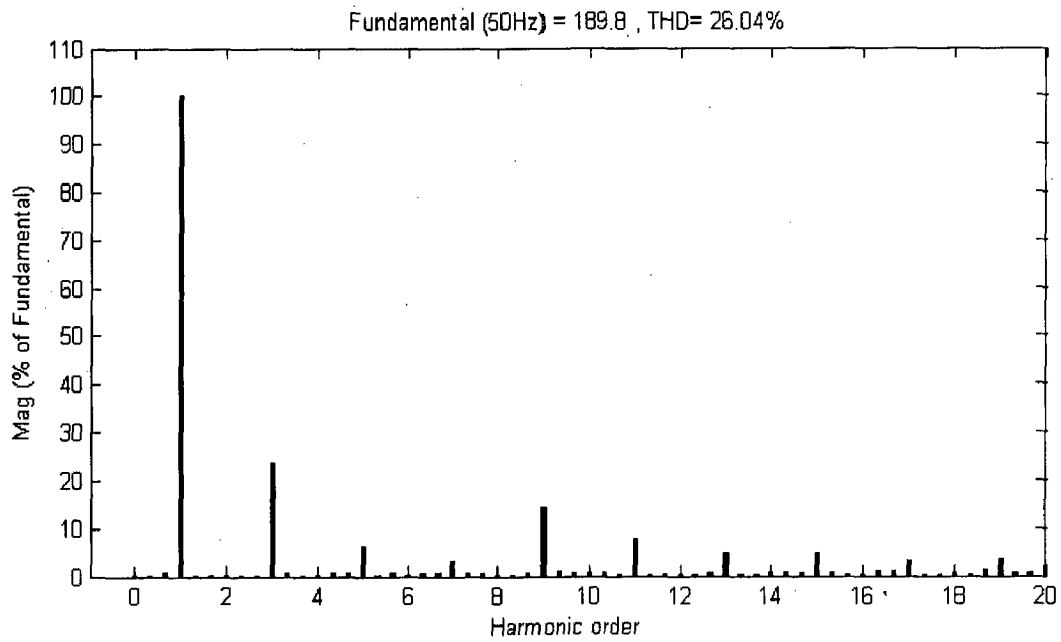
- Determine the switching time ( $T_a$ ,  $T_b$ , and  $T_c$ ) of each switch.
- Generate the inverter output voltages.
- Send data to Workspace

3). Plot simulation results using Matlab

#### 4.4 simulation results

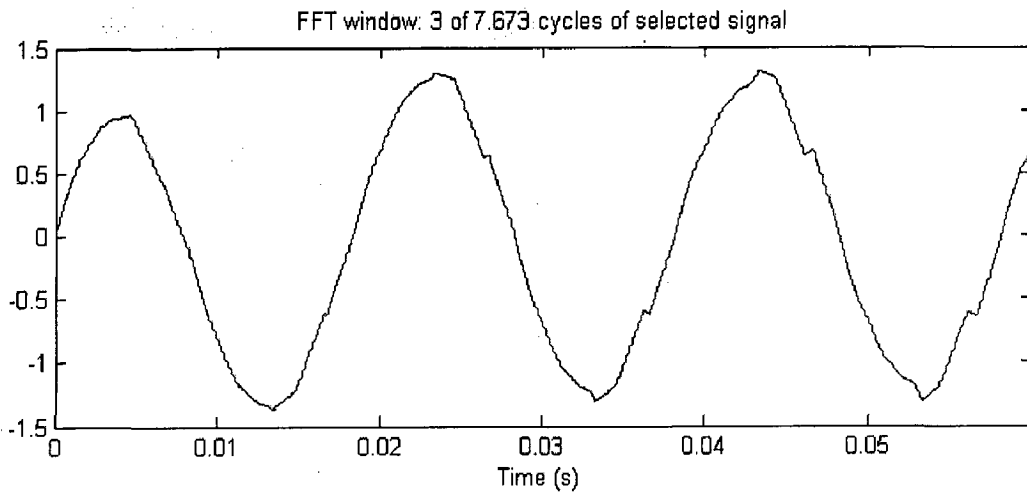


(a)

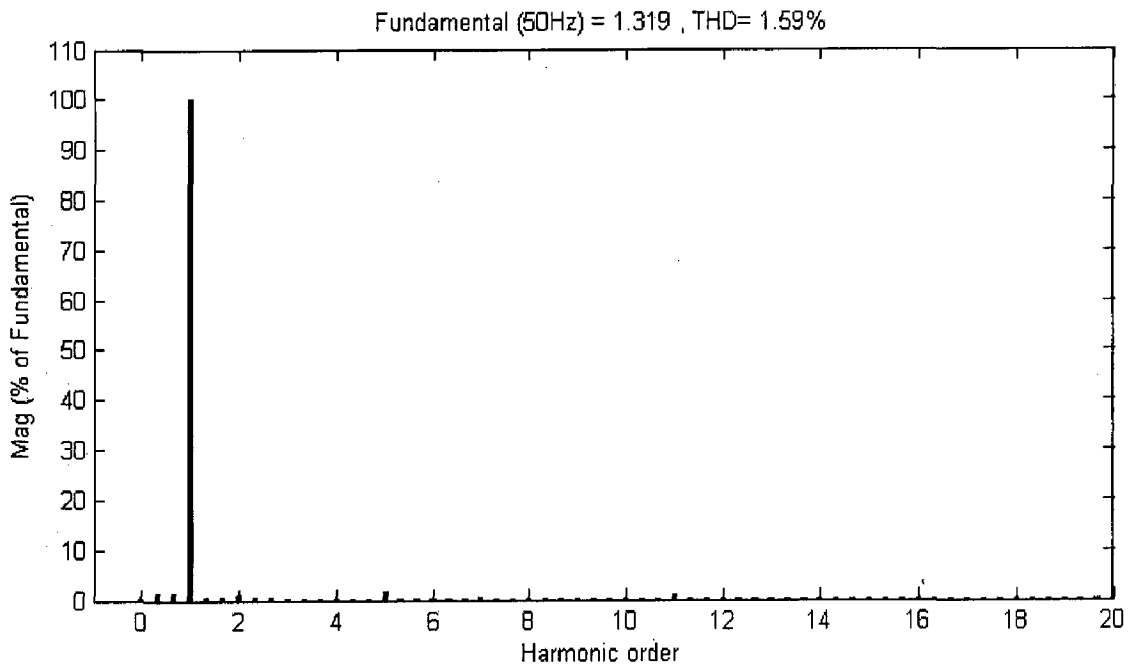


(b)

**Fig 4.28 (a) Inverter phase voltage  
(b) Harmonic spectrum**



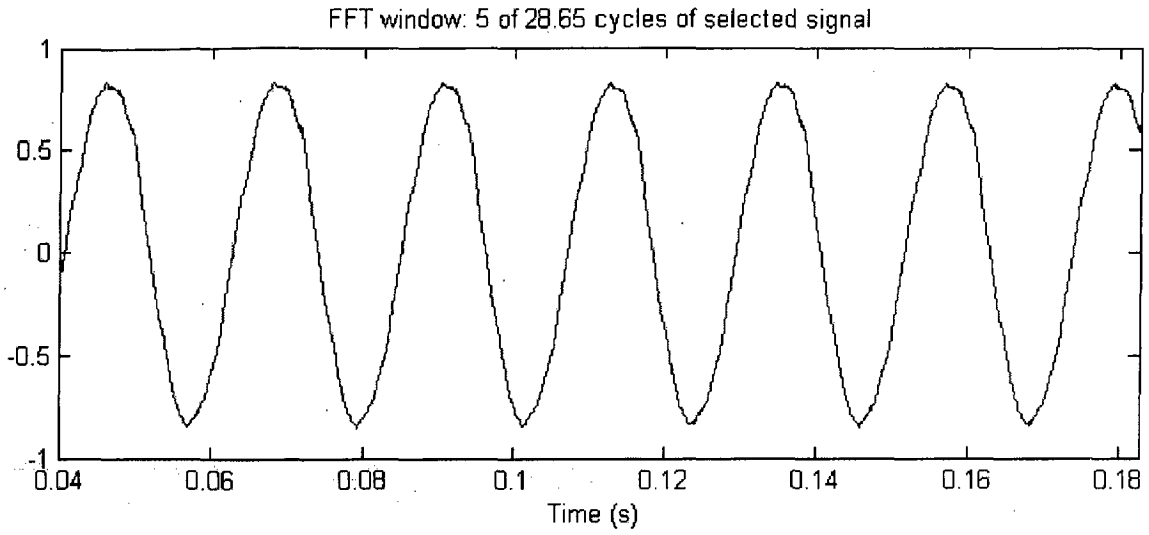
(a)



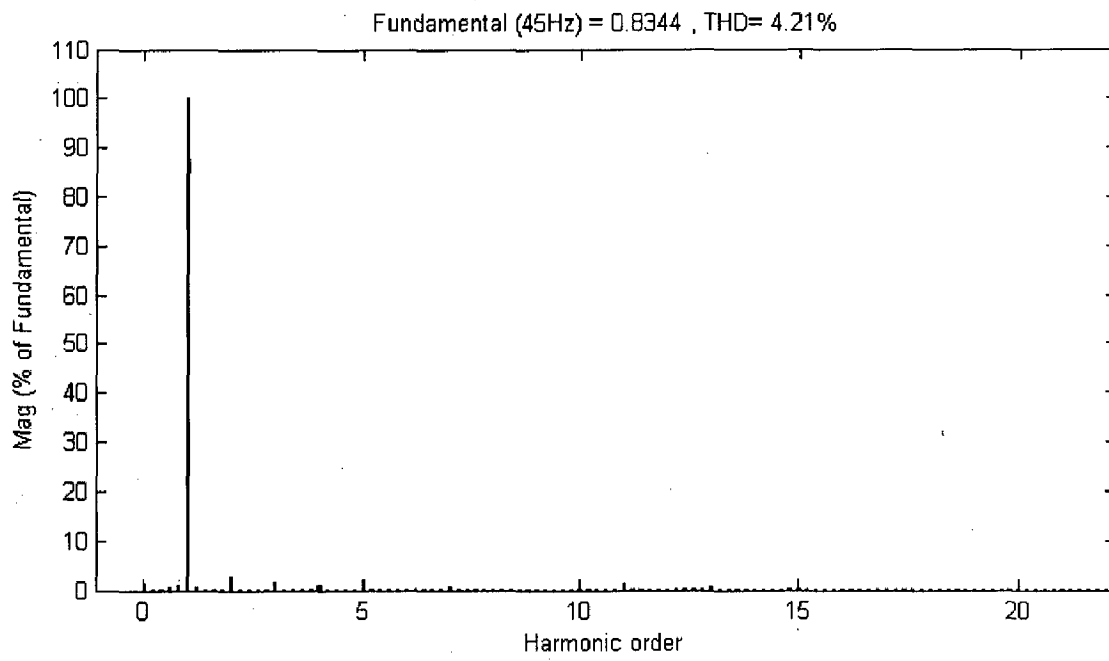
(b)

**Fig 4.29 (a) Load current ( $R=75\Omega$ ,  $L=0.4$ ,  $f=50$  Hz)  
(b) Harmonic spectrum**





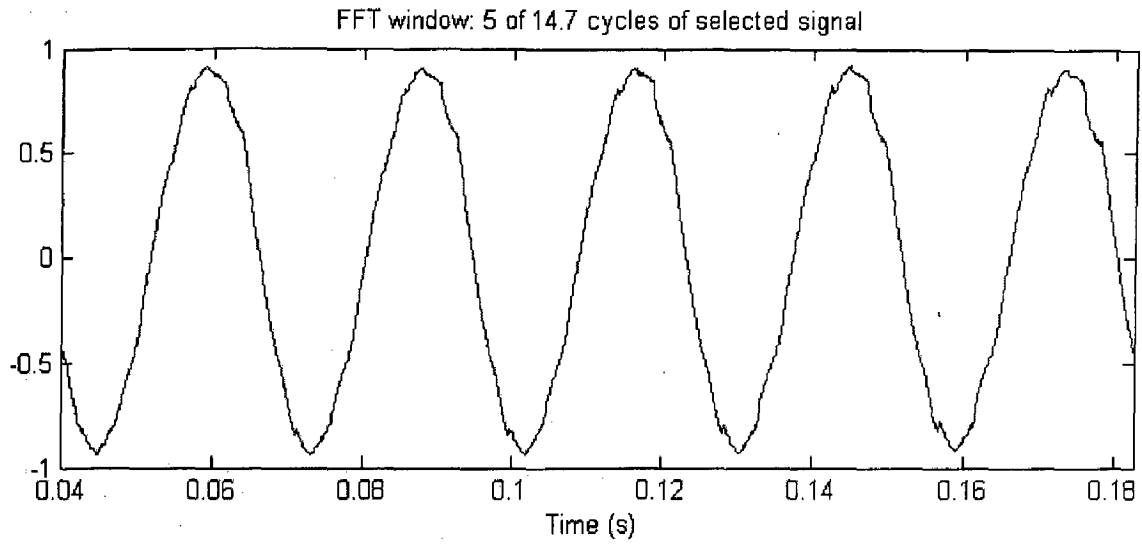
(a)



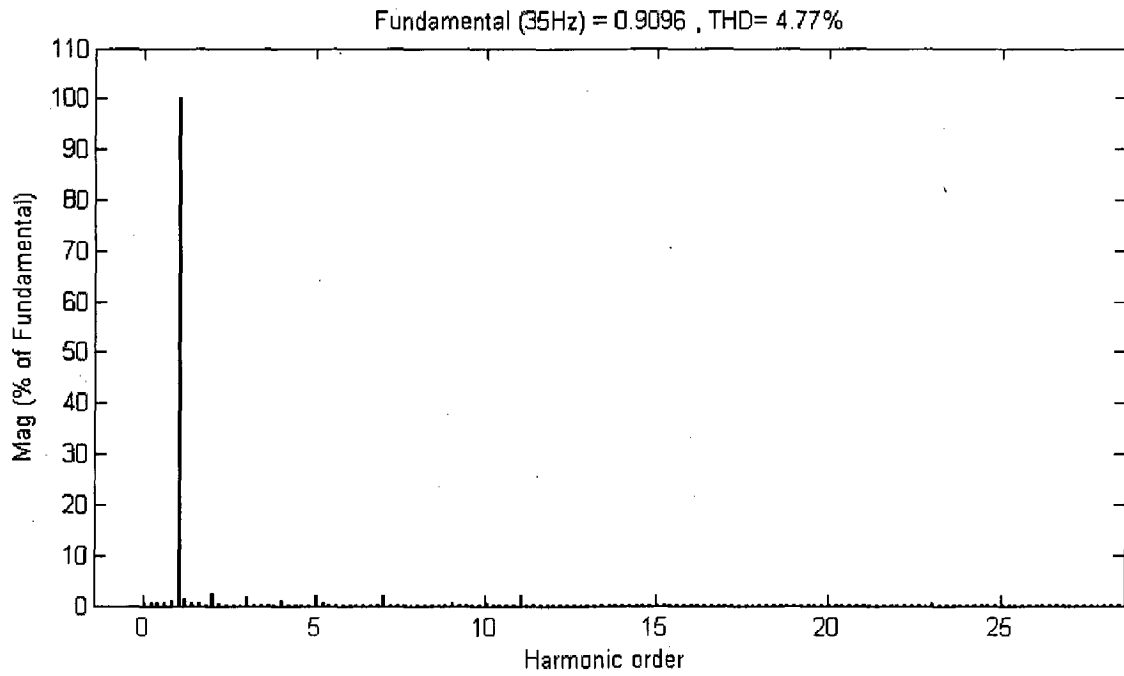
(b)

**Fig 4.30 (a) Phase a load current**

**(b) Harmonic spectrum(R=75, L=0.4H, f= 45 Hz)**

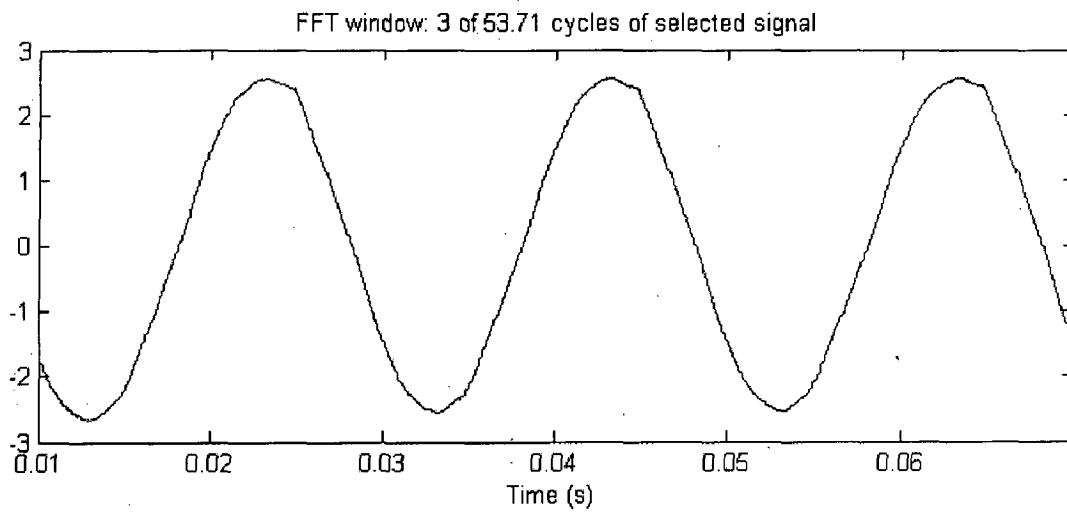


(a)

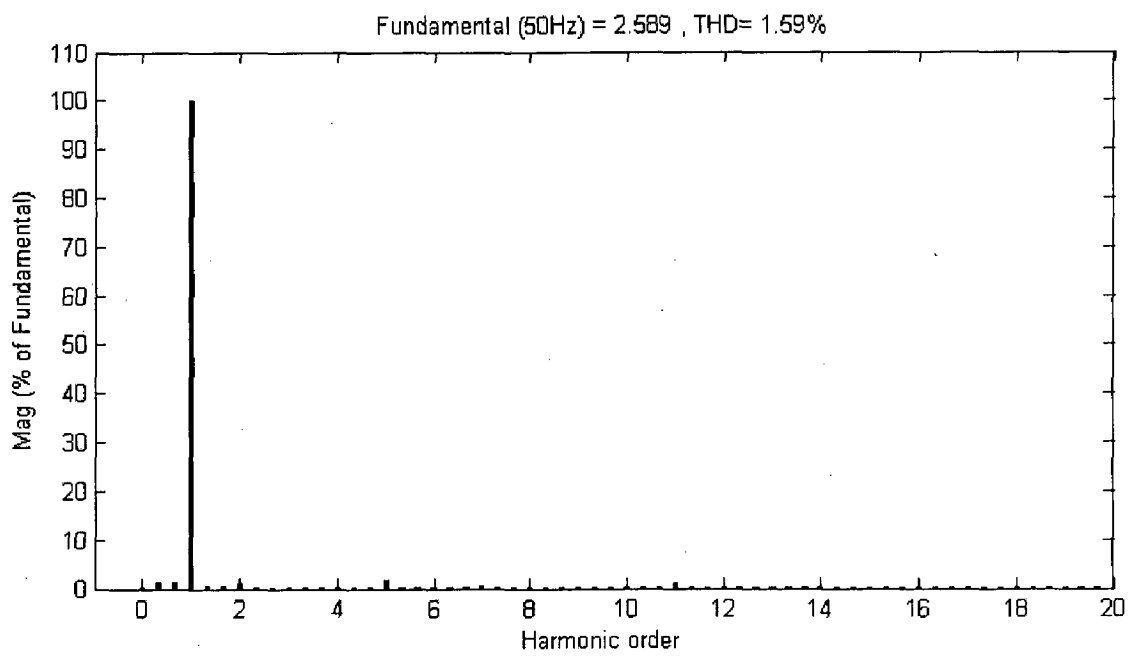


(b)

**Fig 4.31 (a) Phase a load current**  
**(b) Harmonic spectrum (R=75,L=0.4H, f= 35 Hz)**

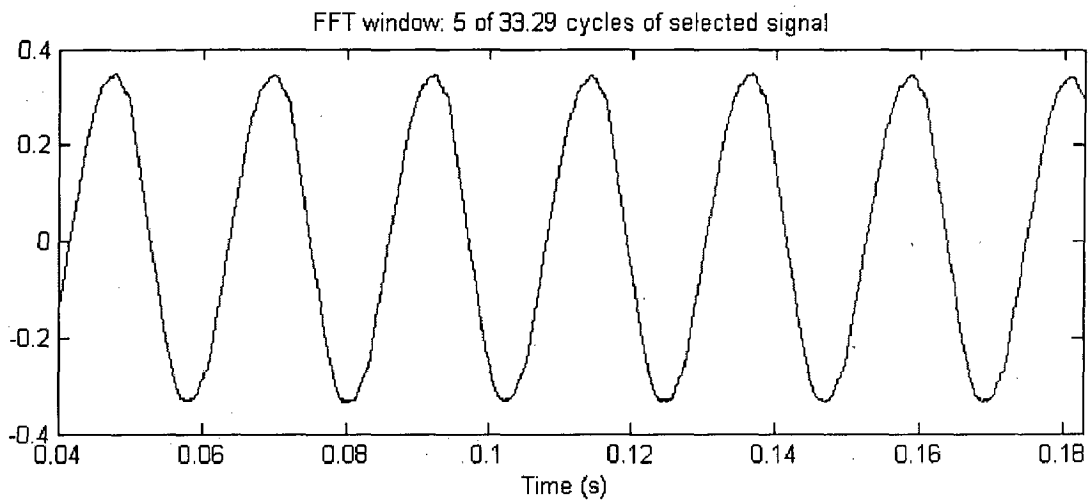


(a)

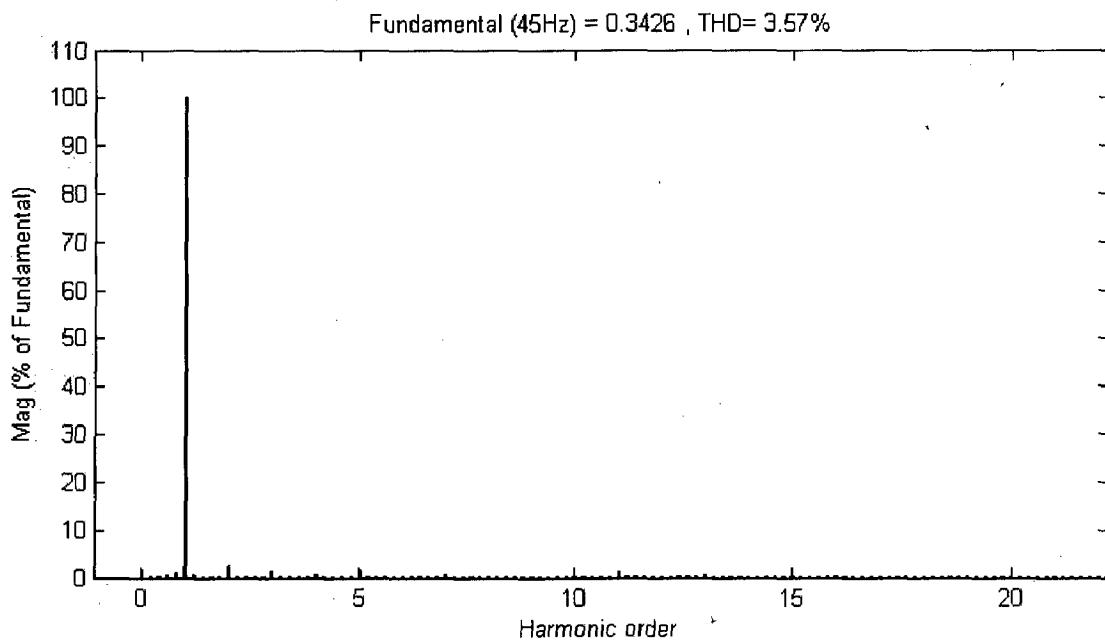


(b)

**4.32 (a) R-L load current ( $R=100\Omega$ ,  $L=0.5H$ ,  $f=50$  Hz)**  
**(b) Harmonic spectrum**

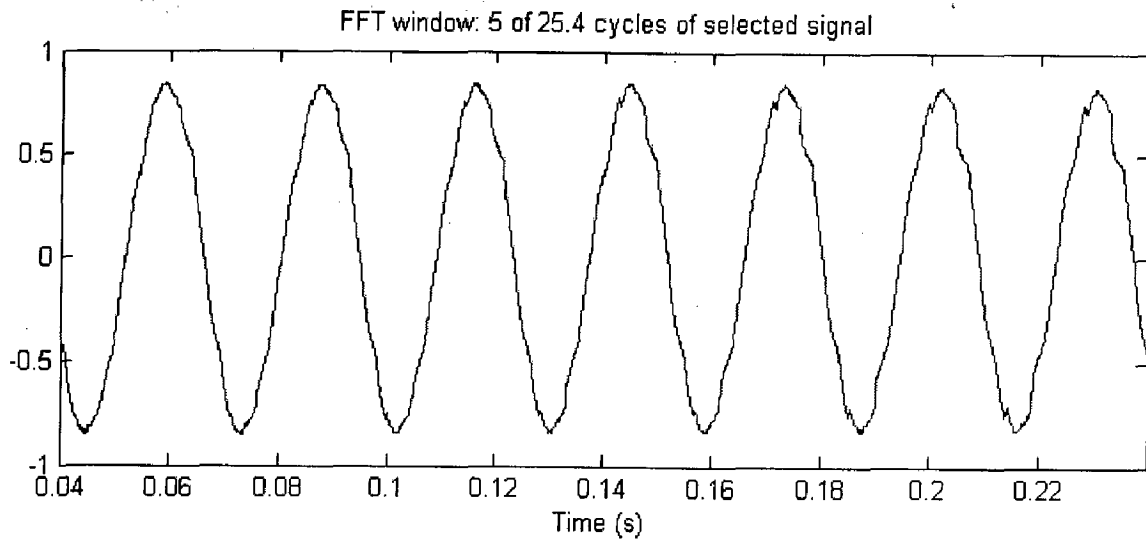


(a)

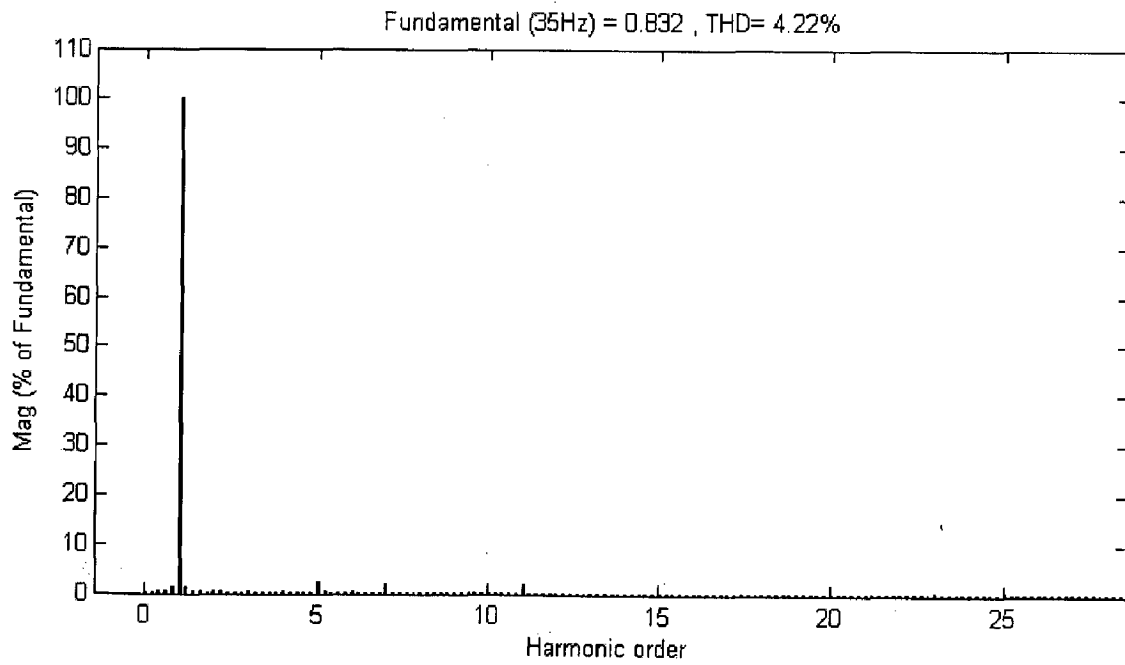


(b)

**Fig 4.33 (a) Load current**  
**(b) Harmonic current ( $R=100\Omega$ ,  $L=2H$ ,  $f=45\text{ Hz}$ )**

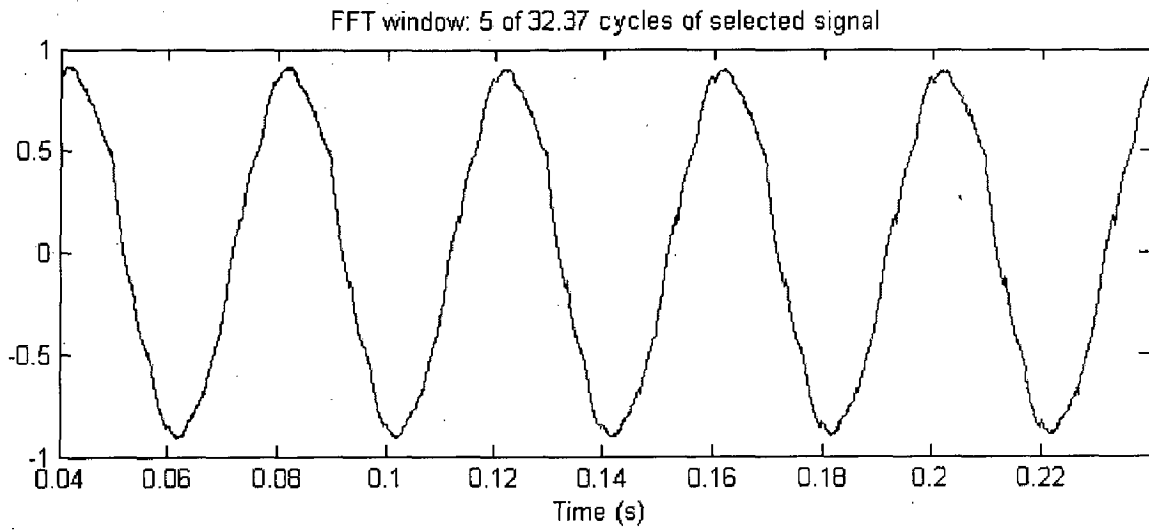


(a)

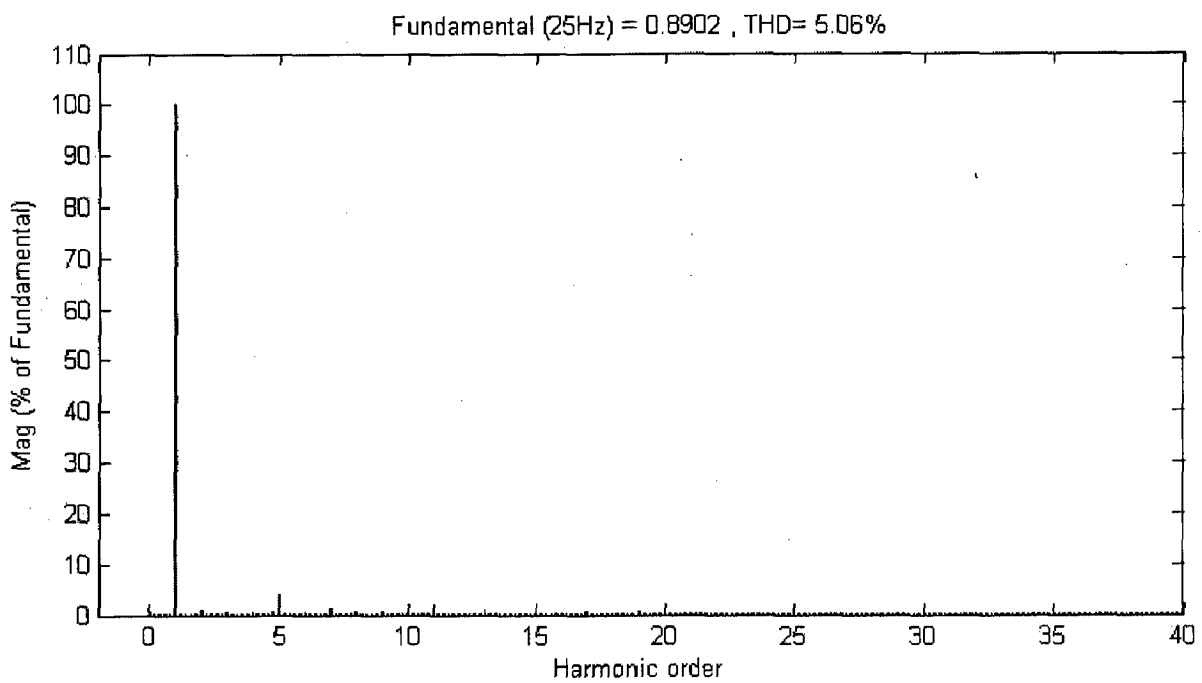


(b)

**Fig 4.34 (a) Load current**  
**(b) Harmonic current ( $R=200\Omega$ ,  $L=0.5H$ ,  $f=35\text{ Hz}$ )**

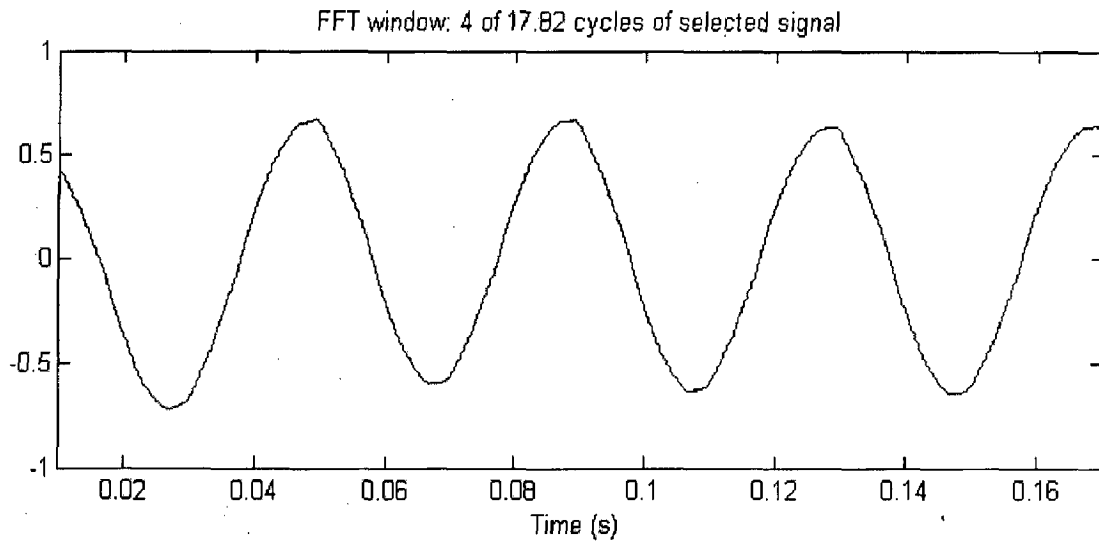


(a)

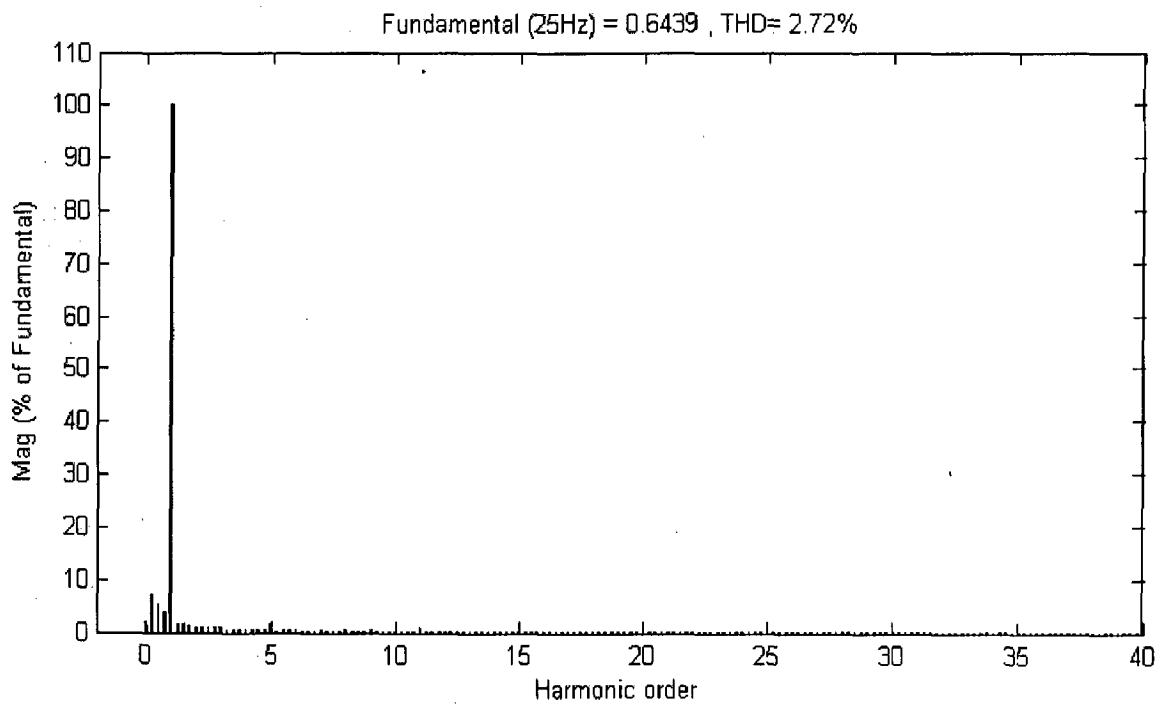


(b)

**Fig 4.35 (a) Load current**  
**(b) Harmonic current ( $R=200\Omega$ ,  $L=0.5H$ ,  $f=25\text{ Hz}$ )**



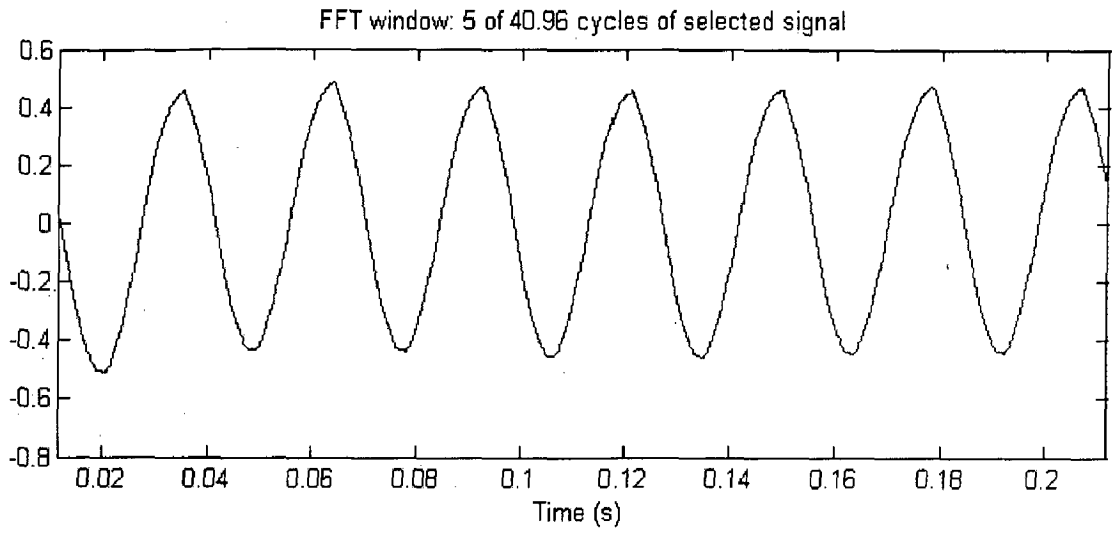
(a)



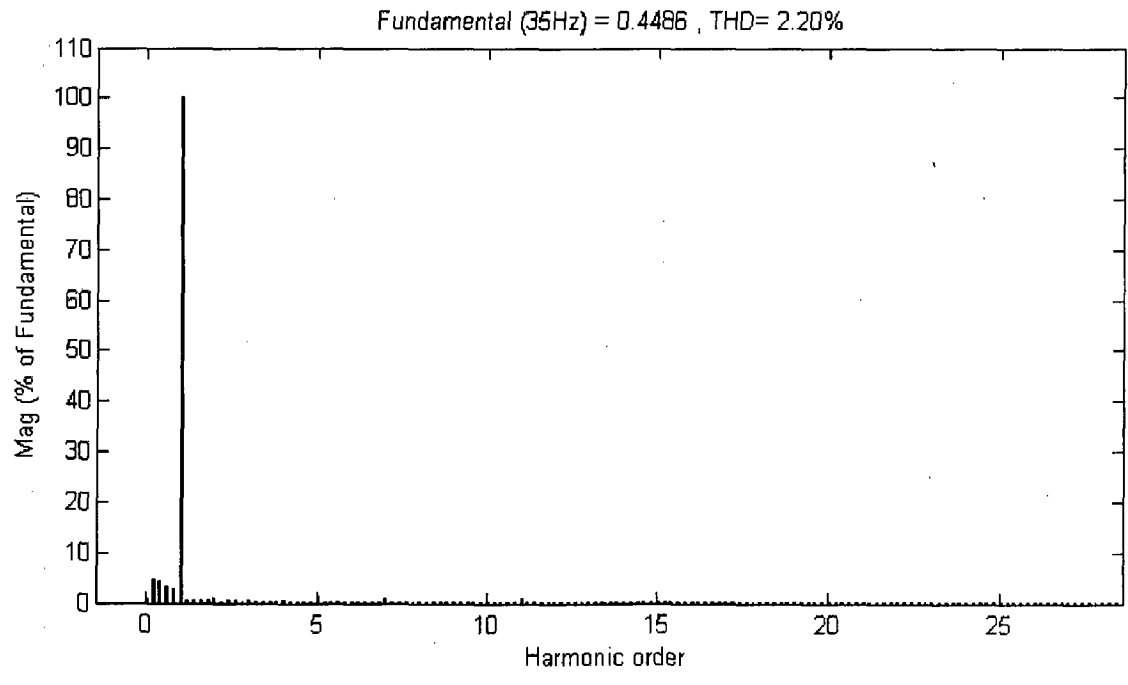
(b)

Fig 4.36 (a) Load current

(b) Harmonic current ( $R=100\Omega$ ,  $L=2H$ ,  $C=200\mu f$ ,  $f=25$  Hz)



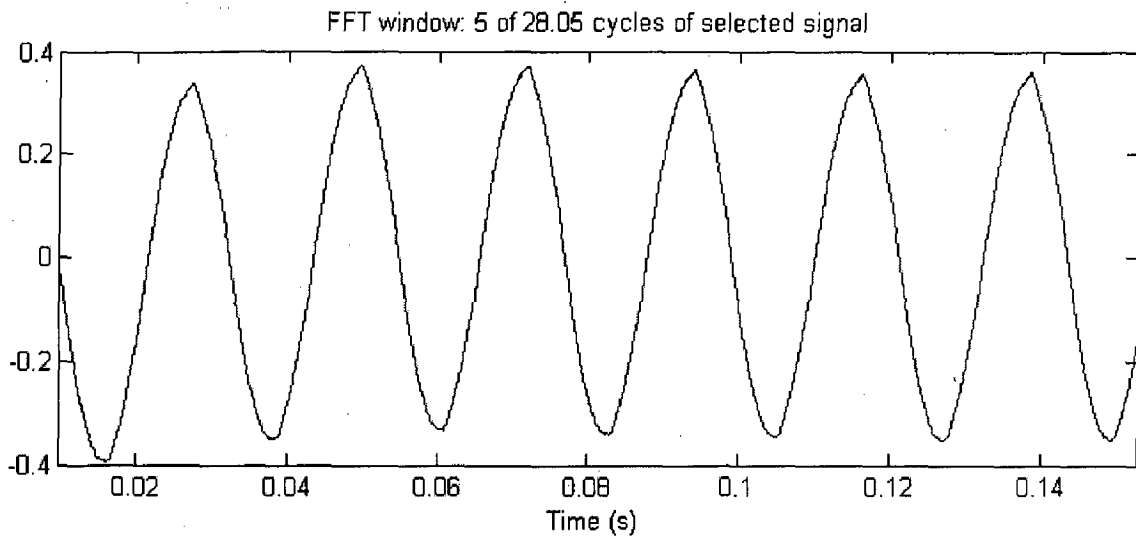
(a)



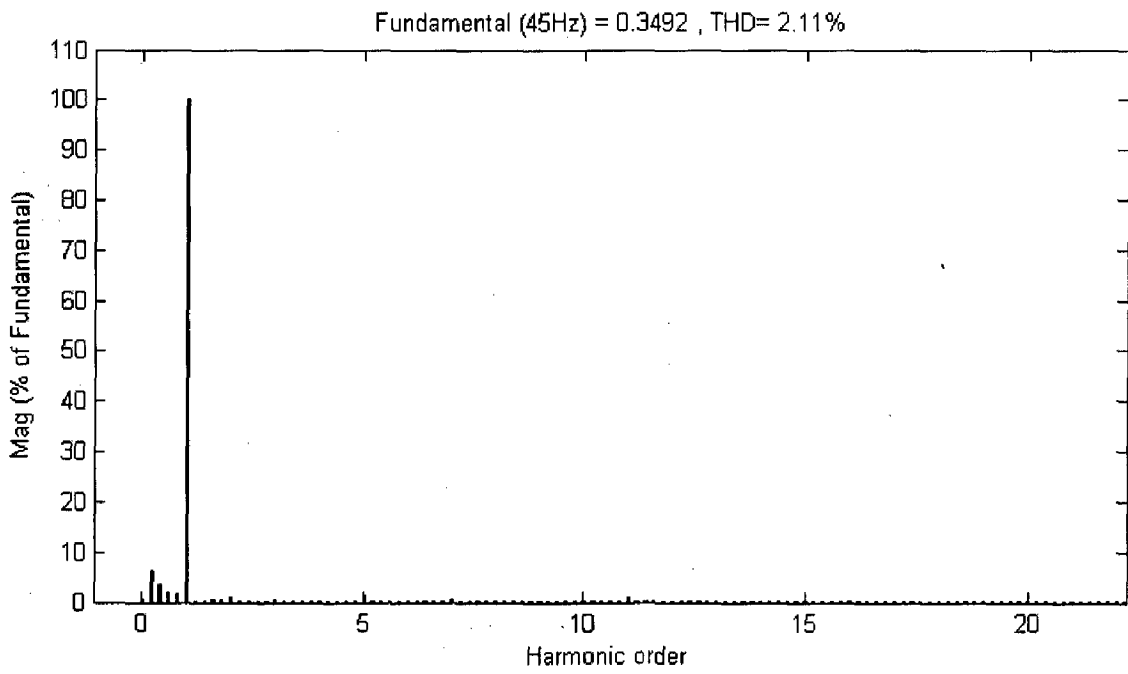
(b)

**Fig 4.37 (a) Load current**  
**(b) Harmonic current (R=100Ω, L=2H, C=200μf, f=35 Hz)**



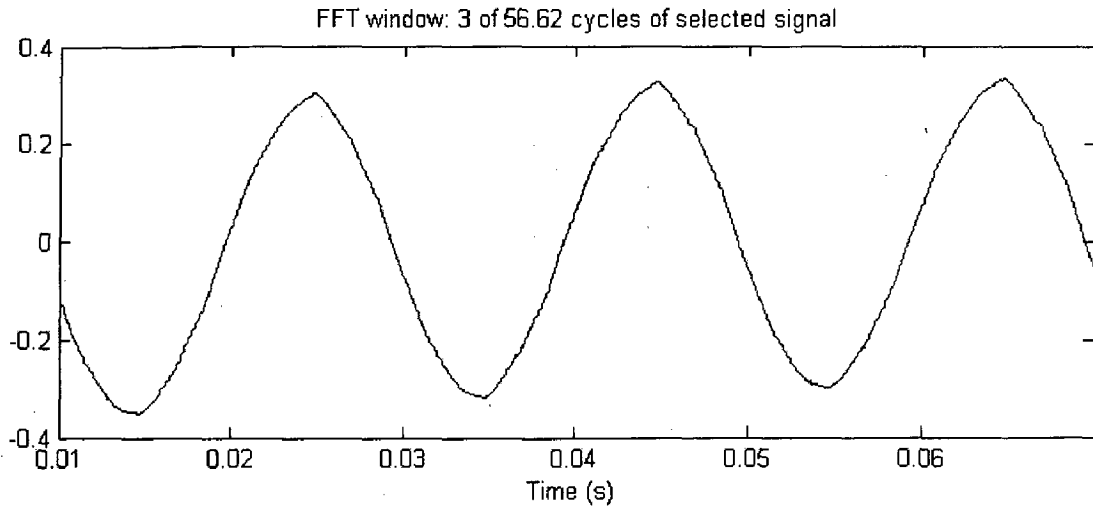


(a)

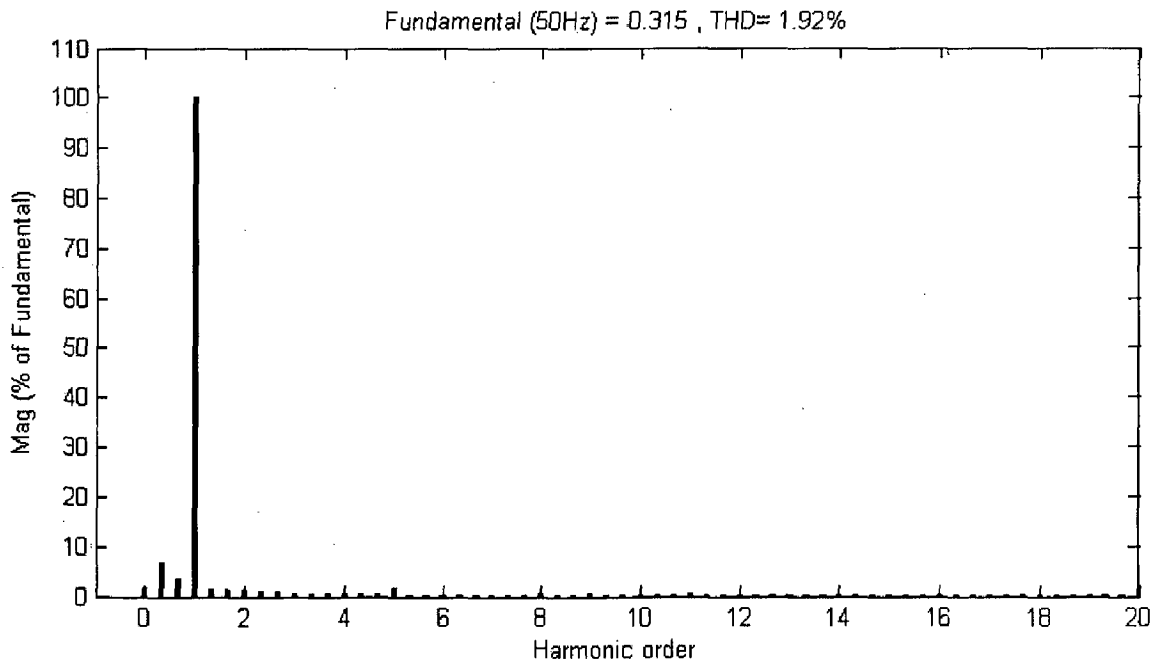


(b)

**Fig 4.38 (a) Load current**  
**(b) Harmonic current ( $R=100\Omega$ ,  $L=2H$ ,  $C=200\mu f$ ,  $f=45\text{ Hz}$ )**

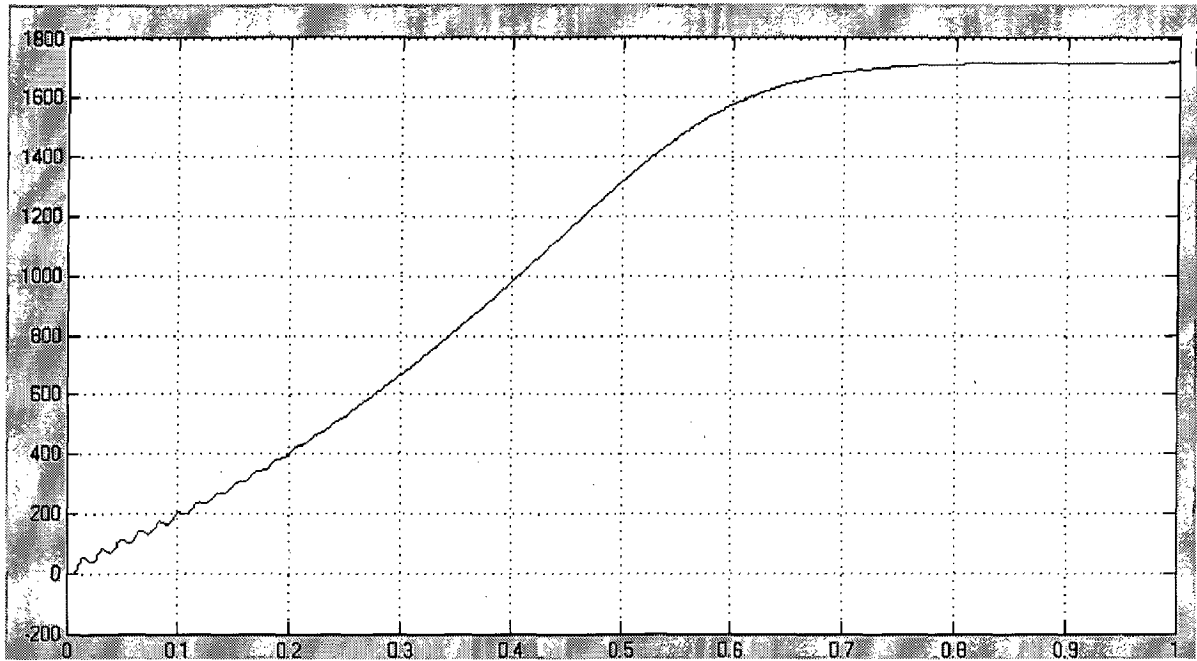


(a)

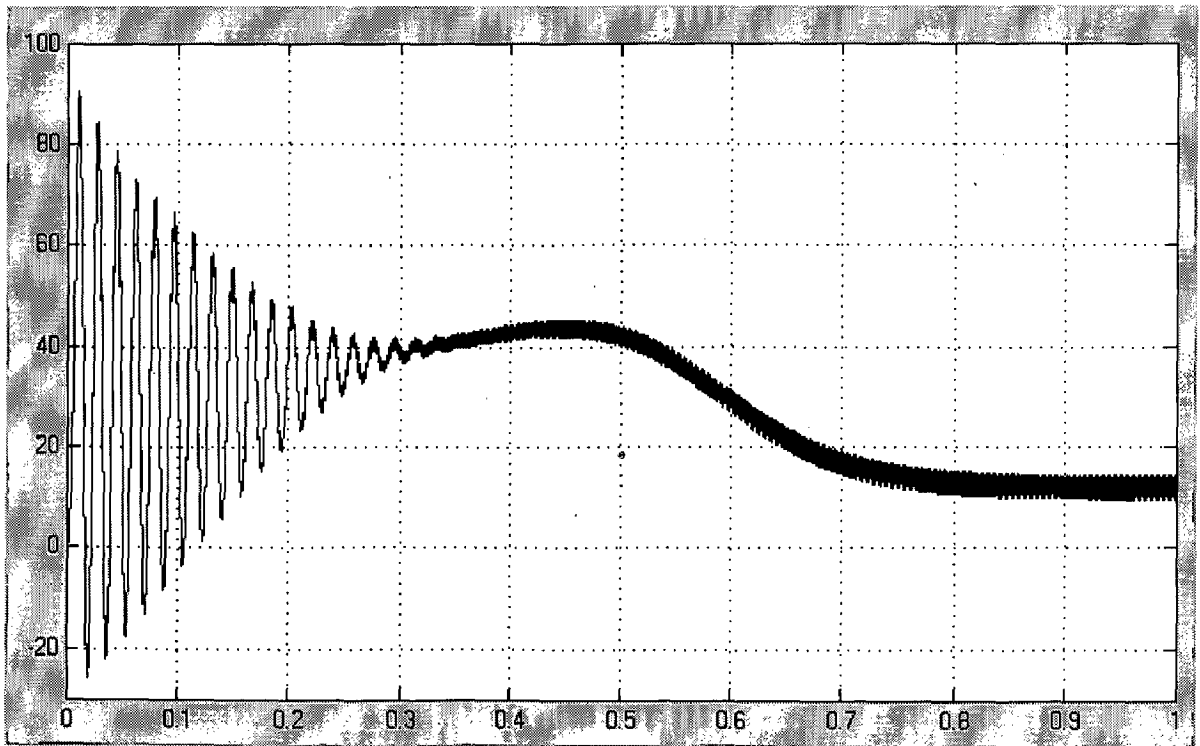


(b)

Fig 4.39 (a) Load current  
 (b) Harmonic current ( $R=100\Omega$ ,  $L=2H$ ,  $C=200\mu f$ ,  $f=50$  Hz)



(a)



(b)

**Fig 4.40 (a) Speed characteristic  
(b) Torque characteristic (3HP, 1725 RPM, 220V )**

## 4.5 Conclusion

From the results shown in figure 4.28-figure 4.40 it can be concluded that space vector modulation can be used to generate an averaged-sinusoidal voltage. Space vector modulation technique utilizes DC bus voltage more efficiently and generates less harmonic distortion in a three phase three level inverter. We observe that the harmonic distortion of the (R-L) load current for different operating frequency (between 25 Hz and 50 Hz) the total harmonic distortion remains between 1% to 5%. So space vector modulation technique synthesizes the reference vector efficiently.

### Conclusion

---

#### 5.1 Conclusion

There is need to analyze the causes for instability and the factor affecting the instability conditions in the induction motor drive systems. For this analysis the dynamic equations of the induction motor and its modeling is important. These dynamic equation and modeling of the drive system is briefly discussed in this thesis from reference [6]. This gives brief idea about the factor affecting the stability condition of the machine. The solution of the problem from the point of view of a linearized model is given. An analytical solution is given for two problems: Under what conditions is the oscillation is exited, and how is the oscillation range determined in the stator voltage versus frequency

(V/f) plane. A Physical explanation is given for the analytical results. Analysis of an induction motor verifies that the unstable range can be determined analytically. The factor restricting the upper limit of the stator frequency regarding the unstable range is the existence of transient inductance. The proposed linearized model is sufficiently appropriate to use as an analytical explanation of the experimental results.

Modeling of Voltage Source Converter (VSC) is always carried out independent of the type of application, for analysis of the system for various test conditions. In the present thesis continuous time and discrete time, linear time varying modeling of three phase three level VSC is analyzed. The effect of DC-link unbalance is ignored and no Pulse Width Modulation is considered for ease.

In the field of high power, high performance applications, the three level inverter seems to be the most promising alternative. In this thesis a simplified space-vector PWM method for the three level inverter is proposed and described in detail. Using MATLAB simulation software packages the simulation study of the three level inverter using space vector modulation technique is carried out in this thesis.

## **5.2 Future Scope**

Much of the research in the induction motor drives area is focused on sensorless methods of speed control, and methods of obtaining robust indirect flux-oriented drives through the use of parameter estimation and other schemes. Microcomputers have profoundly influenced the technology of power electronics and drives systems. Their implementation has not only brought about simplification of hardware and improvement of reliability, but also permitted performance optimization and powerful diagnostic capability which was not possible before by dedicated hardware control. Microcomputer provides intelligence to power electronic and motion control system. In real time context the execution speed of the control function is primary importance. With hardware implementation the execution speed is very fast but hardware complexity increases as the function are added. With software implementation the hardware complexity is fixed and execution time decreases as the functions are added. The trend is that the hardware engineer has to make some trade-off between the software and hardware. In a fully digital control system all the function are implemented by the software with a minimum of hardware used to interface between control system and power circuit.

## References

---

1. Lawrenson, P.J., and Bowes, S.R., "Stability of reluctance machines", *Proc IEE*, 118, 2, Feb. 1971, pp. 356-369.
2. Krause, P.C., "Methods of stabilizing a reluctance synchronous machine", *IEEE Trans. Power Appar. Syst.*, PAS-87, 3, Mar. 1968, pp. 641-649.
3. Risberg, R.L., "A wide speed range inverter fed induction motor drive", *conf. Rec. IEEE Ind. Gen. Appl. Group Annual Meeting*, 1969, pp. 629-633.
4. Fallside, F., and Wortley, A.T., "Steady-state oscillation and stabilization of variable-frequency inverter-fed induction motor drives" *Proc IEE*, 116, 6, June 1969, pp. 991-999.
5. Mongkol, S., and Somboon, S., "Averaging Analysis Approach for Stability Analysis of Speed-Sensorless Induction Motor Drives with stator resistance estimation", *IEEE Trans. On Ind. Elec.* Vol. 53, NO. 1, February 2006.
6. Ryuzo Ueda, Toshikatsu Sonoda, Kunio Koga, and Michiya Ichikawa., "Stability Analysis In Induction Motor Driven By  $V/f$  Controlled General Purpose Inverter" *IEEE Trans. On Ind. Appl.* Vol. 28, NO. 2, March/April 1992.
7. Ping Hsu, "Stability Analysis of AC Steady-State Control for Inverters" *IEEE Pros.*, September 2000.
8. Ulf Jonsson, and Maria-Christina Laiou, "Stability Analysis of Systems with Nonlinearities", *Proceedings of the 35<sup>th</sup> Conference on Decision and Control Kobe, Japan December 1996.*
9. Jee H.J., Gang Y.J., and Bong H.K., "Stability Improvement of  $V/f$ -Controlled Induction Motor Drive Systems by a Dynamic Current Compensator", *IEEE Trans. On Ind. Elec.*, Vol. 51, No. 4, August 2004.
10. R.Itoh, DrEng, "Stability of a PWM current-source rectifier/inverter fed induction motor drive", *IEE Pros.*, Vol.137, Pt. B, No. 6, November 1990.
11. Bimal K. Bose, "Modern Power Electronics And AC Drives".
12. Slemon G.R., "Electrical Machines For Variable-Frequency Drives", *IEEE Pros.*, Vol. 82, pp. 1123-1139, Aug. 1994.

13. Lazhar BEN-BRAHIM, "Improvement of the stability of the V/f controlled induction motor drives systems",
14. Chien F.H., Rong B.H., and Chang H.L., "Stability Analysis and PI Controller Tuning for a Speed-Sensorless Vector-Controlled Induction Motor Drive", *IEEE Ind. Elec.* November 2-6, 2004.
15. Leon M. T., Fang Z. P., and Thomas G. H., "Multilevel Converters for Large Electric Drives", *IEEE Trans. On Ind. Appl.* Vol. 35, No. 1, January/February 1999.
16. Lehn P.W., and Iravani M.R., "Discrete Time Modeling and Control of the voltage source Converter for Improved Disturbance Rejection", *IEEE Trans. On Power Elec.*, Vol. 14, No. 6, November 1999.
17. Lehn P.W., "Exact Modeling of the Voltage Source Converter", *IEEE Trans. On power delivery.* Vol.17, NO. 1, January 2002.
18. Humberto H., Claudia M., and Gérard-André C., "An Equivalent Internal Circuit of the Induction Machine for Advanced Spectral Analysis", *IEEE Trans. On Ind. Appl.* Vol. 40, No.3, May/June 2004.
19. Rathnakumar D., Lakshmana Perumal J., and Srinivasan T., "A new software implementation of Space vector PWM"
20. Keliang Z., and Danwei W., "Relationship Between Space-Vector Modulation and Three-Phase Carrier-Based PWM: A Comprehensive Analysis", *IEEE Ind. Elec.* Vol. 49, No. 1, February 2002.
21. Jobing R., Vander Merwe F.S., Kamper M.J., "Digital Implementation of Bus Clamped Space Vector Modulation", *IEEE Trans. On energy conversion*, Vol. 9, No.2, June 1994.
22. Domenico C., Giovanni S, and Angelo T., "Implementation of a Direct Torque Control Algorithm for Induction Motors Based on Discrete Space Vector Modulation", *IEEE Trans. On Power Elec.* Vol. 15, NO. 4, July 2004.
23. Yamamoto K., Shinohara K., "Comparison Between Space Vector Modulation And Subharmonic Methods For Current Harmonics of DSP-Based Permanent-Magnet AC Servo Motor Drive System", *IEE Proc. Elec. Power Appl.*, Vol.143., No. 2, March 1996.



24. Hyo L. Liu and Gyu H. Cho., "Three-Level Space Vector PWM In Low Index Modulation Region Avoiding Narrow Pulse Problem", *IEEE Trans. On Power Elec.* Vol. 9, NO. 5, September 1994.
25. Remus T. Frede B., John. K. P., Ekrem C., and Prasad N. E., "Multilevel Inverter by Cascading Industrial VSI", *IEEE Trans. On Ind. Elec.*, Vol. 49, No. 4, August 2002.
26. Yo-Han Lee, Bum-Seok Suh, and Dong-Seok Hyun, "A Novel PWM Scheme For A Three-Level Voltage Source Inverter With GTO Thyristors ", *IEEE Trans. On Ind. Appl.*, Vol.32, No. 2, March/April 1996.
27. Xiaoming Y., Ivo B., "Fundamentals of A New Diode Clamping Multilevel Inverter", *IEEE Trans. On Power Elec.*, Vol. 15, No. 4, July 2000.
28. Ratnayake K.R.M.N., Murai Y, and Watanabe T., " Novel Carrier PWM Scheme TO Control Neutral Point Voltage Fluctuations In Three-Level Voltage Source Inverter", *IEEE International Conference On Power Electronics and Drive Systems* ,July 1999, Hong Kong.
29. Annette V.J., Shaoan D., and Haoran Z., "A Multilevel Inverter Approach Providing DC-Link Balancing, Ride-Through Enhancement, and Common-Mode Voltage Elimination", *IEEE Trans. On Ind. Elec.*, Vol. 49, NO. 4, August 2002.
30. Khaled E.A., William S., and Hulley L.N., "Induction Motor Speed Control Using A Microprocessor-PWM inverter", *IEEE Trans. On Ind. Elec.* Vol. 36, No. 4, November 1989.

Space vector representation of the 3 phase quantity

$$\vec{V}^* = V_\alpha + jV_\beta = \frac{2}{3}(V_a + aV_b + a^2V_c) \quad (\text{A-1})$$

Where

$$a = e^{j\frac{2\pi}{3}}$$

$$|V| = \sqrt{V_\alpha^2 + V_\beta^2}, \alpha = \tan^{-1}\left(\frac{V_\beta}{V_\alpha}\right) \quad (\text{A-2})$$

$$V_\alpha + jV_\beta = \frac{2}{3}\left(V_a + e^{j\frac{2\pi}{3}}V_b + e^{-j\frac{2\pi}{3}}V_c\right) \quad (\text{A-3})$$

$$V_\alpha + jV_\beta = \frac{2}{3}\left(V_a + \cos\frac{2\pi}{3}V_b + \cos\frac{2\pi}{3}V_c\right) + j\frac{2}{3}\left(\sin\frac{2\pi}{3}V_b - \sin\frac{2\pi}{3}V_c\right) \quad (\text{A-4})$$

Equating real and imaginary parts:

$$V_\alpha = \frac{2}{3}\left(V_a + \cos\frac{2\pi}{3}V_b + \cos\frac{2\pi}{3}V_c\right) \quad (\text{A-5})$$

$$V_\beta = \frac{2}{3}\left(0V_a + \sin\frac{2\pi}{3}V_b - \sin\frac{2\pi}{3}V_c\right) \quad (\text{A-6})$$

$$\begin{pmatrix} V_\alpha \\ V_\beta \end{pmatrix} = \frac{2}{3} \begin{pmatrix} 1 & \cos\frac{2\pi}{3} & \cos\frac{2\pi}{3} \\ 0 & \sin\frac{2\pi}{3} & -\sin\frac{2\pi}{3} \end{pmatrix} \begin{pmatrix} V_a \\ V_b \\ V_c \end{pmatrix} \quad (\text{A-7})$$

$$\begin{pmatrix} V_\alpha \\ V_\beta \end{pmatrix} = \frac{2}{3} \begin{pmatrix} 1 & -0.5 & -0.5 \\ 0 & \frac{\sqrt{3}}{2} & -\frac{\sqrt{3}}{2} \end{pmatrix} \begin{pmatrix} V_a \\ V_b \\ V_c \end{pmatrix} \quad (\text{A-8})$$

Dynamic equation of an induction motor:

$$\vec{V}_1 = r_1\vec{i}_1 + L_{11}\vec{\dot{i}}_1 + L_{22}\vec{\dot{i}}_2 \quad (\text{A-9})$$

$$0 = r_2\vec{i}_2 + (L_{12}\vec{\dot{i}}_1 + L_{22}\vec{\dot{i}}_2) - j\omega_r(L_{12}\vec{i}_1 + L_{22}\vec{i}_2) \quad (\text{A-10})$$

$$T_e = qL_{12} I_m[\vec{i}_1 \times \vec{i}_2^*] \quad (\text{A-11})$$

$$\frac{J}{n} \dot{\omega}_r = T_e - T_{sh} \quad (\text{A-12})$$

Equivalent magnetizing current  $\vec{i}_0$  is

$$\vec{i}_0 = \vec{i} + \frac{L_{22}}{L_{12}} \vec{i}_2 \quad (\text{A-13})$$

So (B-9)-(B-11) becomes

$$\vec{V}_1 = r_1 \vec{i}_1 + L_1 \dot{\vec{i}}_1 + L_0 \dot{\vec{i}}_0 \quad (\text{A-14})$$

$$0 = r_2'(\vec{i}_0 - \vec{i}_1) + L_0 \dot{\vec{i}}_0 - j\omega_r L_0 \vec{i}_0 \quad (\text{A-15})$$

$$T_e = qL_{12} I_m [\vec{i}_1 \times \vec{i}_0^*] \quad (\text{A-16})$$

Substituting (B-15) into (B-14) and eliminating  $\vec{i}_1$

$$\vec{V}_1 = r_1 \{ \vec{i}_0 + T_0 \dot{\vec{i}}_0 - jT_0 \omega_r \vec{i}_0 \} + L_1 [ \ddot{\vec{i}}_0 + T_0 \ddot{\vec{i}}_0 - jT_0 (\dot{\omega}_r \vec{i}_0 + \omega_r \dot{\vec{i}}_0) ] \quad (\text{A-17})$$

### Information of Data Acquisition Cards

---

The following two cards have been used for the system development.

(1) **Dynalog PCL-812:** The PCL-812 is a high performance, high speed, multi-function data acquisition card for IBM PC/XT/AT and compatible computers. The key features of this card are given below.

- 16 single-ended analog input channels
- An industrial standard 12-bit successive approximation converter (ADC574 or equivalent) to convert analog input. The maximum A/D sampling rate is 30 KHz in DMA mode.
- Switch selectable versatile analog input ranges.  
Bipolar:  $\pm 1V$ ,  $\pm 2V$ ,  $\pm 5V$ ,  $\pm 10V$
- Three A/D trigger modes: Software trigger  
Programmable pacer trigger  
External trigger pulse trigger
- The ability to transfer A/D converted data by program control interrupt handler routine or DMA transfer
- An INTEL 8253-5 Programmable Timer/Counter provides pacer output (trigger pulse) at the rate of 0.5 MHz to 35 minutes/pulse to the A/D. The timer time base is 2 MHz. One 16-bit counter channel is reserved for user configurable applications.
- Two 12-bit monolithic multiplying D/A output channels. An output range from 0 to +5v can be created by using the onboard -5V reference
- 16 TTL/DTL compatible digital input, and 16 digital output channel.

(2) **VYNITICS TIMER I/O CARD:** The key features of this card are shown below.

- 48 programmable Input/Output using two 8255.
- Six channel of 16 Bit Timer/Counter.
- 8 optically isolated Input.
- 8 optically isolated Output.
- Jumper selectable I/O addressing.
- Hardware clock selection for Timer/Counter.